People's Democratic Republic of Algeria
Ministry of Higher Education and Scientific Research
University M'HamedBOUGARA – Boumerdes

Institute of Electrical and Electronic Engineering
Signals and Systems Research Laboratory

PHD DISSERTATION

PRESENTED BY:

DJERIOU Salim

IN PARTIAL FULFILMENT OF THE REQUIREMENTS FOR THE DEGREE OF

DOCTORATE

FIELD:ELECTRICAL ENGINEERING
OPTION: POWER ENGINEERING

TITLE:

Performance Improvement of Photovoltaic Pumping System

JURY MEMBERS:

Mr. BENTARZI Hamid	Pr	IGEE/UMBB	President
Mr. KHELDOUN Aissa	MCA	IGEE/UMBB	Supervisor
Mr. KHODJA Djalal-Eddine	MCA	U.MBM'sila	Co-Supervisor
Mr. HADJ ARAB Amer	DR	CDER-Alger	Examiner
Mr. KABACHE Nadir	MCA	U.Médea	Examiner

Registration Number:……../2018

Dedication

To my lovely parents Smail and Nacera, they are both responsible for the good values that guide my life.

To my dear brothers Nouredinne, Mouloud,

To my sweet sisters

To my wife and my Son Anes, Born of love, Raised with love, always loved

You shoulders gave me the courage to share our theses.

Thank you

Salim

SCIENTIFIC WORK

Journal papers

***1-Salim Djeriou**, Aissa Kheldoun,Adel Mellit,'' Efficiency improvement of induction motor driven solar water pumping system using Golden Section Search algorithm"* Arab J *Sci Eng, Vol 43 issue 6, pp 3199-3211, June 2018*

***2-Salim Djeriou,** Aissa Kheldoun and Radhwane Sadouni '' Fuzzy indirect field oriented control of a dual star induction motor water pumping system fed by photovoltaic generator'' Engineering intelligent systems, Vol 23 No 2 June 2015.*

***3**-Radhwane Sadouni, MEROUFEL Abdelkader,**DJERIOU Salim** and Aissa Kheldoun''a fuzzy sliding mode robust control for a field oriented dual star induction machine fed by photovoltaic power supply with mppt algorithm '',Article · Oct 2016 · Mediterranean Journal of Measurement and Control*

***4**-Aissa Kheldoun, **Salim Djeriou**, Abdelmalek Kouadri, Larbi Refoufi,'' A simple and accurate maximum power point tracking algorithm for photovoltaic systems, Progress in Clean energy, Volume 02,Chapter 50, DOI 10.1007/978-3-319-17031-2-50©Springer International publishing, Switzerland 2015.*

***5**-R. Sadouni, A. Meroufel and **Salim Djeriou**: "Study and Simulation of Direct Torque Control (DTC) for a Six Phase Induction Machine (SPIM)", International Journal of Energy, Issue 2, Vol. 7, 2013*

Conference papers

***1**-SADOUNI Radhwane, MEROUFEL Abdelkader, **DJERIOU Salim** and KHALDOUNE Aissa Field Oriented Control of a Dual Star Induction Machine Fed by Photovoltaic Solar Panel with MPPT'' 2ème conférence Internationale des énergies renouvelables CIER-2014,Tunisie*
***2**-Aissa Kheldoun, **Salim Djeriou**, Abdelmalek Kouadri, Larbi Refoufi "Using Golden Section Search Technique for Maximum Power Point Tracking in Photovoltaic Systems" 13th International Conferance o Clean Energy, June 2014 Istanbul, Turky*

***3**-Aissa Kheldoun, **Salim Djeriou**, Abdelmalek Kouadri, Larbi Refoufi " Fuzzy Logic-Based Aproach For Maximum Power Point Tracking In Photovoltaic Systems"7th International Symposium on Hydrocarbons and Chemistry,May 2014 Boumerdes,Algeria.*

***4-Salim Djeriou**, Aissa Kheldoun ,Radhwane Sadouni and Bahri Hamza'' Vector control of Dual Star Induction Motor-Water Pumping System Fed by Photovoltaic Generator using Fuzzy Controller''Pais 2016 khanchla,Algeria .*

***5**-Aissa Kheldoun, **Salim Djeriou**'' A GSO -based maximum power point tracking algorithm for photovoltaic systems'', The 5th International Conference on Electrical Engineering – Boumerdes (ICEE-B),October 29-31, 2017, Boumerdes, Algeria.*

Acknowledgment

Our sincerest and deepest thanks to God, the most gracious most merciful for helping us finish this modest work. It is our belief in him that helped us persevere at times when it seemed impossible to go on.

I wish to express my sincere gratitude to Prof. Refoufi Larbi (May God bless him) who, although no longer with us, continues to inspire by his example and dedication to the students he served over the course of his career.

We would like to express our deep felt gratitude to our supervisor Dr. A.KHELDOUN for his wisdom, guidance and support.

Finally, I thank my family for their valuable support and encouragement.

ملخص

هذه الأطروحة تتناول تقنيتين مختلفتين تستعملان في أنظمة ضخ الماء باستخدام الطاقة الشمسية للحصول على مردودية أكبر. في الطريقة الأولى، قمنا باستخدام تقنية جديدة و هي طريقة تحسين تعتمد على البحث عن المقطع الذهبي. بالمقارنة مع التقنية التقليدية التي تعتمد على البحث عن نقطة الاستطاعة القصوى مثل تقنية الإضطراب و الملاحظة، طريقة البحث عن المقطع الذهبي لها فائدتين اثنتين: الإستجابة السريعة وعدم وجود إضطراب. الإستطاعة القصوى المحولة من اللوح الشمسي إلى مضخة الطرد المركزي يتم ضمانها بواسطة الإختيار الأمثل لسرعة الإشتغال للمحرك اللاتزامني. هذه الطريقة تبين فاعلية و نجاعة الطريقة المقترحة. فيما يخص الطريقة الثانية قمنا باستخدام الآلة اللاتزامنية ثنائية النجمة (سداسية الطور) بدلا من الآلة اللاتزامنية الكلاسيكية (ثلاثية الطور) معتمدين على تقنية الإضطراب و الملاحظة لمتابعة نقطة الاستطاعة القصوى للمولد الشمسي عند اختيار السرعة المثلى للمحرك، وذلك لضمان تحويل أقصى استطاعة للمضخة. لتحقيق هذا الهدف قمنا باستخدام تقنية التحكم بتوجيه تدفق الجزء الدوار لتسهيل هذا التحويل عن طريق تحسين ميزات الفصل بين الجزء الميكانيكي و الجزء الكهربائي. بالإضافة على ذلك، و من أجل التحكم الجيد في سرعة المحرك، قمنا باستخدام ضابط سرعة جديد يعتمد على المنطق الغامض عوضا عن الضابط التقليدي. هذا الضابط الجديد يعطي نتائج أفضل من الضابط التقليدي من حيث عدم التأثر بتغير عوامل النظام. اعتمدنا على أداة المحاكاة المدمجة في برنامج الماتلاب للحصول على النتائج الخاصة بالطريقتين السابقتين تحت شروط مناخية مختلفة.

الكلمات المفتاحية

أنظمة ضخ الماء باستخدام الطاقة الشمسية, المحرك اللاتزامني, متابعة نقطة الاستطاعة القصوى, البحث عن المقطع الذهبي, السرعة المثلى, الآلة اللاتزامنية ثنائية النجمة ,التحكم بتوجيه تدفق الجزء الدوار ,المنطق الغامض ,مضخة الطرد المركزي.

ABSTRACT

This thesis presents two work frames schemes of solar water pumping system with maximum overall operating efficiency. In the first scheme, a new technique based on Golden-Section-Search (GSS) optimization method is used. Compared to conventional MPPT tracking method such as Perturb and Observe (P&O), GSS technique offers two advantages namely: quick response and perturbation free. The maximum power transfer from the photovoltaic panel to the centrifugal pump is ensured by optimal selection of induction motor's operating speed. This technique demonstrates the effectiveness of the proposed architecture. Regarding the second scheme, a tentative to employ a Dual Star Induction motor (DSIM) instead of the conventional induction motor is investigated. The conventional Perturb and Observe (P&O) algorithm is adopted to track the maximum power from the PV generator while optimum rotor speed selection is adopted in order to ensure maximum power transfer to the pump. To achieve this goal the indirect rotor field oriented control scheme is to facilitate this transfer by improving the decoupling performances. Besides, a fuzzy logic- based PI controller instead of the conventional PI speed controller is used for speed control. This controller is known to be more robust than the conventional one in terms of system uncertainties. Matlab/Simulink package is used to simulate and predict the performances of the two proposed SWPS work frame under different climate conditions.

Keywords

Water pumping system, Induction motor, MPPT, Golden Section Search Algorithm, Optimal speed, Dual Star Induction Motor, Indirect Field Oriented Control, Fuzzy Logic Controller, Photovoltaic Generator, , Centrifugal Pump.

RESUME

Cette thèse présente deux architectures de système de pompage d'eau solaire avec une efficacité de fonctionnement globale maximale. Dans le premier schéma, une nouvelle technique basée sur la méthode d'optimisation Golden-Section-Search (GSS) est utilisée. Comparée à la méthode de suivi MPPT conventionnelle telle que Perturb et Observe (P & O), la technique GSS offre deux avantages: une réponse rapide et une absence de perturbation. Le transfert de puissance maximal du panneau photovoltaïque à la pompe centrifuge est assuré par une sélection optimale de la vitesse de fonctionnement du moteur à induction. Cette technique démontre l'efficacité de l'architecture proposée. En ce qui concerne le deuxième schéma, une tentative d'utilisation d'un moteur à induction double étoile (DSIM) au lieu du moteur à induction conventionnel est étudiée. L'algorithme conventionnel Perturb and Observe (P & O) est adopté pour suivre la puissance maximale du générateur PV tout en adoptant une vitesse de rotor optimale afin d'assurer un transfert de puissance maximal à la pompe. Pour atteindre cet objectif, le schéma de la commande vectorielle indirecte par orientation du flux rotorique doit faciliter ce transfert en améliorant les performances de découplage. En outre, un contrôleur PI basé sur la logique floue à la place du contrôleur de vitesse PI classique est utilisé pour le contrôle de la vitesse. Ce contrôleur est connu pour être plus robuste que le contrôleur conventionnel en termes d'incertitudes système. Le logiciel Matlab / Simulink est utilisé pour simuler les performances des deux architectures proposées dans différentes conditions climatiques.

Mots clés

Système de pompage photovoltaïque, Moteur à induction, MPPT, Golden-Section-Search, Vitesse optimale, Moteur à induction double étoile, Commande vectorielle indirecte par orientation du flux rotorique, la logique floue, Générateur photovoltaïque, Pompe centrifuge.

Nomenclacture

PV	Photovoltaic
P	Power [w]
V	Voltage [V]
I	Current [A]
I_{PV}	Photovoltaic current
V_{PV}	Photovoltaic voltage
PI	Proportional-Integrator
I_O	Saturation current [A]
V_{mp}	Maximum power point voltage
I_{mp}	Maximum power point current
V_{OC}	Open circuit voltage
I_{sc}	Short circuit current
N_S	Number of series connected cells
MPP	Maximum Power Point
STC	Standard test conditions [25°C, 1sun]
G	Irradiance [W/m^2]
$P\&O$	Perturb and observe
IC	Incremental conductance
P_{max}	Maximum power
DC	Direct current
AC	Alternating current
K_P	Proportional constant
K_I	Integrator constant
PWM	Pulse Width Modulation
I_{ph}	photocurrent
I_d	junction diode current
I_0	reverse saturation current
R_s	series resistance
R_{sh}	parallel resistance
A	diode factor

k	Boltzmann's constant
T	Cell temperature
Eg	gap energy (1.12 eV for Crystalline-Silicon)
q	electron charge
α_v	Open circuit voltage/temperature coefficient
α_i	Short circuit current/temperature coefficient
T_{ref}	reference temperature of PV cell in Kelvin (K), usually 298K (25^0C)
η	efficiency of the module
Pint	Power in incident spectrum.
FF	the fill factor
M	index to the module
n_s	number of cells connected in series
n_p	number of cells connected in parallel
R_{sM}	Series resistance of module.
IsrM	is the reference saturation current of Module
IccrM	the reference short circuit of module
I_{scM}	The short circuit of the array under given environmental conditions
D	The duty cycle.
L	The value of inductor
ΔI_L	Ripple current
C	capacitor
GSS	Golden section search
MPPT	Maximum Power Point Tracking
SWPS	solar water pumping system
PVG	Photovoltaic generator
IRFOC	Indirect Rotor Field Oriented Controller
a,b,c	Indices denoting actual three phase axes
d,q	Indices denoting axes rotating synchronously with supply frequency
$\alpha.\beta$	Indices denoting stator-fixed axes
s	Laplace operator
R_s	Stator resistance
R_r	Rotor resistance
R_m	Iron loss resistance
L_s	Stator self inductance
L_r	Rotor self inductance

L_{ls}	Stator leakage inductance
L_{lr}	Rotor leakage inductance
P	Number of pair poles
θ_r	Rotor electrical angle
θ_e	Angle between the synchronous frame and the stationary frame
ω	is angular electrical speed
ω_r	the speed of d-q axes in the rotor repair
ω_s	the speed of d-q axes in the stator repair
T_e	Electromagnetic toque
T_L	Load torque
Ω_r	Mechanical speed
J	Rotor inertia
T_{fr}	Time constant rotating leakage
σ	Dispersion coefficient
DSIM	Dual Star Induction Machine
Φ	Flux
FLC	Fuzzy Logic Controller

Table of contents

Chapter III: Adaptation stage and MPPT

Chapter IV: MPPT for Solar water pumping system using induction motor

List of Figures

List of tables

General Introduction

General Introduction

The increasing of the consumption of electrical energy with fossil fuels (oil, coal, natural gas, etc…) has traditionally provided adequate costs, and as results many problems such as the crisis of energy and more recently climate change. Therefore, fossil energy generation is responsible for 40% of global CO_2 emissions from greenhouses [1] and the sustainability of our civilization is seriously threatened by the world widely energy demand. It has been looking to alternative sources of energy for reducing carbon dioxide emissions and ensuring secure, clean and affordable energy. Our sun "Solar Energy" is one of the greatest alternative sources, a solution for achieving more sustainable energy systems, and it is the environment friendly energy sources.

Solar energy is available in abundance, clean and sustainable; which makes it very attractive source of electricity supply for industrial as well as for domestic applications. It is totally free, produces no pollution, widely available, no emission of carbon footprint and it is one of the most widely used renewable source of energy.

The most important aspect of a photovoltaic generator (PVG) is that to produce electrical energy directly from collecting sunlight based a solar cell, made up of silicon cells. Although each cell outputs a relatively low voltage, when the many cells are connected in series and in parallel, a PVG is formed. Thus, it is necessary to extract as much energy as possible from a PVG during utilization, because it was a high cost of solar cell module.

The variation of ambient environmental conditions (the level of solar irradiation, temperature, the intensity of sunlight,) influenced for a supply maximum power at one particular operation point known the maximum power point (MPP). However, it is desirable to operate PV systems at its MPP. Thus, power electronic converters are required for maximum power point tracking (MPPT) techniques, which provides maximum power. And they are also needed to transfer the PV power to a load. In this case, many algorithms have been studied in literature to seek this maximum power point from which one can list the following algorithms Perturb and Observe (P&O) algorithm, the Incremental Conductance (InCond) algorithm, …etc. But the main drawback of this algorithm is the difficulty to tune the algorithm such that fast dynamic response is obtained without affecting the steady state stability.

In Algeria, the most popular application of the photovoltaic energy is stand-alone water pumping system driven by electrical motors. Indeed, it is the best adopted energy resource to supply drinking and agricultural applications in remote regions which economically cannot benefit from the national grid connection [2]. In fact, much research has been studied to investigate the performance of solar water pumping systems (SWPS) in different countries. These countries are located in tropical regions of the earth and therefore strongly support the use of SWPS.

Many types of motors are available for use in SWPS. At early stage brushed DC motors were extensively used to drive water pumps [3, 4] and continue to be used [35, 48]. After that it has been turned out that the reliability of SWPS can be improved by using brushless DC motors [5] and switched reluctance motors [6]. For high power and/or when high reliability SWPS is required, AC induction motors seem to be the adequate alternative [51, 52] compared to the aforementioned motor types.

Background and scope of this thesis:

Several MPPT methods have been developed for either stand-alone or grid-connected PV systems .However, to the author best knowledge, there are few published papers treating the application of MPPTs for SWPS. Much focus has been on Perturb and Observe (P&O) and Incremental Conductance (IC) MPPT methods [10], [29]. These methods are known to be the perturbation MPPT techniques that share the same principle in which the value of the operating parameter, such as voltage, current or duty cycle is permanently varied with predefined step size to approach the MPP. This increasing or decreasing allows converging to the MPP. These techniques are robust but introduce oscillations around the MPP which results in energy waste.

New modified technique P&O have been developed using Fuzzy Logic (FL) in order improve the performance of the MPPT in terms of time response [55, 40]. In ref [55], a global efficiency improvement using FL is proposed. The fuzzy logic-based P&O developed in [29] has as first input the variation of the power with respect of the voltage and the second input is the variation of the first input. The output of this MPPT controller is the variation of the chopper duty cycle. The proposed FL based-MPPT shares the same principle as the classical P&O except that the step size of the chopper ratio or duty cycle which is variable due to the use of fuzzy rules. Artificial Neural Network (ANN) was used in [11] to truck the MPP of PV array supplying power to centrifugal pump being driven by a separately excited DC motor.

ANN-based MPPT, once trained, exhibits superior dynamic performance in comparison to PO and IC MPPTs. However, these performances are limited to training data and consequently great amount of training data is needed in case of PV systems where MPP depends on many parameters.

For AC machines, the multiphase motor drive is one of the most interesting and extensively discussed in literature. And it has become attention due to developments in numerous popular applications. Hence a pumping system based on an IM (Three phase or multi phase) can be an appealing proposal where reliability and maintenance are important. Water flow rate depends on head and speed of the IM. The speed can be controlled by many techniques by the inverter to the motor. So, the regulation includes the DC link voltage and the frequency of the inverter [12].

The main aims of this research work are:

1) The application of Golden Section Search-based MPPT algorithm in solar water pumping system. The proposed method will be compared with the conventional P&O in terms of 1) effectiveness in tracking the maximum power point under varying climate conditions, 2) simplicity and 3) dynamic tracking convergence. It will be taking into consideration the steady state energy waste as well. The latter is the result of perturbation process in conventional MPPT methods such as P&O algorithm.

2) A new framework of solar water pumping system (SWPS) using a Dual Star Induction motor (DSIM). This is the first attempt to apply DSIM with optimum speed control to such a system. The PV output maximum power is tracked using the conventional Perturb and Observe (P&O) algorithm. DSIM is driving centrifugal pump whose speed needs to be optimized to maximize the pump's hydraulic parameters. To achieve this goal the indirect rotor field oriented control scheme is adopted to overcome the motor's nonlinear coupling. Besides, instead of using the conventional PI speed controller, the paper suggests the use of fuzzy sets based – PI controller which shows better dynamic performances and robustness against system uncertainties.

Chapter I

Literature Review

I.1 Introduction

According to UN World Water Development Report published in 19 March, 2018, it is estimated that the global demand for water has been increased by a rate of about 1% per year over the past decades as a function of population growth, economic development and changing consumption patterns, and one billion do not have sufficient drinking water [13]. In this situation, water resources are essential for satisfying human needs, ensuring food production and protecting health, as well as for social and economic development [13, 14]. Water pumping has throughout history been a technical challenge. There has been always a need to supply drinking water and satisfy regular agricultural demands throughout the development of civilization in human societies [15]. Now, it is a necessary need to supply sustainable energy for the provision of potable water at lower financial and environmental cost, especially domestic, livestock and irrigation water supplies in remote areas. Remote water pumping system is a first solution for satisfying need the future. It is also be proprietary of the purification and desalination plants to produce drinking water.

Water pumping worldwide is generally dependent on electricity or diesel generated electricity. The diesel is expensive and not available in countryside of many developing countries and even when the fuel is available in the country, transporting it to remote areas is not an easy task. This is because there are no roads or supporting infrastructure in most of the remote villages [15]. The electricity must be economic and takes minimum maintenance when this power is available from the nearby grid. In rural areas, the installation of a new transmission line and transformers is extremely expensive for irrigation or drinking water. Solar water pumping systems minimizes this great dependence of diesel and lines of transmission. Besides, they are environmental friendly and require low maintenance with no fuel cost [16]. Photovoltaic pumping is one of the most promising applications of solar energy; the technology is similar to any other conventional water pumping system except that the power source is solar energy [17].Table I.1 shows the comparisons of different stand-alone type water pumping systems.

In recent years, due to non availability of electricity and increase in diesel prices, solar pumping has become a wide scope to utilize for water supplies in rural, community, urban, industry and educational institutions. However, it is estimated that the PV electricity will contribute with 7% of the world electricity needs by the years 2030, and this will increase to reach 25% by the year 2050 [19].

Table I.1 Comparison between water pumping systems powered by PV and diesel generator [18]

System type	Advantages	Disadvantages
PV system	➢ Clean energy ➢ Easy to install and movable technology ➢ low maintenance ➢ Reliable long life ➢ Unattended operation ➢ No fuel no fumes ➢ Low environmental pollution ➢ Low life cycle cost in remote areas ➢ Does not require frequent site visits	➢ Relatively high initial cost ➢ Low output in shading
Diesel system	➢ Easy to install ➢ Can be portable ➢ Extensive experience available ➢ Rapid installation and movable technology ➢ Linear and control operation and does not depend on the weather condition	➢ Noise, fume, dirt problems ➢ Needs high maintenance and replacement ➢ Site visits necessary ➢ Fuel often expensive ➢ High environmental pollution

Internationally, many studies have shown that the main rural application areas are located in Africa, Asia and Latin-American. In are areas, there are available wells along with plenty of uninterrupted sunshine favoring solar PV water pumping [20].

Solar water pumping systems (SWPS) are composed of different components, which can be classified as mechanical, electrical and electronic components. These components have different constructions, working and performance characteristics. In general, SWPS poses difficulty in operation and leads to overall poor performance [21]. This has motivated

researchers around the world from all fields of engineering to investigate this topic. Mainly, objective of these investigations is to make SWPS a cost effective solution and more efficient compared to conventional water pumping systems.

I.2 Configuration and classification of SWPS

SWPSs are based on PV technology that converts sunlight into electricity to drive the pump. The PV panels are connected in series and parallel to drive a motor (DC or AC) which converts electrical energy supplied by the PV array into mechanical energy [17]. In general, the SWPS consists, more or less, of the following components [18]:

1) PV array,
2) Charge controller,
3) pump controller,
4) Batteries,
5) inverter,
6) Motor – Pump,
7) Storage tank.

Different classifications of SWPS which depend on the available components are listed as follows [22]:

a. SWPS based on energy storage

Based on the storage components, SWPS can have different configurations such as: with water tank, with battery and without any storage. The simplest configuration is direct connected SWPS. The latter system consists of a PV array directly connected to pump without using battery storage or water tank. This type is relatively simple and low cost and is used for small applications. The second configuration includes battery storage as backup during the night [22]. In addition, batteries are able to satisfy transient surges of current that are much higher than the instantaneous directly obtainable from a PV panel [23]. To avoid battery, water tank can be used and allows satisfying maximum water demand. The topology of this system is presented in Figure 1.1.

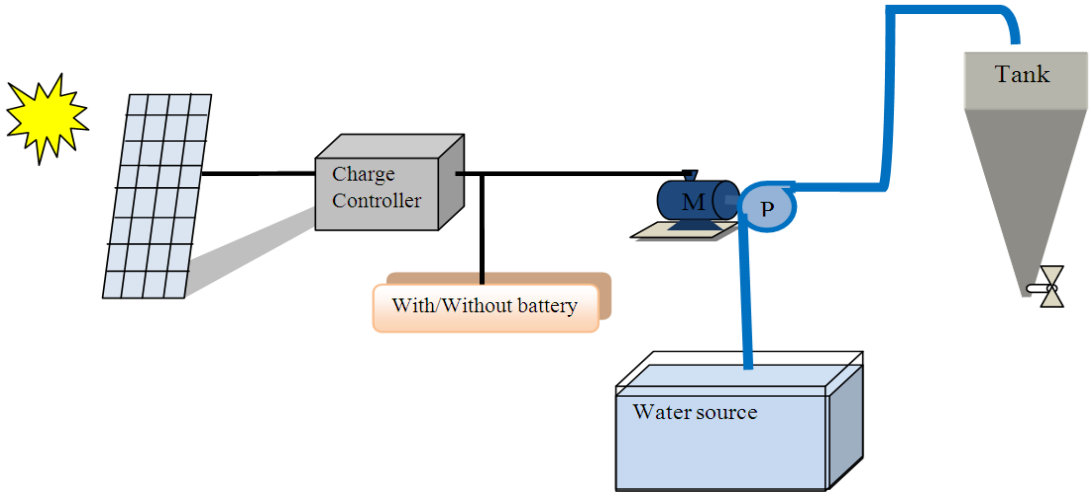

Figure 1.1 PV water pumping system with/ without battery

b. SWPS based on form electric power input [18]

The performance of the solar interface system depends on load operating condition. This can be connected with DC pump motor or AC pump motor by an inverter. The DC motor driven pump is of two types; DC motor with brushes and brushless DC motor (BLDC). For standard DC driven pumps, brushes of the commutator must be periodically changed to ensure good operation of the motor - pump. This increases maintenance cost of the whole system. Brushless DC motor is a self synchronous machine with an electronic commutator. Permanent brushless DC motor (PMBLDC) has become popular choice in SWPS due to high efficiency, silent operation, high reliability, and low maintenance requirement. The SWPS with DC motor is shown in Figure 1.2.

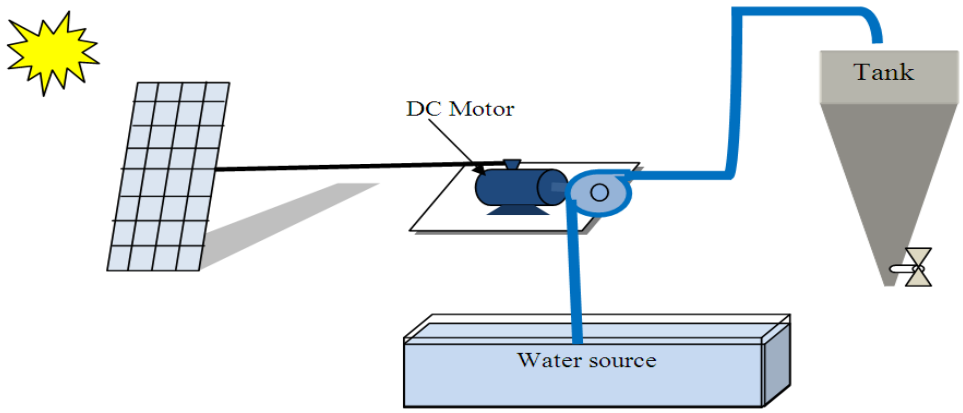

Figure 1.2 Direct coupled DC/ PV water pumping system

AC water pumping system consists of an AC motor driven pump where a suitable inverter is required to convert DC to AC electrical power (Figure 1.3). The advantage of the AC SWPS is that it can run during all the day. Besides, it offers the possibility of grid connection when sunshine is not available particularly during night. The AC SWPS has many attractive features such as reliable and maintenance free and provide more possibilities for control strategies in comparison to DC motors [24].

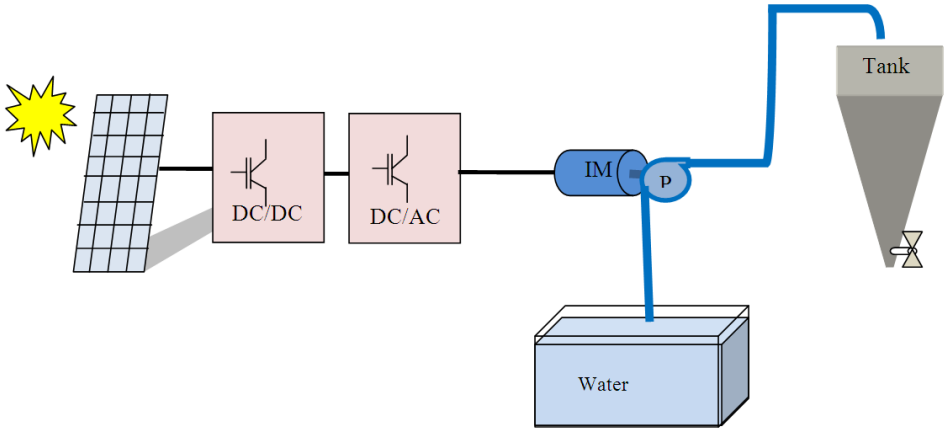

Figure 1.3 Direct coupled AC/ PV water pumping system

c. SWPS based on type of pump [18]

The pumps are rated per voltage supplied and require sometimes accessories like filters, switches and float valves, to function optimally. Different configurations of SWPS are available according to the type of pump being used

1. submersible pumps draws water from deep well(Figure 1.4)
2. Surface pump draws water from shallow wells, tanks, rivers(Figure 1.5)
3. Floating water pumps draws water from tanks with adjusting height ability (Figure1.6)

In general, pumps can be organized in two categories based on operating principal:

1. Dynamic pumps operate by developing a high liquid velocity and pressure in a diffusing flow passage like centrifugal pumps and axial flow pumps.
2. Positive displacement pumps operate by forcing a fixed volume of fluid from the inlet pressure section of the pump into the discharge zone of the pump like screw pump and piston pump.

The performance of PV water pump manly depends on the flow rate which is influenced by:

- ✓ Solar radiation availability at the local,
- ✓ Total dynamic head,
- ✓ Flow rate of water,
- ✓ Total quantity of water requirement.

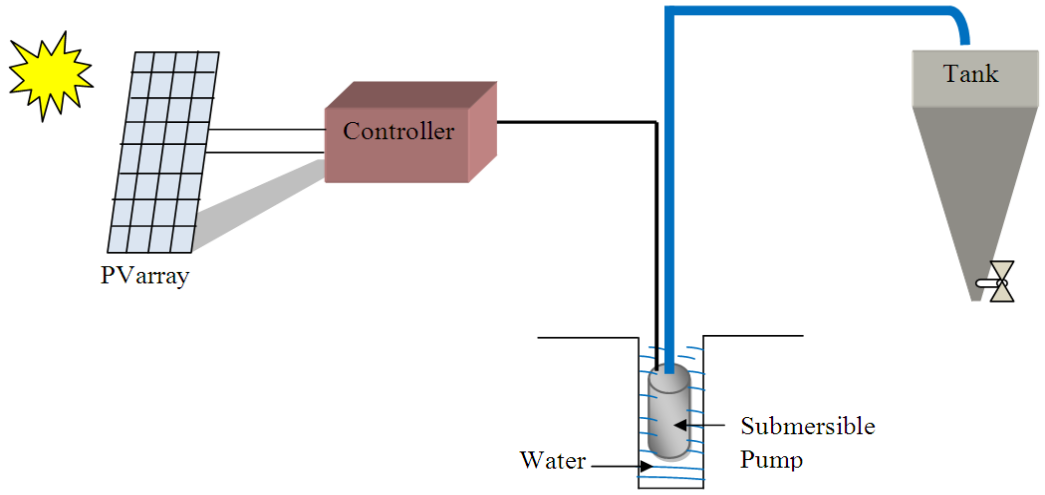

Figure 1.4 a solar water pumping system with submersible pump

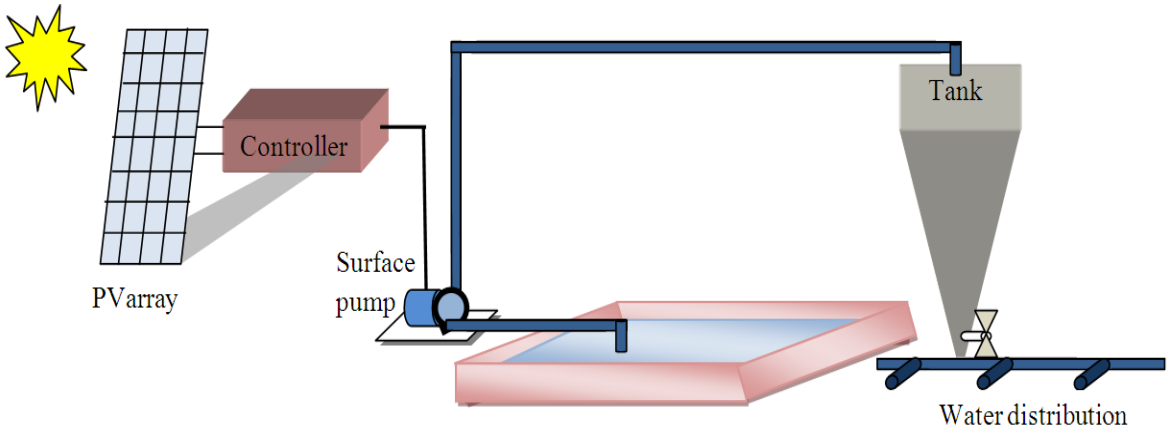

Figure 1.5 a solar water pumping system with surface pump

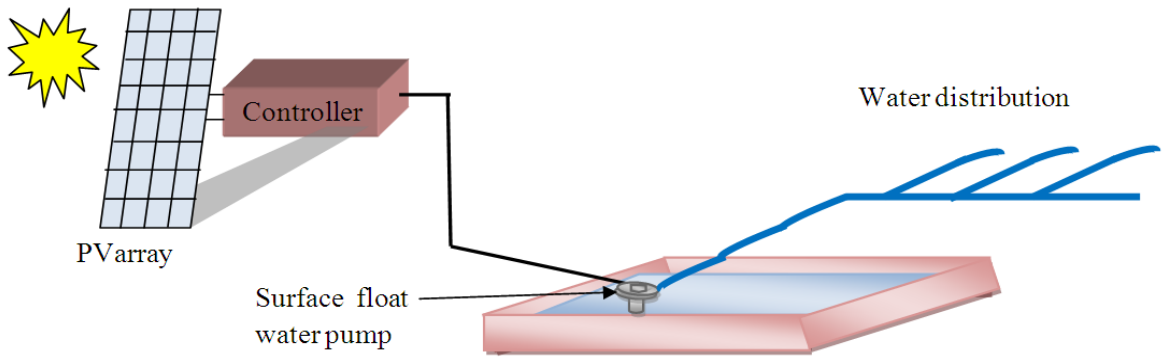

Figure 1.6 Solar water pumping system with surface floating water pump

I.3 Summary of related research

The low PV module conversion efficiency is another factor that restricts the usage of PV systems, therefore a power converter is always embedded into the motor pump with capability of maximum power tracking (MPPT) controller integrated with the PV systems too. This latter is essential to improve the system efficiency. In this section, a comprehensive analysis of the available MPPT algorithms and different types of motors being used in SWPS are reviewed to provide state of art regarding this topic.

Several MPPT methods have been developed for either stand-alone or grid-connected PV systems [25, 26]. However, to our best knowledge, there are few published papers treating the application of MPPTs for SWPS using either DC or AC motors [27].

Akihiro *et al.* [28] investigated the application of two algorithms IncCond and P&O. They analyzed and simulated the performance of directly coupled pump with the PV array in terms of total energy extracted and water flow pumped along the day. They reported that with MPPT the efficiency of the system can be increased by 35% and could utilize more than 99% of PV capacity. A comparison between the direct duty cycle perturbation and the reference voltage perturbation algorithms was reported in [29] under different weather conditions. They found that the direct duty cycle perturbation has a slower response than that of the reference voltage perturbation when climatic conditions are changing rapidly. Furthermore, it has been observed that the direct duty cycle perturbation algorithm offers higher energy utilization efficiency than the reference voltage perturbation algorithm for both rapidly and slowy changing of irradiance.

Katan *et al.* [30] studied the performance of SWPS using helical rotor pump and sun tracker with MPPT; the system has been analyzed while the head is fixed and a sun tracker is

included to get more sunlight. Obtained results showed that overall efficiency could be increased by 36% with respect to the amount of solar energy received by the PV arrays. Mahmoudi *et al.* [31] designed a controller to get a matching between the pump's operating point and the PV generator output for given solar irradiation. They proposed control system increased the quantity of the pumped water by 4.7%. Andoulssi *et al.* [32] proposed a tracking maximum power point (MPP) by using a non-linear control strategy based on feedback linearization and this control is currently under experimental stage. A comparative study between perturb and observ method (P&O), fuzzy logic controller (FLC) and Neuro-fuzzy (NF) technique of MPPT was discussed in [33] under ambient condition using Matlab/Simulink. It has been found that the application of NF algorithm in MPPT increased the daily pumped water quantity and the pumping time. ANN controller is developed in [34] to adjust the duty cycle of the buck-boost converter according to the solar irradiation so that optimal operating point is reached. Mazouz *et al.* [35] used a fuzzy controller to choose the appropriate duty cycle of DC/DC converter to enable the system tracking the maximum power point. Caton [36] utilized a commercial MPPT to match between PV modules and motor-pump system. A fuzzy logic-incremental conductance technique for operating at MPP was proposed in [37] and a DTC strategy is used to drive the motor of SWPS. The IncCond-MPPT technique with V/f method was proposed in [38] to control and seeking the maximum power point of PV panel. Eskander *et al.* [39] used two control methods; the first one allows is the PV array to operate at maximum efficiency with variable flow rate, whereas the second is allows the induction motor to operates at its maximum efficiency but with limited flow rate. The fuzzy logic-based P&O developed in [40] has a first input the variation of the power with respect of the voltage and the second input is the variation of the first input. The output of this MPPT controller is the variation of the chopper duty cycle. The proposed FL based-MPPT shares the same principle as the classical P&O except that the step size of the chopper ratio or duty cycle which is variable due to the use of fuzzy rules. FL-based IC has been proposed in [41] to overcome the main drawback of the classical IC being the difficulty to approximate the identifier factor (*dP/dV*) at zero and near zero voltage deviations. However, the implementation of fuzzy controller with 25 rules is much more complex than that of the P&O and IC. Artificial Neural Network (ANN) that was used in [42] to truck the MPP of the PV array is intended to supply maximum power to centrifugal pump being driven by a separately excited DC motor. ANN-based MPPT, once trained, exhibits superior dynamic performance in comparison to PO and IC MPPTs. However, these performances are limited to training data

and consequently huge training data is needed in case of PV systems where MPP depends on many parameters, load, irradiance, and temperature.

In such applications, high efficiency and reliability are required. Many types of motors are available for use in SWPS. Lawrance *et al.* [43] used a brushless DC motor for driving pump with PV array for livestock watering and it investigated the performance of this system in different applications of irrigation. In [44], Hans *et al.* studied a permanent magnet brushless (PMBL) DC motor system where they reduced the system cost by driving the system with PMBLDC and found that the efficiency is better at low value of climatic condition. Chandrasekaran *et al.* [45] discussed the performance of solar photovoltaic pumping system with permanent magnet DC motor and conventional DC motor. The outcome of this research paper is that using the latter motor, the overall was less efficient than with the permanent magnet DC motor. Singh *et al.* [46] analyzed the dynamic performance of the permanent magnet brushless DC motor by a PV array source coupled to a pump, the results are the following: the system was easy to maintain and simple in construction which reduced the cost of the drive significantly. Kolhol *et al.* [47] investigated the showing of permanent magnet DC motor for different climatic conditions; they investigated the effects on the system due to variation in cell temperature and solar irradiation. The performance of solar water pumping system using induction motor for the desert is performed by and simulated by Daud and Mahmoud in [48]. They showed that when using induction motor, the overall efficiency of the system can increase to more than 3%. In [49], Zaki *et al.* studied and analyzed two different drive systems for the maximum power extracted with the PV array, especially conventional DC motor and IM which were used to drive a pump. They reported that more mechanical power using IM is possible by drawing more power from PV generator and hence more efficiency compared to the DC motor. Hens [50] tested two systems types using brushless DC motor and conventional asynchronous AC motor. He concluded that the latter system was inferior and less efficient than the system with brushless DC motor. Chenni *et al.* [51] analyzed the dynamic performances of asynchronous motor and permanent magnet synchronous motor. Both have shown good transient and steady state performance. Hamidat [52] used asynchronous motor directly coupled with a pump under different irradiations and tested three configurations of PV array for different heads. He found that suitable to fulfill drinking water demand irrigation water requirement with small configuration of PV array in Sahara region. Authors in [53] studied tow control schemes to improve the efficiency of SWPS. The first control scheme employs the InCond as MPPT technique which feeds a

proportional integral (PI) controller by the estimated PV voltage at MPP. On the other hand, the second control scheme employs the direct torque control (DTC) to maintain the flux level and control the torque of the induction motor. As a result, it has been found that the DTC based control scheme offers a rapid response without overshoot and less steady state oscillations for variable climate conditions.

Various strategies used in literature for improving efficiency of PV water pumping systems. Odeh *et al.* [54] studied and simulated SWPS using AC motor with real field data obtained from a system installed in Jordan. They improved water output volume with the increasing PV modules size and decrease PV efficiency. Benlarbi *et al.* [55] developed and maximized the global efficiency of SWPS, which in turn, maximized the water output rate by using a fuzzy logic controller. The SWPS consisted of pump driven by a separately excited DC motor, a PMSM and an IM. The optimization parameter was the drive speed of the motor.

Using an optimization technique for SWPS consisting of mono-cellular centrifugal pump driven by IM is proposed in [56]. This technique achieved a good performance of SWPS that is improving the motor efficiency by minimizing the non-linear criterion and also improved the efficiency of the pump hence flow rate by varying the motor speed.

I.4 Conclusion

In this chapter, different configurations of water pumping have been discussed which electric motor system. It has been shown also the importance of SWPS particularly in remote areas or the desert. These regions are characterized by harsh climate conditions while electricity is not available. SWPS is the appropriate solution in such regions and as many schemes are also available particularly with respect to the motor being used, different related research papers have been listed and analyzed to guide us well settling down the problematic. From the point of reliability point view, induction motor and particularly the squirrel one outperforms most of the motors available in the market. Even from the cost point of view, the motor offers best price. When used to drive the water pump and supplied from a PV array, the DC motor performs better as it is naturally decoupled and hence speed control becomes easier than in squirrel cage induction motors. With the decrease of power electronics power switches and processors, variable speed drive using induction motor has gained more attention including solar water pumping systems. So far, and in the light of reviewed research, most of

the induction motor based SWPS use either P&O or InCond MPPT techniques. In the present thesis, two topics will be investigated:

1. Replacing the conventional induction motor by a double star induction motor while classical P&O MPPT is employed for maximum power harvesting from the PV generator
2. And, employing a new maximum power point while classical induction motor will be used for driving the pump. A comparison with classical P&O will be used to evaluate the performance of the proposed MPPT algorithm.

Chapter II

Photovoltaic generator modeling

II.1 Introduction

Energy has great importance for our life and economy. Fossil fuels consumption has been increased with augmenting of energy demand due to the industrial revolution and population growth. Besides, an increase in the price of all sort of energy has been observed. This huge demand and used on has increased substantially the carbon dioxide emissions. Now, it is really global challenge to research for alternative and renewable energy resources in order to vouch for protection of environment and sustainable development [57].

Among the available renewable energy sources, solar energy is the promising one for the country. It is a free, inexhaustible and non-polluting source of sustainable and renewable energy. The energy the earth receives from the sun is so enormous and so lasting that the total energy consumed annually by the entire world is supplied in as short a time as a half hour. On a clear day the sun's radiation on the earth can be 1kilowtts per square meters depending on the location [58]. It is expected to play a central role in meeting the increasing demand of electricity and therefore limiting the use of fossil resources. Furthermore, it is expected to be used in different industrial applications where some economic constraints must be satisfied, particularly in remote areas. The design and implementation of solar PV systems are necessary and currently facing challenges in terms of efficiency and reliability [59, 60].

The use of solar cells as an electrical energy source has many advantages and among which the flowing are listed [61, 57, and 62]:

- Sustainable and renewable energy,
- Little maintenance and maximum reliability for long periods,
- Non-polluting with no detectable emissions or odors,
- No fossil fuels consume,
- Ease of extension and installation,
- Withstand severe weather conditions including snow and ice.

II.2 PV CELLs

Scientific investigation on photovoltaic effect started in 1839, when the French physicist, Edmund Becquerel discovered that an electric current could be reduced by shining a light into certain chemical solutions and it was not economic until the late 1940's with the development of solid material. The first generation of semiconductor silicon-based PV cell which converted 6% of sunlight falling onto it into electricity developed by Chapin, Pearson in 1954. And Fuller patent in 1957 for the 8% efficient Silicon solar cell. This generation of cells was used in the spacecraft Vanguard 1 in1958 [63].

Unfortunately, solar cells are still far too expensive to produce a significant fraction of the world energy needs. However, the cost of PV cells per watt of peak output has decreased dramatically since the 1970's. The commercially available silicon solar cells have efficiencies of about 10-18%. Silicon solar cells are made using single crystal wafers, polycrystalline wafers or thin films [64]. Today, the cost of PV cells is essential for the technology to further extend its use especially among utilities.

Solar cell uses semiconductor materials to convert sunlight into electricity. When these materials are exposed to light, it will absorb the photons that have a higher energy than the band gap energy of the semiconductor materials. This absorption of a photon knocks the electron free from their atom, allowing this electron to flow through the cell junction to produce electricity. This process of converting light energy (photons) to electricity (voltage) is called the photovoltaic effect Figure 2.1.

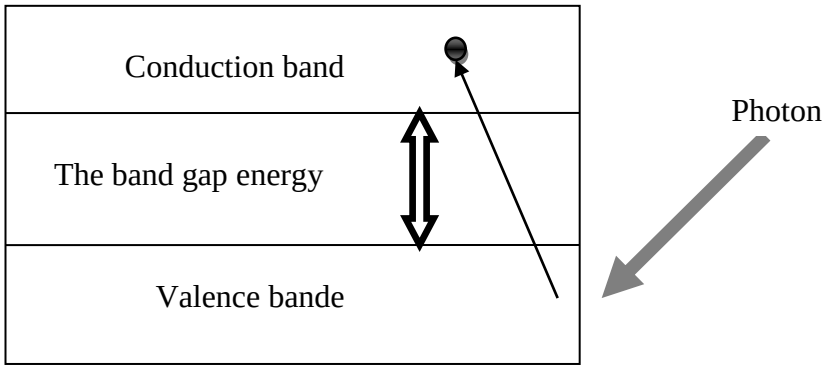

Figure 2.1The semiconductor of converting light energy

The operation of a solar cell can be represented by a simple p-n junction diode where the electrons flow from the n layer side to the p layer side of the photovoltaic cell via an

external wired connection. A schematic diagram of the p-n junction is depicted in Figure 2.2 [65]

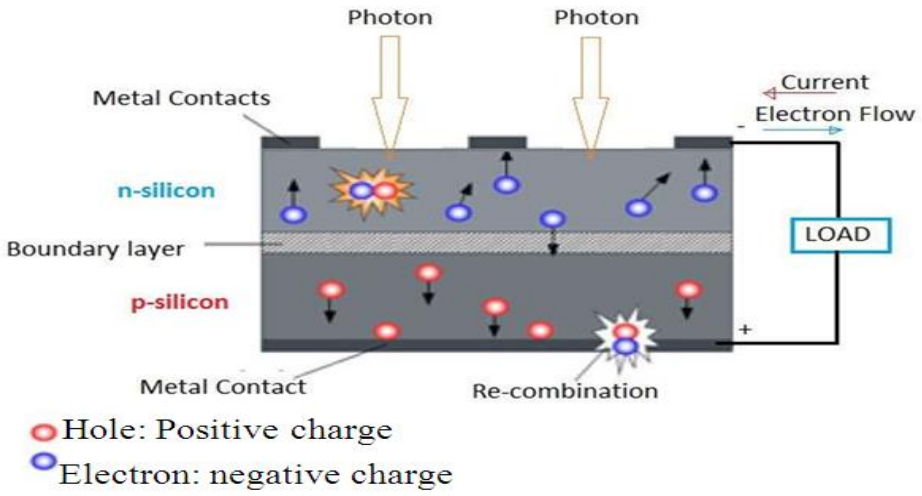

Figure 2.2 Solar cell principle

II.3 PV generator

Under standard test conditions (1000W/m^2, 25^{0}C), the maximum power delivered by silicon cell of 150cm^2 is about 2.3Wc with a voltage 0.5V. An elementary photovoltaic cell therefore constitutes a low power generator that is insufficient as such for most domestic or industrial applications.

In general, the module comprises group of cells connected in series and parallel to supply the desired output power and voltage as depicted in Figure 2.3. Generator or arrays are made up of some combination of series and parallel modules to increase power.

The connection of cells in series will directly multiply the voltage handling capability of the system and connection in parallel will directly multiply current production.

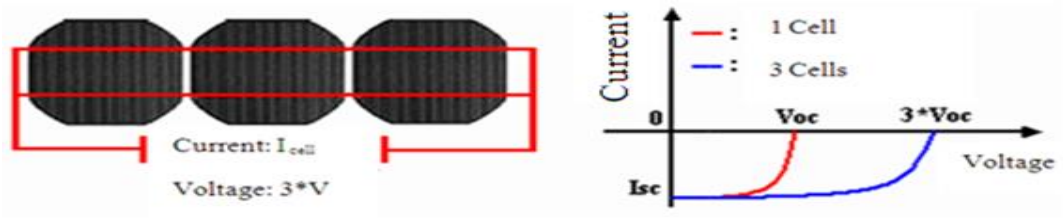

(a)

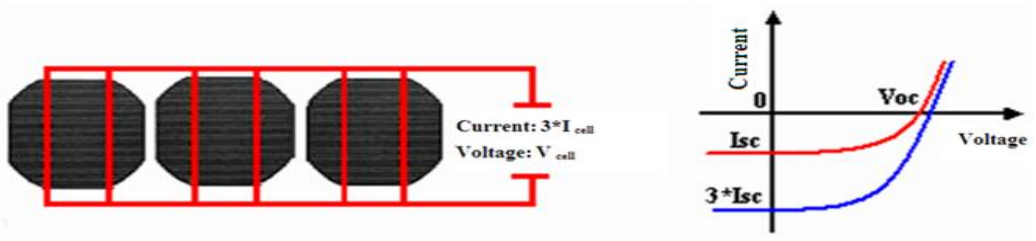

(b)

Figure 2.3 Series (a) and parallel (b) connection of identical cells

II.4 PV cell model

The strategy of modeling a PV module is not different from modeling a PV cell. The ideal solar cell, theoretically, can be modeled as a current source with a diode in anti-parallel (Figure 2.4). The direct current, generated when the cell is exposed to light, varies linearly with solar radiation.

The model includes a current source I_{ph}, one diode and series resistance R_s that represents the resistance inside each cell and in connection between cells. R_p is a loss associated with a small leakage of current through a resistive path in parallel with the intrinsic device. Its effect is much less conspicuous in a PV module compared to series resistance's one, and it will only become noticeable when a number of PV modules are connected in parallel for larger system. The net current I is the difference between the photocurrent I_{ph} and the both of parallel resistance current I_p and the normal diode current I_d [66].

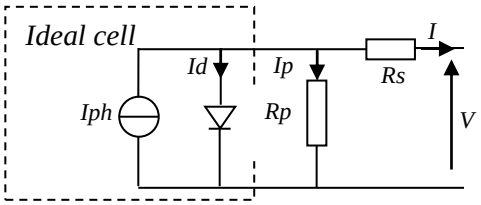

Figure 2.4 Equivalent circuit of PV cell

Application of KVL to the circuit of Figure 2.4 results in the characteristic equation of the photovoltaic cell [18]

$$I_{Ph}=I_D+I+I_{R_P} \quad \text{(II.1)}$$

In this single diode model, I_D is modeled using the Shockley equation for an ideal diode:

$$I_D=I_s[e^{\frac{(v+IR_S)}{nV_t}}-1] \quad \text{(II.2)}$$

Where Vt is the array thermal voltage given by

$$V_t=\frac{KT}{q} \quad \text{(II.3)}$$

The I_s is the saturation current:

$$I_s=K_1T^3e^{-\frac{E_g}{KT}} \quad \text{(II.4)}$$

Writing the parallel current as

$$I_{R_P}=\frac{V+IR_S}{R_P} \quad \text{(II.5)}$$

Where:

n:is the diode ideality factor

*k:*is the Boltzmann's constant(1.381×10^{-23}J/k)

*K_1:*is a constant ($1.2A/cm^2K^3$)

*T:*is the cell temperature in Kelvin(*K*).

q: is the electron charge(1.602×10^{-19}C)

Eg: is the gap energy (1.12 eV for Crystalline-Silicon)

The equation of the PV cell can be represented with I(V) characteristic as:

$$I=I_{ph}-I_s[e^{\frac{(V+IR_S)}{nV_t}}-1]-\frac{V+IR_S}{R_P} \quad \text{(II.6)}$$

Where: I is the output current from the cell, V is the voltage across the PV cell

II.5 Identification of PV Model parameters

For simplicity, in this thesis the single diode, known as the five parameter model {I_{ph}, I_s, n, R_s, R_p}, is as a model for the identification of photovoltaic cell parameters. A simplified considers the value of the parallel resistance (R_s<<< R_p) is high enough that it can be neglected. However, the equation whose parameters need to be identified is (II.7). The aforementioned unknown parameters can be determined as follows [67] [68].

$$I=I_{sc}-I_s[e^{\frac{(V+IR_S)}{nV_t}}-1] \quad \text{(II.7)}$$

Then the photo-induced current is calculated straightforwardly, because it is significantly higher than the diode current, so that it is assumed to be equal to the short-circuit current in STC:

$$I_{ph} \approx I_{sc} \tag{II.8}$$

In the open-circuit condition, starts by applying (II.6)

$$0 = I_{ph} - I_{sr}[e^{\frac{V_{oc}/ns}{nV_{Tref}}}-1] \approx I_{sc} - I_{sr}[e^{\frac{V_{oc}}{nV_{Tref}}}] \tag{II.9}$$

Consequently, it is

$$V_{OC}=nV_T\ln(1+\frac{I_{sC}}{I_s}) \tag{II.10}$$

When Isc >>I_s, it is possible V_{oc} writing with:

$$V_{OC}=nV_T\ln(\frac{I_{sC}}{I_s}) \tag{II.11}$$

The diode ideality factor is calculated by means of (II.12)

$$n = \frac{\alpha_v - \left(\frac{V_{oc,stc}}{T_{stc}}\right)}{n_s.V_{stc}\left\{\frac{\alpha_i}{I_{ph,stc}} - \frac{3}{T_{stc}} - \frac{E_{gap}}{k.T_{stc}^2}\right\}} \tag{II.12}$$

Where:

α_v: Open circuit voltage/temperature coefficient

α_i: Short circuit current/temperature coefficient

In order to calculate I_{sr}, the open circuit conditions can be used as well, that from (II.9) it is

$$I_{sr} \approx I_{scr}/[e^{\frac{V_{Oc}}{nV_{Tref}}}] \tag{II.13}$$

The series resistance can be calculated by [69]:

$$R_s = \frac{n_s.n.V_{t,stc}.Ln\left\{1-\frac{I_{mpp,stc}}{I_{ph,stc}}\right\} + V_{oc,stc} - V_{mpp,stc}}{I_{mpp,stc}} \tag{II.14}$$

The equation (II.8),(II.12), (II.13) and (II.14) allow calculation of the values of the unknown parameters in (II.7) starting from the data sheet of panel {V_{oc}, I_{sc}, α_i, α_v,V_{mpp},I_{mpp}}in the STC available in the PV panel data sheet provided by the manufacturers.

Solving equation (II.7) using the parameters of the panel being derived from the datasheet at STC. It may be possible to find the answer by simple iterations, the Newton's method is chosen for rapid convergence of the answer [70].

It is possible to rewrite (II.7):

$$f(I)=I_{sc}-I-I_s[e^{\frac{(V+IR_S)}{nV_T}}-1] \quad \text{(II.15)}$$

The Newton's method is described as:

$$x_{n+1}=x_n-\frac{f(x_n)}{f'(x_n)} \quad \text{(II.16)}$$

Where:

$f'(x_n)$: is the derivative of the function

x_n : is a present value

x_{n+1}: is a next value

Rewriting the equation (II.15)

$$I_{n+1}=I_n-\frac{I_{cc}-I_n-I_s[e^{\left(\frac{V+R_S.I}{nV_T}\right)}-1]}{-1-I_s\left(\frac{R_S}{nV_T}\right).[e^{\left(\frac{V+I_n.R_S}{nV_T}\right)}]} \quad \text{(II.17)}$$

The established equations are valid only under operating conditions (STC). To generalize modeling for different irradiance and temperature, we use the model that moves the reference curve to new locations.

For operation under environmental conditions, the equations for short circuit current and the saturation current can be written as [71]:

$$I_{sc}(G,T)=I_{scr}\frac{G}{1000}[1+\alpha i(T-T_{ref})] \quad \text{(II.18)}$$

Where:

- I_{scr} at T_{ref} is given in datasheet (measured under irradiance of 1000W/m^2)
- α_i is the temperature coefficient of I_{sc} in per cent change per degree temperature also given in the datasheet.
- T_{ref} is the reference temperature of PV cell in Kelvin (K), usually 298K (25^{0}C)

$$I_s(T) = I_{sr}(T_{ref}) \left(\frac{T}{T_{ref}}\right)^{\frac{3}{n}} e^{\left(\frac{-qE_g}{nk}\right)\left(\frac{1}{T}-\frac{1}{T_{ref}}\right)} \quad \text{(II.19)}$$

The power is the product of the voltage and the current in a DC electrical circuit. The power is described by the following mathematical equation:

$$P = VI \quad \text{(II.20)}$$

Theoretical maximum power is maximum current in photovoltaic cell being generated when the cell is short circuited times the maximum voltage denoted V_{oc} being the one measured across the cell without load. Under the latter condition, no current flows in the circuit because it is open.

In practical, at the maximum power point, both the voltage and current are maximized to provide the largest amount of power from the PV module (Figure 2.5). V_{mp} is the voltage value at P_{max} and I_{mp} is the current value at P_{max}:

$$P_{max} = V_{pmax} \; I_{pmax} \quad \text{(II.21)}$$

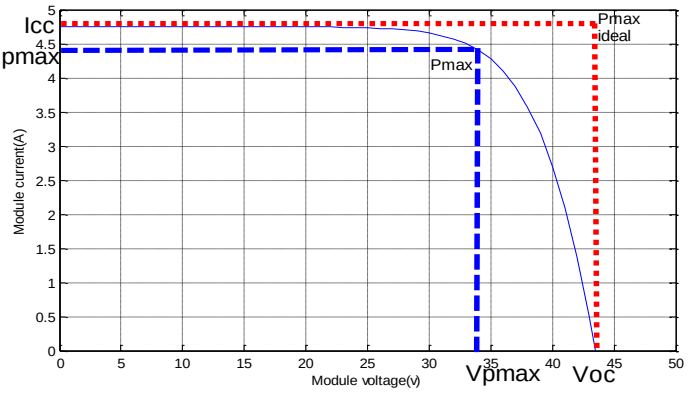

Figure 2.5 Power ideal and practical

The efficiency of the module is calculated by [72]:

$$\eta = \frac{P_{max}}{P_{in}} \quad \text{(II.22)}$$

Where

P_{int} is the power in incident spectrum.

Another important characteristic of module is the fill factor, which indicates an important role when comparing the performance of different photovoltaic module. A high fill factor is equal to a high quality module which has low internal losses.

$$FF = \frac{V_{pmax} I_{pmax}}{V_{oc} I_{sc}} \quad \text{(II.23)}$$

II.6 Photovoltaic Module

In a typical PV system, the modules are configured in a series-parallel structure to obtain large power generation or high voltage being suitable for grid connection. Figure 2.6 shows a module of several PV cells which are electrically connected in series and parallel.

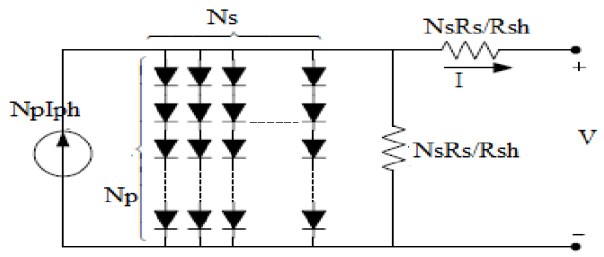

Figure 2.6 Equivalent circuit of series and parallel connected PV cells

Given that in a series connection voltages sum and in a parallel connection currents sum the following relation for [73]:

$$\begin{cases} I_M = n_p I \\ I_{ccM} = n_p I_{cc} \\ V_M = n_S V \\ V_{ocM} = n_s V_{oc} \\ I_{sM} = n_p I_s \end{cases} \quad \text{(II.24)}$$

Where:

M: index to the module

n_s: number of cells connected in series

n_p: number of cells connected in parallel

Remembering that and substituting these into equation (II.7) results in:

$$I_M = I_{ccM} - I_{sM}\left[e^{\frac{(V_M + I_M R_{sM})}{n_S n V_T}} - 1 \right] \quad \text{(II.25)}$$

In short circuit at ($T=T_{ref}$), equation (II.25) can be writing for the current I_{srM} as follows:

$$I_{srM} = \frac{I_{ccrM}}{\left[\, e^{\frac{(V_{coM})}{nn_sV_{tref}}} - 1 \,\right]} \qquad \text{(II.26)}$$

With

$R_{sM}=(n_s/n_p)R_s$: is series resistance of module.

I_{srM}: is the reference saturation current of Module

I_{ccrM}:is the reference short circuit of module

II.7 Photovoltaic Array

The array connection refers to the number of solar modules connected in series to form a string and the number of parallel strings used to form the array Figure (2.7).The short circuit of the array under given environmental conditions is calculated by (II.27)

$$I_{scM}(G,T) = I_{scrM}\frac{G}{1000}[1 + \alpha i(T - T_{ref})] \qquad \text{(II.27)}$$

The diode current which is function of the saturation current given by the following equation:

$$I_{sM}(T) = I_{srM}(T_{ref})\left(\frac{T}{T_{ref}}\right)^{\frac{3}{n}} e^{\left(\frac{-qE_g}{nk}\right)\left(\frac{1}{T}-\frac{1}{T_{ref}}\right)} \qquad \text{(II.28)}$$

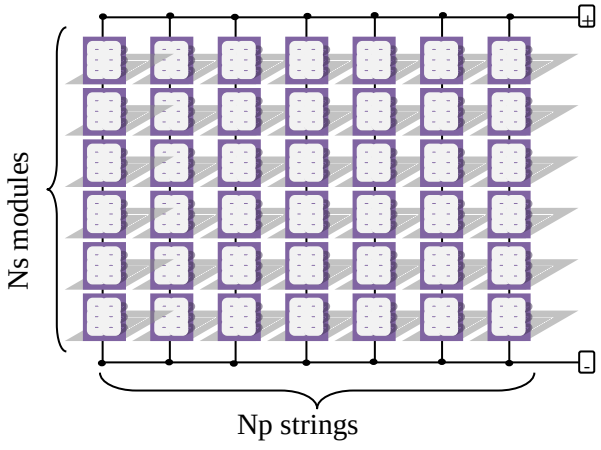

Figure 2.7 Configuration of the PV array

II.8 MATLAB simulation of PV module

For this project, the Bp SX150S module, which contains 72cells, has been chosen, its STC parameters are shown in Table II.1.

Table II.1 PV module parameters at STC

Parameters	Value
Maximum Power (P_{max})	150W
Voltage at Pmax (V_{mpp})	34.5V
Current at Pmax (I_{mpp})	4.35A
Open-circuit voltage (V_{oc})	43.5V
Short-circuit current (I_{sc})	4.75A
Temperature coefficient of V_{oc}	-160 ± 20 mV/ ºC
Temperature coefficient of I_{sc}	0.065 ± 0.015 %/ ºC
Temperature coefficient of power	-0.5 ± 0.05 %/ ºC
Number of cells	72

Results of computation of model parameters of this module based on datasheet values are shown in Table II.2.

Table II.2 Model parameters of BP SX 150s module

Parameters	Value
I_{ph}	4.75 A
Rs	0.6279Ω
I_0	2.3539e-006 A
n	1.3696

The electrical characteristic of the module is always described by two factors, the short circuit current I_{sc} and the open circuit voltage V_{oc}. The I_{sc} is the point where the curve intersects with vertical axis and it is the maximum possible current in the circuit and it is expressed in Amps. V_{oc} is the point where the curve intersects with the horizontal axis and represented the maximum output voltage from the circuit.

The power drawn by the photovoltaic module at any point along the curve $I(V)$ is expressed in watts.

Figure 2.8 shows an I-V curve of a solar module with three points commonly provided on specification sheets.

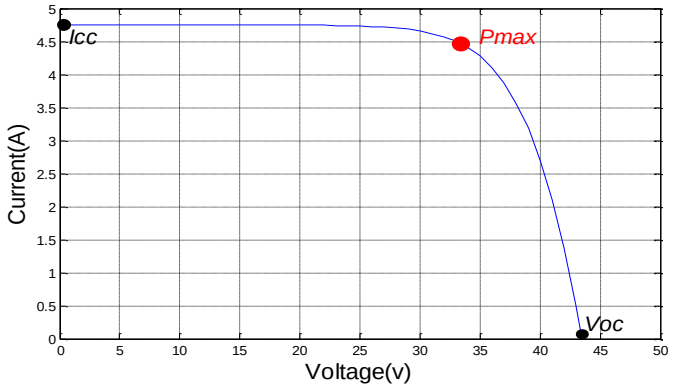

Figure 2.8 I-V characteristic of the PV module

While the module can operate according to this curve, it is most efficient when operating at the maximum power point, labeled P_{max} . This is the point on the curve where the product of the operating voltage and current is the highest.

II.8.1 Effect of temperature and irradiation

The goal of this section is to validate the PV model, described in this chapter. It is shown how the model simulates the influence of irradiation and of temperature on the PV module. These two parameters are dependent on the geographical area of installation and the different year's seasons.

II.8.1.1 Effect of irradiation

The MATLAB simulation of the PV module is used to perform a simulation of the PV module for different values of irradiation, Figure 2.9-2.10 illustrate how the I-V and P-V curves of the PV module are affected by irradiation, when the temperature is kept constant at 25^0C.

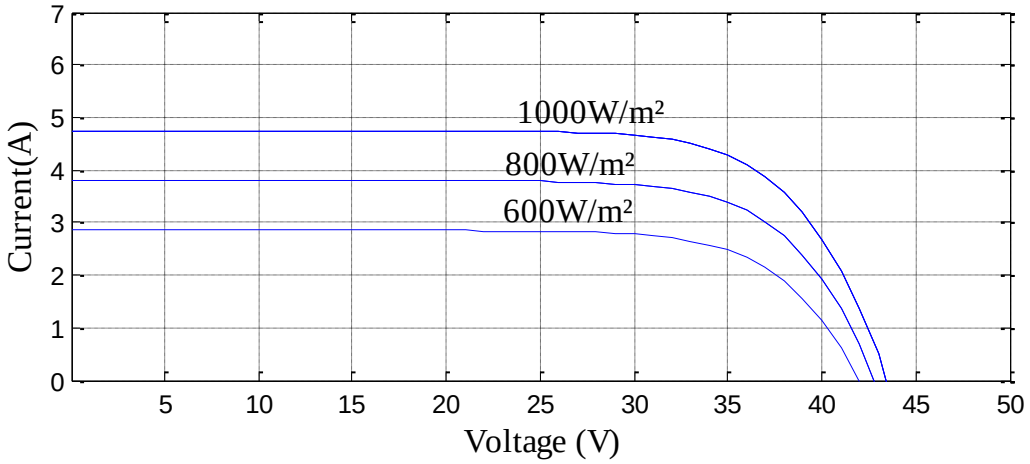

Figure 2.9 I-V curves at various sun radiations

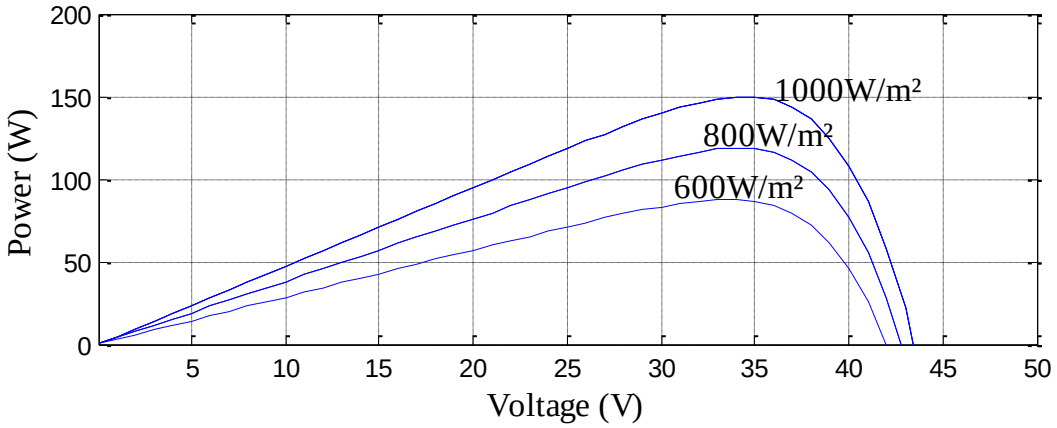

Figure 2.10 P-V curves at various sun radiations

It can be observed from both figures, the output power is directly proportional to the irradiation. A smaller irradiance will result in reduced power output from the PV module. In general, the increment of the irradiation level leads to a theoretical increment in the maximum power when there is no change in the temperature.

II.8.1.2 Effect of temperature

A PV module's temperature has a great effect on its performance. It is observed in Figure 2.11-2.12 that the temperature mainly affects the voltage; the power delivered by PV is inversely proportional to the temperature. However, the reason of that is due to the band gap energy decreases and more photons have enough energy to create electron-hole pairs. Therefore the module efficiency is reduced [74].

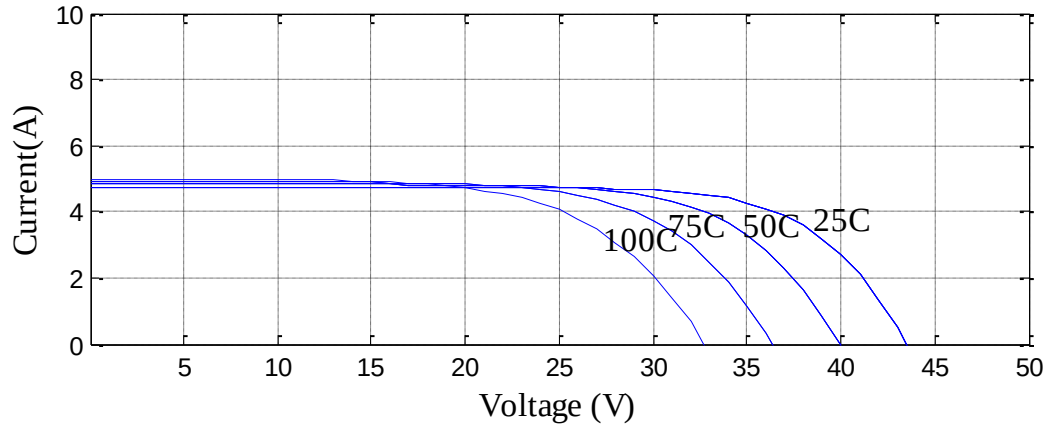

Figure 2.11 I-V curves at various temperatures

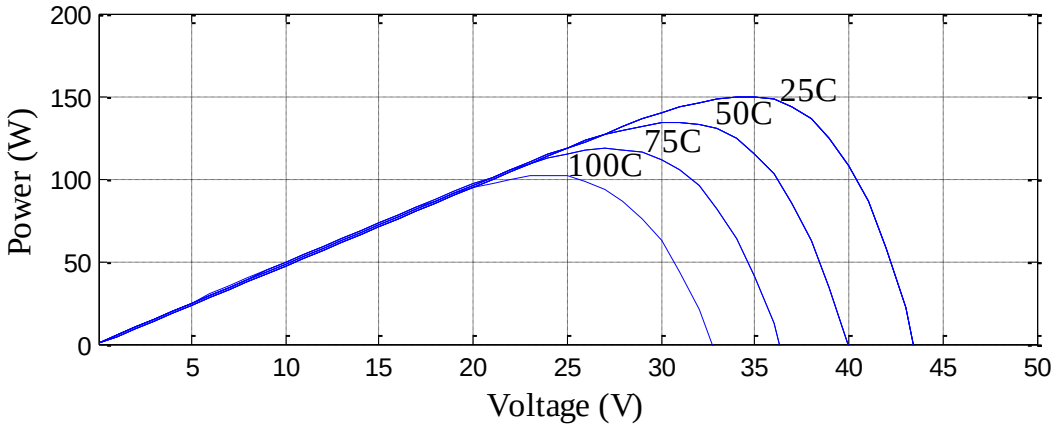

Figure 2.12 P-V curves at various temperatures

II.8.2 Effect of series resistance

A small variation in R_s has a large impact on the slope of the I-V curve. In fact, increasing the series resistance increases the slop of the I-V characteristic in the voltage source region, as shown in Figure 2.13. Therefore the maximum power changes significantly as depicted in Figure 2.14. Hence the value of R_s is derived by equation (II.14) from datasheet of the panel.

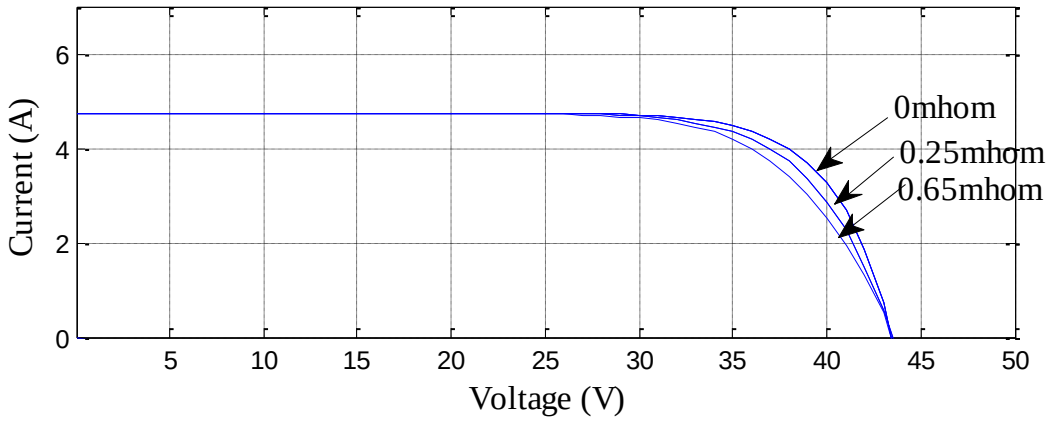

Figure 2.13 Effect of series resistance on the I-V curve

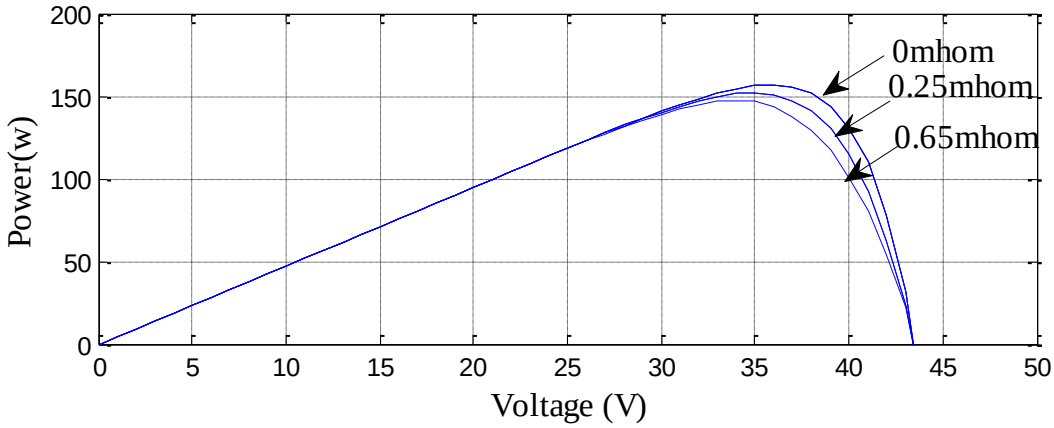

Figure 2.14 Effect of series resistance on the P-V curve

II.8.3 Effect of diode ideality factors

The diode ideality factor (n) is calculated by equation (II.12) from datasheet of the module. The ideality factor is an empirical factor that is added to the Shockley equation in order to reproduce the real behavior of a PV cell. It takes a value between one and two. Figures 2.15- 2.16 show the effect of the varying ideality factor

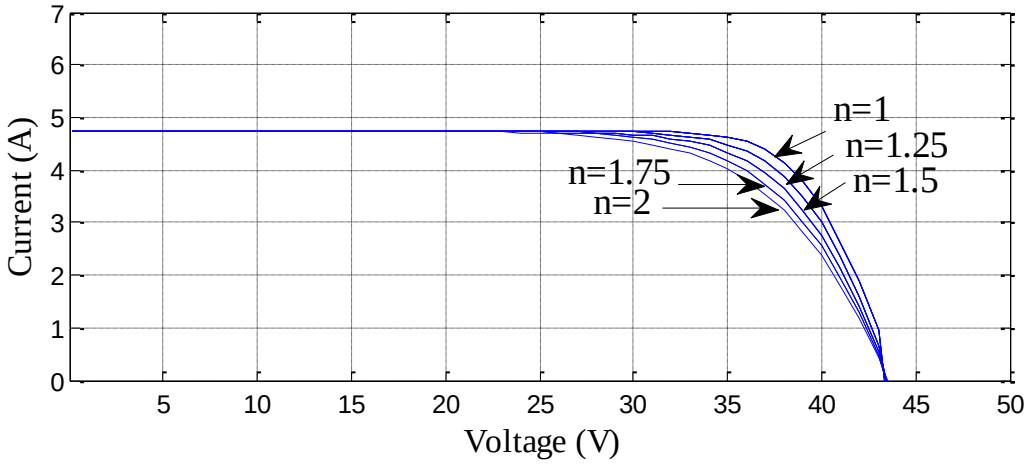

Figure 2.15 Effect of diode ideality factors on the I-V curve

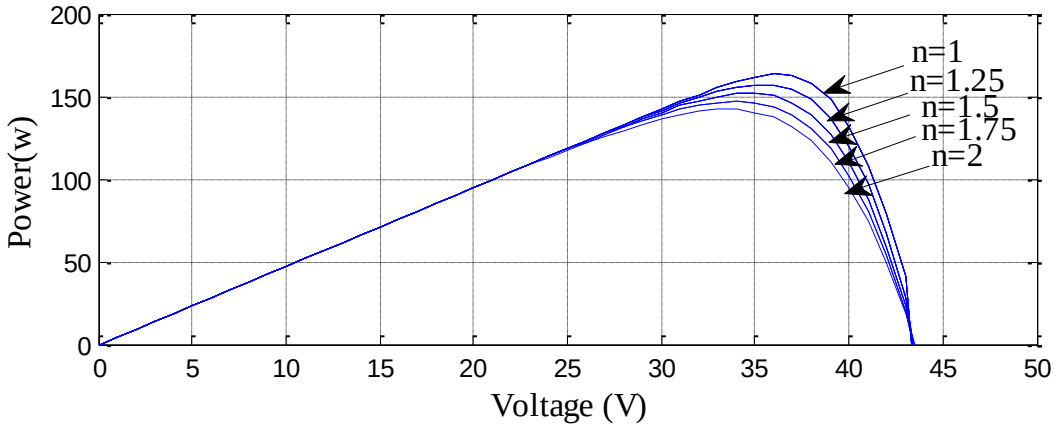

Figure 2.16 Effect of diode ideality factors on the P-V curve

II.9 Conclusion

In this chapter we have seen the modeling of the PV module using the equivalent a single diode PV cell model and applied a method of identification of PV cell parameters from datasheet.

It is well known that environmental conditions like temperature and irradiation affect the PV module. To this, the effect of varying temperature on PV module is explained here with P-V and I-V characteristic. The power produced from the PV panel is directly proportional to the irradiance and inversely proportional to the temperature. It is important to operate the system at the MPP of PV module in order to harvest the maximum power from the

module. However, the environment in which the PV module is installed has seldom the parameters of STC. Therefore, the power delivered is not maximal if the operating point is different than the critical one on the P-V characteristic of the PV. The next chapter investigates the converter that allows tracking this critical point, maximum power point.

Chapter III

Adaptation stage and MPPT

III.1 Adaptation stage in solar system

III.1.1 Introduction

A PV array in a uniform and constant irradiation has I-V characteristics, for any irradiance level, there is only one operating point called the Maximum Power Point (MPP), at which the PV array operates at maximum efficiency and produces a maximum of power (P_{max}). Therefore, when a solar photovoltaic system is directly connected to a load for given climate conditions, Figure 3.1 [75], the operating point (V, I) will be at the intersection of the I-V characteristics of the PV array and that of the load line (R_1, R_2 and R_3), as depicted in Figure 3.2. A part from point B, in general this intersection point is not the maximum power point of the PV array (such as A or C). For this reason, PV arrays are connected to loads through DC-to-DC converter. The latter allows to PV arrays to be constrained to an appropriate operating voltage (or current) by adapting load line so that intersection point would be point B. To this, an intermediate stage, (chopper or inverter according to desired output) must be used to match this characteristic. The converter is controlled by a Maximum Power Point tracking (MPPT) algorithm. The latter adjusts the duty cycle of the converter to control the voltage or current independently of the load. Thus, the duty cycle can be adjusted to change any load to match optimal load at under any climatic condition [76].

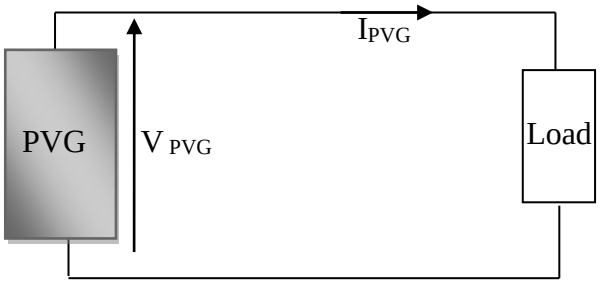

Figure 3.1 Direct coupled system with resistive load

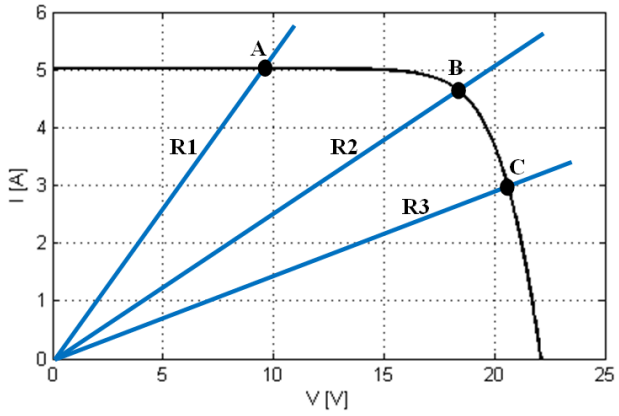

Figure 3.2: Different operating points of the PV module

III.1.2 DC-DC converter

The DC-DC converter allows supplying a regulated DC output from a DC input. They are used as an interface between the PVG and the load in photovoltaic systems, as shown in Figure3.3. The load must be adjusted to match the current and voltage of the solar generator as to deliver maximum power and therefore it will be variable due to the changes in temperature and irradiation. In power electronic, DC-DC converter is presented for the switching circuits with it transform the form of input voltage to another output voltage [77].

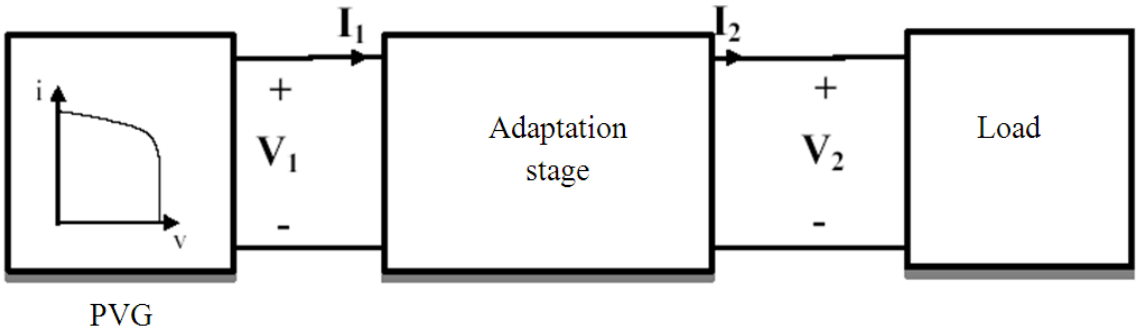

Figure 3.3 Block diagram of a typical standalone PV system

III.1.3 Topologies

There are different topologies of DC-DC converters. They are classified into isolated and non-isolated topologies [78].

The isolated topologies are used for small sized and high frequency electrical isolation transformer which provides the benefits of DC isolation between input and output by changing the transformer turns ratio. Popular topologies for such applications are flyback,

half-bridge and full bridge. These types used when electrical isolation is preferred for safety reasons [79].

The non isolated topologies do not have isolation transformer. They are further categorized into three types:

- Buck converters (step down)

- Boost converters (step up)

- Buck-Boost converters (step up and down)

The Table III.1illustrates the transformer turns ratio K and duty cycle D with different topologies.

Table III.1 the transformer turns ratio with different converters.

Converters	Transformer ratio and duty cycle	Galvanic isolation
Buck	D	No
Boost	$\frac{1}{1-D}$	No
Buck-Boost	$\frac{-D}{1-D}$	No
Cuk	$\frac{-D}{1-D}$	No
SEPIC	$\frac{D}{1-D}$	No
Flyback	K $\frac{D}{1-D}$	Yes
Push-pull	KD	Yes
Forward	KD	Yes

III.1.4 Boost converter

In PV applications, the boost topology is used for stepping up the voltage when they are connected to utility mains through an inverter stage. In this type of converter the output voltage is always greater than the input voltage [80]. Therefore the step up chopper can be applied to MPPT systems where the output voltage needs to be greater than the input voltage [81]. The circuit topology is shown in Figure3.4.

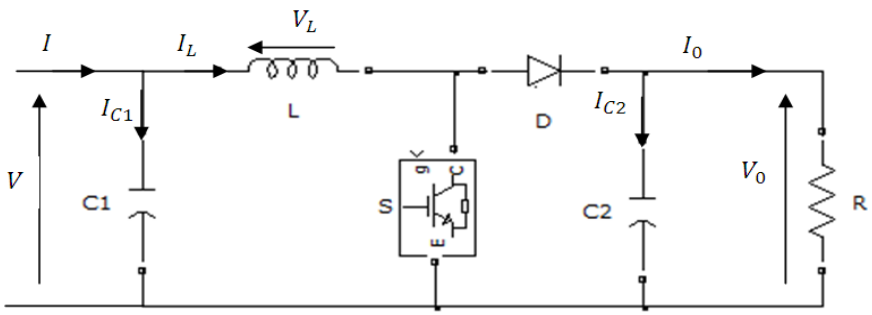

Figure 3.4 Boost converter

III.1.4.1 Waveforms

The waveform of the current and voltage of the Boost converter during continuous conduction mode is show below in Figure 3.5 [82].

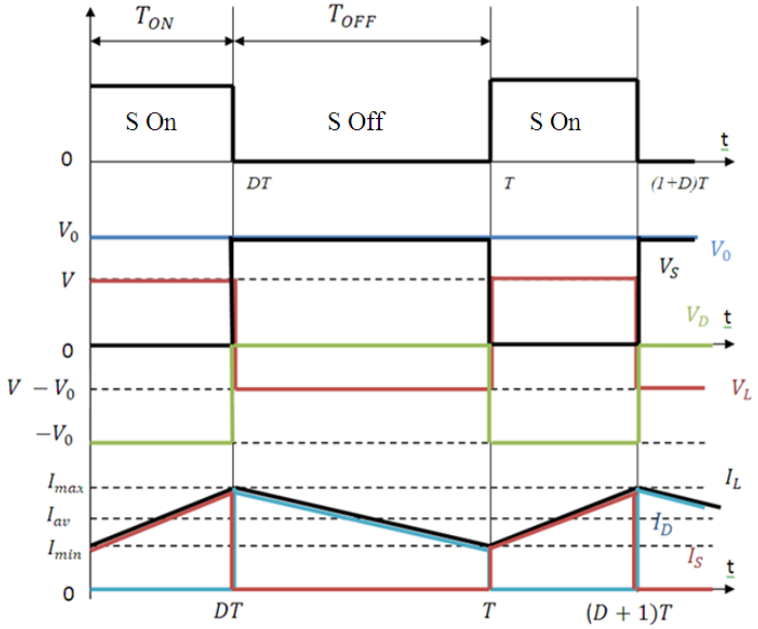

Figure 3.5 Circuit schematic of Boost converter

When the switch S is on, from t=0 to t = t_{on}, the diode D is reverse biased. Consequently, the current in the inductor L rises linearly due to the input voltage source, and the output stage is isolated. Whereas the capacitor C is partially discharging and supplying power to load .The equivalent circuit is shown in Figure 3.6

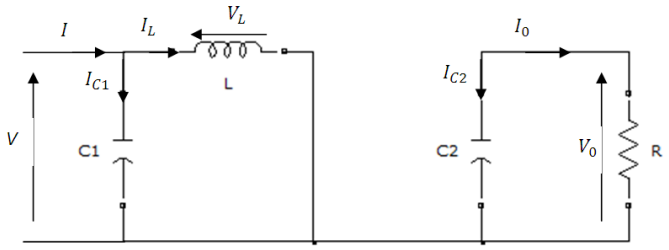

Figure 3.6 Equivalent circuits when S is on

When the switch S is off from t=t_{on} to t = T (duration =t_{off}), the diode is conducting and during this time the output stage receives energy from both the inductor and the input source. The equivalent circuit is shown in Figure 3.7

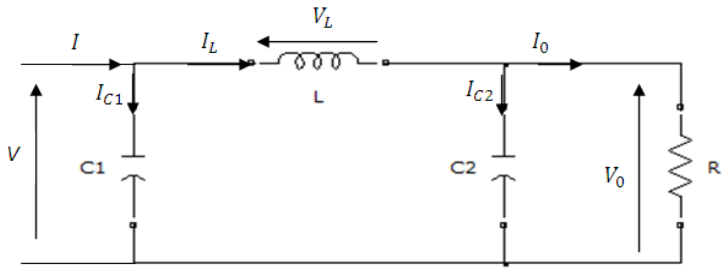

Figure 3.7 Equivalent circuits when S is off

III.1.4.2 Voltage output Calculated

Since in steady state time integral of the inductor voltage over one time period must be zero [83]:

$$V\,T_{ON} = T_{OFF}\,(V_0 - V) \tag{III.1}$$

Dividing both sides by T and rearranging items yield

$$\frac{V}{V_0} = \frac{T}{t_{off}} = \frac{1}{1-D} \tag{III.2}$$

Then:

$$V_0 = \frac{1}{1-D}\,V \tag{III.3}$$

Where:

T: The switching period.

D: The duty cycle.

It's clear from equation (III.2) the value of V_0 is greater than that of V, hence the name of Boost.

III.1.4.3 Calculation of I_0

The diode current is given by [83]:

$$I_D = I_0 + I_{C_2} \quad \text{(III.4)}$$

Current I_0 can be calculated using the following equation:

$$I_{0\ aver} = I_{D\ aver} - I_{C_2\ aver} \quad \text{(III.5)}$$

Similarly, when S is turned off, the following approximation is used:

$$I_0 = I_{L\ aver}\ (1 - D) \quad \text{(III.6)}$$

III.1.4.4 The ripple current and voltage

The inductance voltage is given by:

$$V\ T_{ON} = L\ \Delta I_L \quad \text{(III.7)}$$

We can determine ΔI_L with:

$$\Delta I_L = \frac{V}{L\ f}\ \mathrm{D} \quad \text{(III.8)}$$

And the corresponding waveform of voltage ΔV_0 is:

$$\Delta V_0 = \frac{1}{f C_2}\ D\ I_0 \quad \text{(III.9)}$$

Where:

f: is the chopping frequency.

III.1.5 Design chopper for PV application

When the voltage with MPP of the panel shown in Table II.1 is V=34.5V. We are solving for imposed voltage (in this section, we have V_{out} at 48V for example).

III.1.5.1 Duty cycle

By equation II.3, we can solve for V_{out}:

$$D = -\frac{V}{V_0} + 1 = -\frac{34{,}5}{48} + 1 = 0.28$$

Knowing that I_L=I=4.35A, the current I_0 is:

$$I_0 = 4.35\ (1 - 0.28) = 3.132\ A$$

III.1.5.2 Load calculation

$$R = \frac{V_0}{I_0} = \frac{48}{3.132} = 15.32\ \Omega$$

III.1.5.3 Inductor

The value of inductor is calculated by equation II.8:

$$L\ = D\frac{V}{f\Delta I_L}$$

Ripple current is 5% of I_L

$$\Delta I_L = I_L\, 0.05 = (0.05)4.35 = 0.2175\ A$$

When the f=50 KHz, we have:

$$L = 0.28\frac{34.5}{50\ 10^3 0.2175} = 0.888mH$$

III.1.5.4 Capacitor

Using equation II.9, we get:

$$C_2 = \frac{D\, I_0}{f\Delta V_0}$$

Ripple voltage is constrained to be less than 5% of V_0

$$\Delta V_0 = V_0\ 0.05 = (0.05)48 = 2.4\ V$$

Then,

$$C_2 = \frac{0.28\ \ 3.132}{50\ 10^3 2.4} = 7.3\ \mu F$$

To ensure maximum power available at the terminals of the PV and transfer it to the load, the voltage of the PV array must be adjusted to the appropriate value. The technique conventionally employed is to use an adaptation stage between the PV array and the load. In our study we use a boost converter, known also as voltage elevator, which is mostly used in photovoltaic systems, especially in photovoltaic pumping system.

This converter allows performing the load matching task between the PV array and the load. This ensures, by changing the duty cycle of the converter regardless of climate conditions (irradiation and temperature), the load impedance can be reached using MPPT algorithms and that will be the aim of next section.

III.2 MPPT based on GSS algorithm

III.2.1 Introduction

MPP tracking technique that ensures that the PV gives the maximum available power under any change in irradiance level and the temperature condition. However, there is a need to track the MPP in order to maximize the power delivered to the load from the PV array under any circumstance. By adjusting the duty cycle for Boost converter which is connected between the PV array and the load is possible to track the MPP. Figure 3.8 illustrate a Boost switching power converter along with an MPPT control algorithm to operate the PV system in such way it transfer the maximum capable power to the load. There are several algorithms to track the MPP of PV system that have been studied, developed and published over the last decades. In [15], the authors have developed many MPPT control technique. There are variations between these techniques in terms of simplicity, sensors requirement, cost, and convergence speed and hardware implementation. Some MPPT algorithms outperform the others under the same operating conditions.

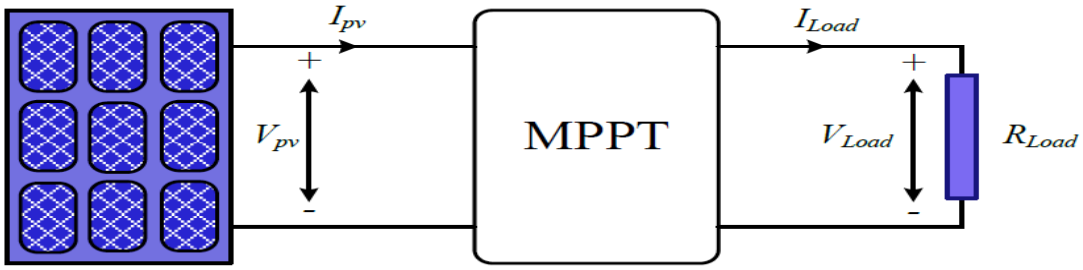

Figure 3.8 Boost converters acting as MPPT

III.2.2 Specification of MPPT control algorithm

The performances of a new or modified MPPT control algorithms for successful design depend on dynamic response, steady-state error and tracking efficiency [15].

III.2.3 MPPT algorithms

Many studies are made on MPPT methods and developed for ether stand-alone or grid-connected PV systems were installed in wide-ranging power capacities and by using various technologies [84]. Conceptually, MPPT is a simple problem, it is originally an operating point matching between the PVG and power converter. The tracking the correct maximum power point is essential in PV systems to ensure the best energy harvesting from the environment conditions [85]. Such as Constant Voltage Control (CVC) applied in [7] performs to reduce the power losses caused by dynamic tracking errors under rapid weather changing conditions. The Perturb and Observe (P&O), the hill climbing (H&C) and Incremental Conductance (IC) MPPT techniques [29, 86, 88, 89]. These methods are known to be perturbation MPPT techniques that share the same principle in which the value of the operating parameter. These techniques are robust but introduce oscillations around the local MPP and remains there indefinitely which result in energy waste, and there are used as MPPT due to the simple implementation and also fewer sensor requirements.

The fuzzy logic controllers have been introduced in the tracking of the MPP in PV systems [90]. T advantages are robust and relatively simple to design. ANN based MPPT, once trained, exhibits superior dynamic performance in comparison to PO and InCond MPPTs. However, these performances are limited to training data and consequently huge training data is needed in case of PV systems where MPP depends on many parameters. The MPPT efficiency varies depending on cell temperature and fill factor with the climatic conditions and features of geographic region [42].

Developing a new MPPT algorithm known Golden section optimization is the scope of this thesis. The proposed method preserves the main advantages of P&O that is simplicity and effectiveness in trucking the MPP under varying climate conditions. In addition to that, it is faster and does not need perturbations to converge to MPP. This results in oscillation free operation of the algorithm and subsequently better efficiency. In this section we are presented two algorithms P&O and GSO based MPPT algorithm is depicted. Simulation and discussion of results for different climate conditions are given in present chapter.

III.2.4 MPPT based Perturb and observe (P&O)

The Perturb and Observe (P&O) is easy to implement, it works based on the PV array which is perturbed of a radiation of direction. The algorithm measures the present power and compares it to the initial one and pursuant to the difference the duty cycle is updated. The duty cycle is stepped up or down to move from the new point towards another in the P-V characteristics in which it is expected to obtain more power. The PV system is always perturbed such as the tracking is ensured. However, this technique require limited time to identify the MPP and the PV system oscillate proximately of MPP. When the oscillation can be minimize by using smaller step sizes [26]. The flowchart corresponding to this method is given in Figure 3.9. A disadvantage of P&O is at steady stat around the peak point. The operating point oscillates in the region of the MPP giving rise to the waste of energy.

This algorithm has two parameters:

-The time interval between the times when measurement is done and the time when operating point moves from its optimal value.

-The increment of the movement of the operating point itself.

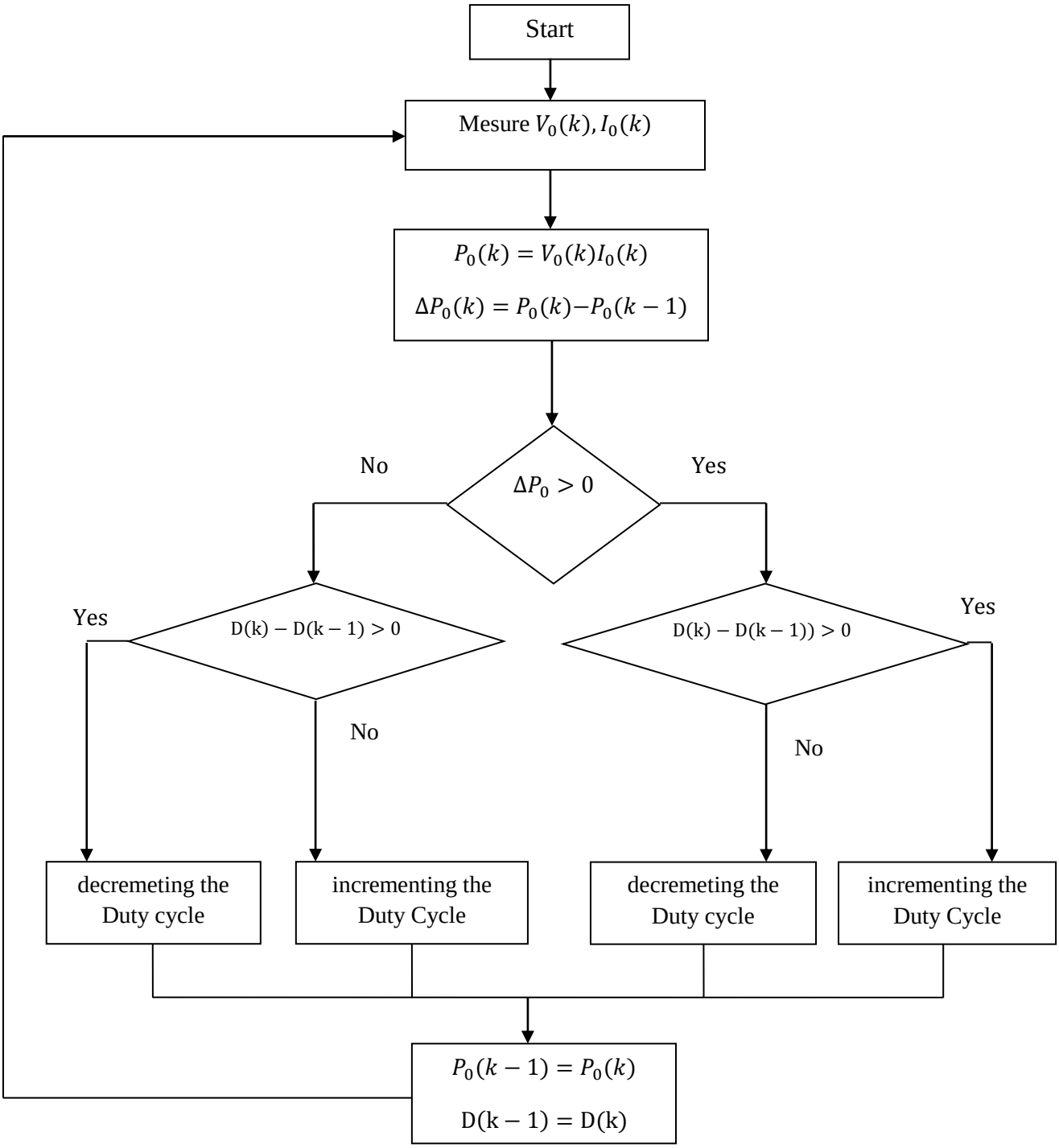

Figure 3.9 Flowchart of P&O MPPT algorithm

III.2.5 Control of MPPT

The MPPT technique tells a MPPT controller how to move the operating voltage. Then, it is a MPPT controller's task to bring the voltage to a desired level and maintain it. We have many methods often used for MPPT [13].

III.2.5.1 PI Control [91]

The proportional and integral (PI) controller regulates the input voltage of converter, Where the MPPT takes measurement of PV voltage and current and then taking algorithm calculates the reference voltage(V_{ref}) when the PV operating voltage should move next. The algorithm set to V_{ref} only, and repeated periodically with a slower rate. The PI controller task is minimize error between V_{ref} and the measured voltage by adjusting the duty cycle as shown in Figure 3.10.

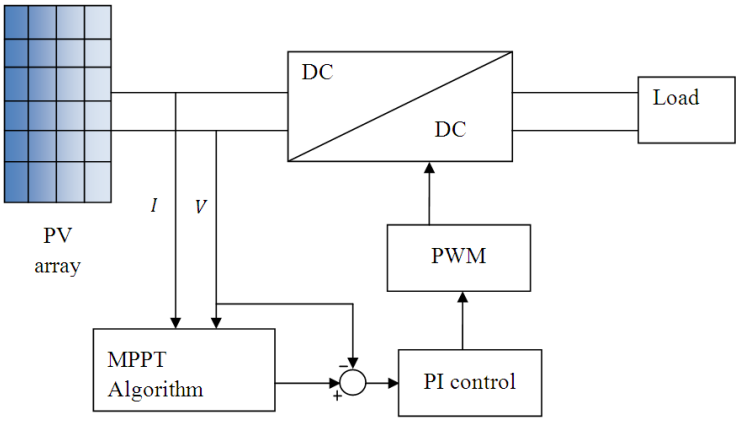

Figure 3.10 Block diagram of PV generator systems with the PI controller

III.2.5.2 Direct Control [13]

One of the most used controllers is the direct controller that is simpler and uses one control loop and it performs the adjustment of duty cycle. This is shown graphically in the Figure 3.11.

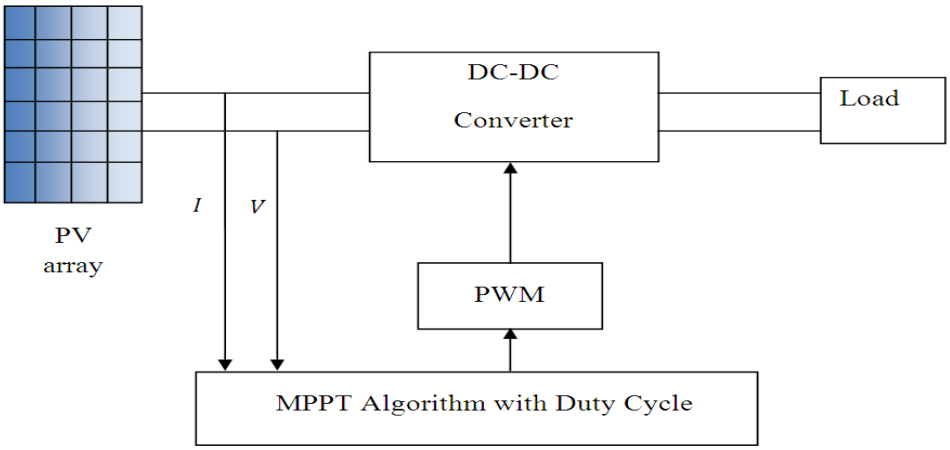

Figure 3.11 Block diagram of PV generator systems with the direct control

III.2.5.3 Control by pulse width modulation (PWM)

The PWM control is to cut the output voltage generated by the converter into a series of elementary patterns with low frequency, and variable duty cycle in time [92]. The variation of the duty cycle of each switch is then determined by a modulating signal. The control commands are formed by the intersection between a triangular wave of higher frequency and the reference signal [93].

The converter forces the PV module to operate at maximum power, whatever the illumination and transfer to the load for a duty cycle defined by the P&O MPPT method. Actually the real effect of MPPT is seen when there are changes in environmental conditions (temperature and irradiance). The only way to see real difference is to use different conditions with the same duty cycle, when we seen in the next sections.

III.2.7 MPPT based Golden section search technique

The **American Jack Carl Kiefer** discovered the new optimization technique known Golden Section Search or Golden Ratio Method or Golden Mean Method in 1953[94], and then developed Fibonacci method. This technique can be utilized for solving many problems particularly for unimodal functions which have only on optimum point (minimum or maximum on the interval [x1, x2])[95]. The advantages of this method are the no requirement of both number of iterations and the function derivative [96]. GSS method is similar to bisection one in the sense that it defines an interval with a single maximum inside, then it divides the segment in three sections by adding two internal points between them, the whole technique is described in the flowchart shown in Figure 3.12 [97].

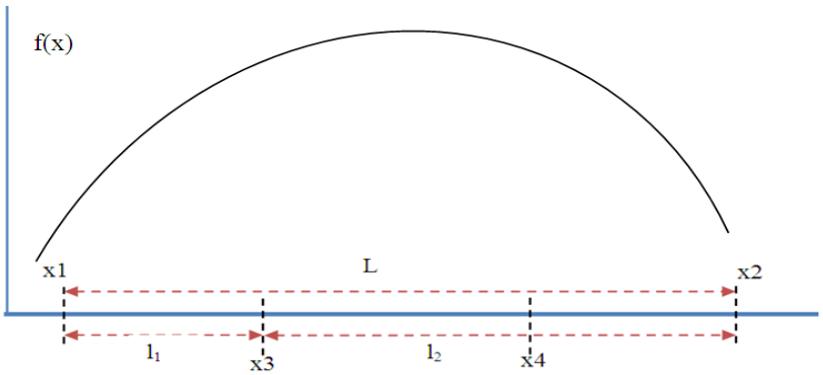

Figure 3.12 Explanatory diagram for GSS

Then it evaluates the function at the two points x3 and x4 such that

If f(x3) >f(x4), the maximum is between x1 and x3 then the new range is x1=x1, x2=x4.

If f(x3) <f(x4), the maximum is between x3 and x2 then the new range is x1=x3, x2=x2.

We have a new interval into three sections and repeat over, and we are close enough to maximum to stop with us use the tolerance of smaller interval [x3, x4] such that:

$$err = \frac{1}{2}(x_3 + x_4) \quad \text{(III.10)}$$

The place of two internal points determine by:

$$L = l_1 + l_2 \quad \text{(III.11)}$$

And

$$r = \frac{L}{l_2} = \frac{l_2}{l_1} \quad \text{(III.12)}$$

Substitute (III.11) in (III.12), we have:

$$r^2 + r - 1 = 0 \quad \text{(III.13)}$$

Solving (III.12) for r:

$r_1 = \frac{\sqrt{5}-1}{2} = 0.61803$ $r_2 = -\frac{\sqrt{5}-1}{2} = -1.618$

Where:

r: is the Golden ratio.

So the result leads to the following equations of x3 and x4:

$$x_3 = x_1 + r(x_2 - x_1) \quad \text{(III.14)}$$

$$x_4 = x_2 - r(x_2 - x_1) \quad \text{(III.15)}$$

III.2.8 GSS-based MPPT algorithm

Figure 3.13 shows the proposed MPPT boost converter configuration of PV system.

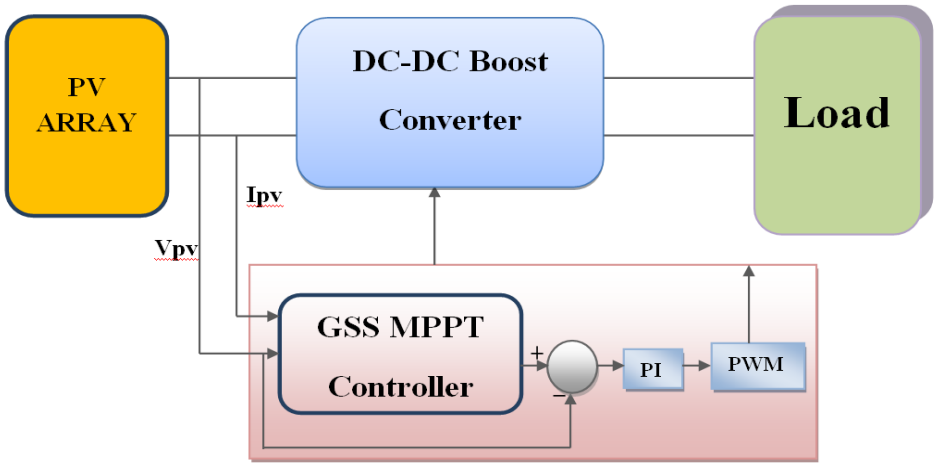

Figure 3.13 Model of the proposed MPPT

In order to apply the GSS into MPPT method in PV systems, the function of f(x) and the variable x should be chosen carefully. Figure 2.3 shows a real power –voltage (P-V) curve of a PV array.

It can be seen that the change in power with respect to voltage approaches zero at the maximum power point. Obviously, the power at short circuit voltage (0V) and open circuit voltage (V_{oc}) are null, so maximum power should not happen in these two points even though the changes in power at these two points are also zero, which is caused by the small powers around these two points. The MPPT is essential to find the root in the function P by regulating the voltage of solar module or solar arrays, where the variable x is the voltage of solar module or solar array and can be written as:

$$f(x) = P(V_{Array}), Initial\ value: x1 = 0\ and\ x2 = V_{OC} \quad \text{(III.16)}$$

To regulate the voltage V_{Array} , converters are required as interface between solar array and load. The following flowchart summarizes the entire proposed algorithm:

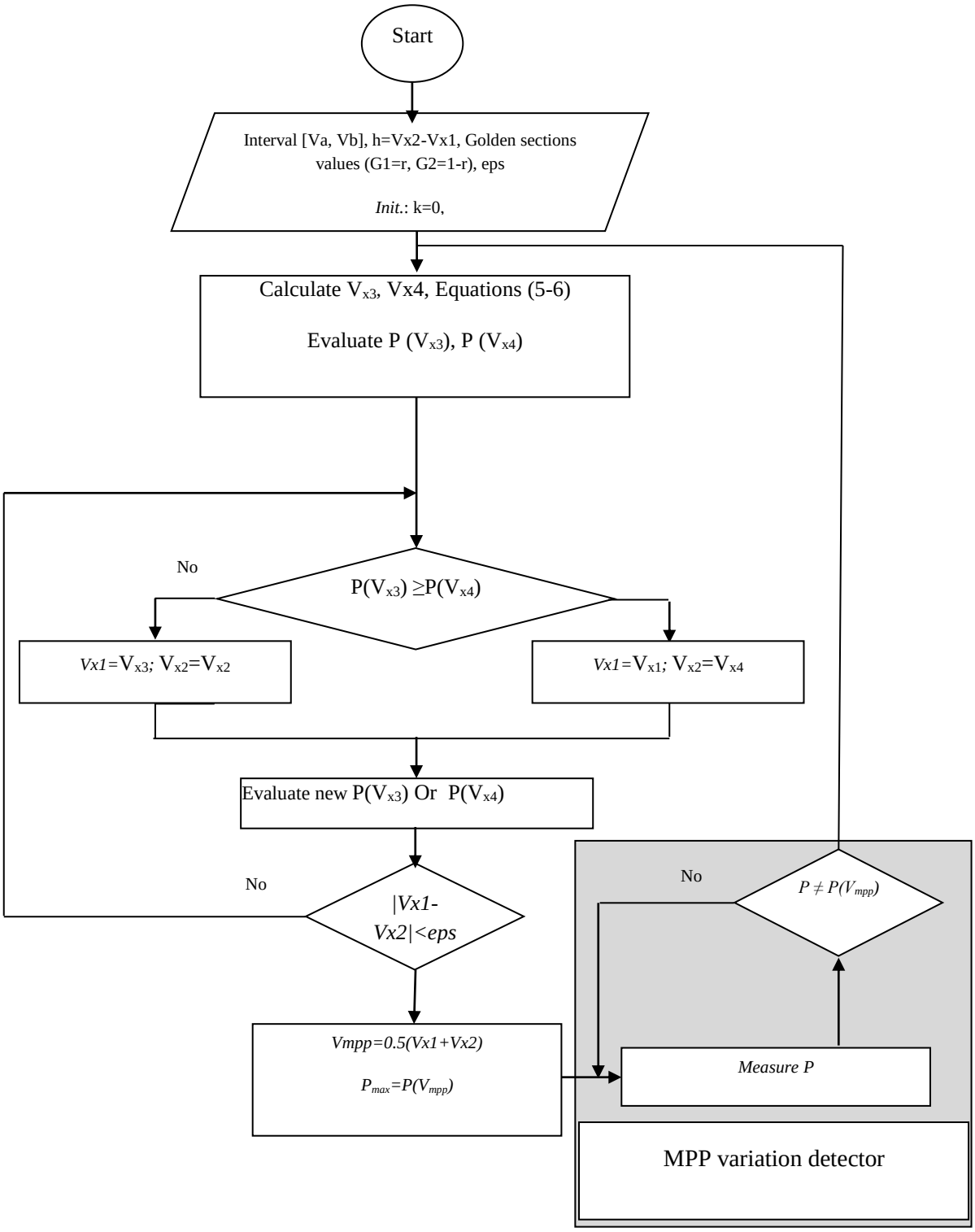

Figure 3.14 Proposed GSS MPPT algorithm flowcharted

III.2.10 Conclusion

In this chapter GSS technique designed present important enhancements to the power extraction skills of the P&O for MPP. Special attention should be the absence of oscillations around the MPP, it has fast convergence speed and there is no requirement of derivatives of voltage and power measured from solar array, when it reduces the complexity in computation and hence implementation. Then, the proposed MPPT method is very suitable for the use of PV system where we are seen in the next chapter.

Chapter IV

MPPT for Solar water pumping system using induction motor

IV.1 Introduction

In recent years, The non- availability of electricity in rural and remote areas and increase in diesel prices affects the pumping requirement of community water supplies and irrigation, utilizing solar energy for water pumping is promising alternative to conventional electricity and diesel based pumping systems [17]. SWPS is environment friendly and require low maintenance with no fuel cost [16], which is based on photovoltaic technology that converts solar energy to electrical energy to run an AC or DC motor with addition water pump. The PV pumping systems for water supplies are used in urban, rural, industry, community and educational institutions. So for the importance of water supply systems is also dependent on electricity, there is a wide scope to study and develops on ways of sizing, matching and adapting PV pumping systems [98]. In this case, many studies which are listed in [99,100] have been conducted to investigate the performance of solar water pumping systems (SWPS) in different countries. These countries are located in tropical regions of the earth and therefore strongly support the use of SWPS.

The SWPS are two types presented in DC and AC systems. For DC systems, driving by a DC motor with brushes coupled to a pump. This type used for low power direct coupled PV water pumping systems because the high cost and suffer frequent maintenance problems, where we have resulted in the use of AC systems [17].

AC systems have mostly three-phase asynchronous motor pumps which require an inverter to be used between PV generator and the motor. The systems based an induction motor is reliable, rugged and maintenance free with increased efficiency and provides more possibilities for control strategies in comparison to DC motor [31].

IV.2 System description and configuration

A typical configuration of solar-powered water pumping system is shown in Figure 4.1. The photovoltaic generator is a set of PV panels and their connection is chosen according to the power requirement of the association power electronic converters, motor and centrifugal pump.

In PV systems, a DC/DC converter is installed between a PVG and pump which extracted the maximum energy during all the day. In order to extract the maximum power point tracking MPPT is used as online control strategy to track the maximum output power operating point of the PVG for different climatic conditions and it’s important in SWPS

because it reduces the solar array cost by decreasing the number of solar panels needed to obtain the desired output power [101]. In order to perform the DC/AC conversion stage, an inverter must be included which it provides three phase voltage and it can be controlled the speed of the motor according the amplitude and frequency supplies depends of the water flow rate of the pump and variation of the climatic conditions.

The input variable of SWPS in this thesis is the solar irradiation and output variable is the water flow rate. The reference voltage V_{ref} obtained by MPPT algorithm, which mainly depends on irradiance. Water flow rate depends on head and speed of the motor. The speed of the later is controlled by the frequency supplied by the inverter. Indirect Rotor Field Oriented Controller (IRFOC) is the simplest control algorithm which can ensure simultaneously good decoupling of induction motor for our SWPS.

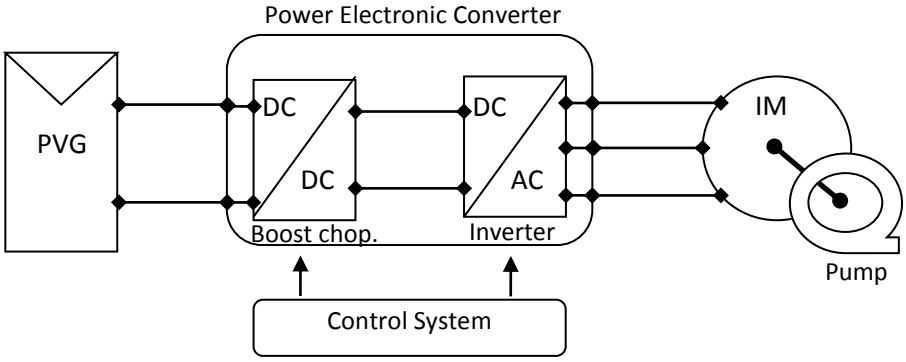

Figure 4.1 Configuration of solar powered water pumping system (SWPS)

The objective of this chapter is the application an algorithm known Golden Section search based MPPT method in SWPS, and the proposed technique will be compared with the conventional P&O method.

IV.3 Modeling of SWPS

IV.3.1 Induction motor model

IV.3.1.1 Introduction

The induction motor is largely used in many industrial applications due to low cost, good torque density and it has numerous advantages such as simple construction and robustness [102]. There is a rotary type with basically a stationary stator and rotating rotor, the stator has a cylindrical magnetic core that is housed inside a metal frame. The stator is

composed of three phases distributed stator windings, connected in star or triangle. The rotor of the machine consists of cylindrical laminated iron core with uniformly spaced peripheral slots to accommodate the windings, similar to the one of stator. That is a three phase winding with same amount of poles as in the stator. The rotor is coupled in star and we distinguished according to this rotor constitution two machines technologies.

For the first technologies, the coiled rotor includes a three-phase winding, similar to the stator connected in star. This connection can be short-circuit or a link to resistor. And the rotor windings are short-circuited second technology.

Industrial realizations generally use a rotor, which is composed of conducting copper or aluminum bars that are short-circuited by a conductor ring at each bound[103].

IV.3.1.2 Equivalent representation

The windings arrangement of a symmetrical induction machine is shown in Figure 4.2. The windings of stator are identical and sinusoidal distributed and displaced 120^0 apart. Similarly the rotor winding are also considered as three identical sinusoidal distributed winding displaced 120^0 apart.

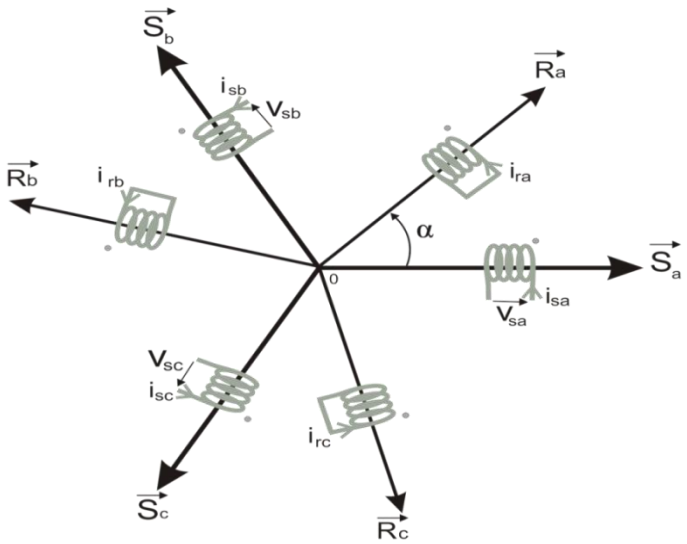

Figure 4.2 Three phase windings arrangement.

For this modeling getting easier the following assumptions will be considered:

-The air gap is uniform

-Magnetic saturation, anisotropy effect, core loss and skin effect are negligible

-Winding saturation and reactance do not vary with the temperature

- Infinitely permeable iron …

IV.3.1.3 Voltage equations

Using Kirchoff's low, the voltage equations for each winding on the stator and rotor can be determined [102].

$$v = Ri + \frac{d\Phi}{dt} \tag{IV.1}$$

The voltage equation for stator windings:

$$[v_{sabc}] = [R_s][i_{sabc}] + \frac{d[\Phi_{sabc}]}{dt} \tag{IV.2}$$

And rotor windings:

$$[v_{rabc}] = [R_r][i_{rabc}] + \frac{d[\Phi_{rabc}]}{dt} = [0] \tag{IV.3}$$

IV.3.1.4 Flux equations

The flux linkage equation is shown in equation (IV.4) and divided into four sub-matrices:

$$\begin{bmatrix} \phi_{sabc} \\ \phi_{rabc} \end{bmatrix} = \begin{bmatrix} [L_s] & [M_{sr}] \\ [M_{rs}] & [L_r] \end{bmatrix} \begin{bmatrix} i_{sabc} \\ i_{rabc} \end{bmatrix} \tag{IV.4}$$

Where L_s is the inductance within the stator winding, L_r is the inductances within the rotor windings, L_{sr} is the inductances between stator and rotor winding and L_{rs} is the inductances between the rotor and stator windings.

Substituting equation (IV.4) into equations (IV.2), (IV.3) gives the following equation:

$$[v_{sabc}] = [R_s][i_{sabc}] + (d/dt)\{[L_s][i_{sabc}] + [M_{sr}][i_{rabc}]\} \tag{IV.5}$$

$$[v_{rabc}] = [R_r][i_{sabc}] + (d/dt)\{[M_{sr}]^t[i_{sabc}] + [L_r][i_{rabc}]\} \quad \text{(IV.6)}$$

IV.3.1.5 Mechanical equations

Performing an energy balance on the system, the mechanical equation is obtained as follows:

$$\begin{cases} J\dfrac{d\Omega}{dt} + f_r\Omega = T_{em} - T_L \\ \omega = p.\Omega \end{cases} \quad \text{(IV.7)}$$

Where:

-T_{em} is electromagnetic torque

-T_L is torque of the mechanical load

-J is inertia of the rotor and the equivalent mechanical load

-f_r is damping coefficient associated with mechanical rotational system of the machine

-Ω is angular rotational speed of the motor

-p is pair poles number

-ω is angular electrical speed

IV.3.1.6 The dynamic d-q model using PARK's transformation

In order to reduce the expressions of the induction motor equation given below and obtain constant coefficients in the differential equations, the Park's transform will be applied. Especially, it can understand as transforming the three windings of the induction motor to jest two windings, as shown in Figure 4.3

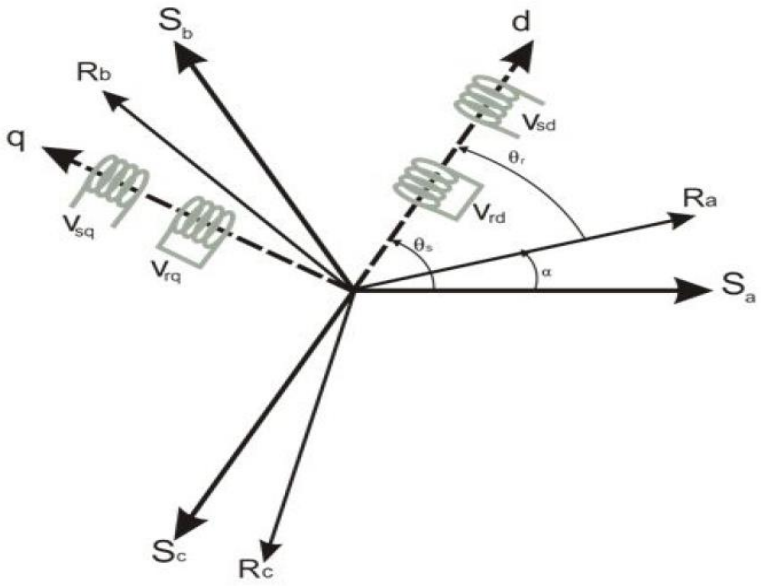

Figure 4.3 Park transform vector diagram

In the symmetrical three-phase machine, the direct and the quadrature axis stator magnitudes are fictitious. The equivalencies for the direct d and quadrature q magnitudes with the magnitudes per phase are as follows:

$$[x_{dq0}] = [P]\,[x_{abc}] \tag{IV.8}$$

Where

[P]: is passing matrix, it determined with:

$$[P] = c.\begin{bmatrix} \cos\psi & \cos(\psi - 2\pi/3) & \cos(\psi + 2\pi/3) \\ -\sin\psi & -\sin(\psi - 2\pi/3) & -\sin(\psi + 2\pi/3) \\ 1/\sqrt{2} & 1/\sqrt{2} & 1/\sqrt{2} \end{bmatrix} \tag{IV.9}$$

Where

($\psi=\theta_s$) for the stator and ($\psi=\theta_r$) for the rotor.

c is a constant that can take either the values 2/3 or 1 for the so-called non-power invariant form or the value $c=\sqrt{(2/3)}$ for the power-invariant form.

It is shown in Figure 4.3 for θ_s and θ_r depends with α, so we can write:

$$(\theta_s - \theta_r) = \alpha \tag{IV.10}$$

The same situation happens between the frame speeds in each frame and the mechanical speed, that is:

$$(\omega_s - \omega_r) = \frac{d\alpha}{dt} = \omega = p\Omega \tag{IV.11}$$

Where:

ω_r is the speed of d-q axes in the rotor reference

ω_s is the speed of d-q axes in the stator reference

ω is angular electrical speed

α is the angle between stator and rotor

IV.3.1.7 Voltage equations

The application of park transformation to the model of induction machines after simplification the dq-model given in (IV.1-10), where the state variables are$I_{ds}, I_{qs}, \phi_{dr}, \phi_{qr} and\ \omega_r$.

$$\begin{cases} v_{sd} = R_s i_{sd} + (d\phi_{sd}/dt) - (d\theta_s/dt)\phi_{sq} \\ v_{sq} = R_s i_{sq} + (d\phi_{sq}/dt) + (d\theta_s/dt)\phi_{sd} \\ v_{rd} = R_r i_{rd} + (d\phi_{rd}/dt) - (d\theta_r/dt)\phi_{rq} = 0 \\ v_{rq} = R_r i_{rq} + (d\phi_{rq}/dt) + (d\theta_r/dt)\phi_{rd} = 0 \end{cases} \tag{IV.12}$$

With:

$$\begin{cases} \omega_s = d\theta_s/dt \\ \omega_r = d\theta_r/dt \end{cases} \tag{IV.13}$$

IV.3.1.8 Flux equations

$$\begin{cases} \phi_{sd} = L_s i_{sd} + M i_{rd} \\ \phi_{sq} = L_s i_{sq} + M i_{rq} \\ \phi_{rd} = L_r i_{rd} + M i_{sd} \\ \phi_{rq} = L_r i_{rq} + M i_{sq} \end{cases} \tag{IV.14}$$

IV.3.1.9 Mechanical equations

$$J\frac{d\Omega}{dt} = T_{em} - T_L - f_r\Omega \tag{IV.15}$$

IV.3.1.10 Expressions of fluxes

$$T_{em} = \frac{pM}{L_r}(\phi_{rd} i_{sq} - \phi_{rq} i_{sd}) \tag{IV.16}$$

By replacing the equations (IV.14) in (IV.12) and derived the currants and the fluxes we obtain the following mathematical model of the induction machine considering the squirrel cage at the stationary rotating frame $\omega_s=0$, $\omega_r=-\omega$:

$$\begin{cases} \dot{i}_{s\alpha} = -\gamma i_{s\alpha} + \frac{k}{T_r}\phi_{r\alpha} + k\omega\phi_{r\beta} + \frac{1}{\sigma L_s} v_{s\alpha} \\ \dot{i}_{s\beta} = -\gamma i_{s\beta} + k\omega\phi_{r\alpha} + \frac{k}{T_r}\phi_{r\beta} + \frac{1}{\sigma L_s} v_{s\beta} \\ \dot{\phi}_{r\alpha} = \frac{M}{T_r} i_{s\alpha} - \frac{1}{T_r}\phi_{r\alpha} - \omega\phi_{r\beta} \\ \dot{\phi}_{r\beta} = \frac{M}{T_r} i_{s\beta} + \omega\phi_{r\alpha} - \frac{1}{T_r}\phi_{r\beta} \end{cases} \tag{IV.17}$$

Where:

- $k = \frac{M}{\sigma L_r L_s}$ et $\gamma = \frac{1}{\sigma L_s}(R_s + \frac{M^2}{L_r T_r})$,
- $\sigma = 1 - \frac{M^2}{L_s L_r}$: Dispersion coefficient
- $T_r = \frac{L_r}{R_r}$: Rotor time constant.

IV.3.2 Inverter model

Inverters are electronic solid state devices used to transform electric energy from DC to AC at desired frequency, current and voltage. There are two types of inverters, current source inverters (CSI) when the input DC source has a high impedance and voltage source inverter (VSI) when the inverter has a DC source with small or negligible impedance [17, 104].It composed of six IGBT switches (k_{11}, k_{12}, k_{21}, k_{22}, k_{31}, k_{32}) each shunted in ant parallel by a fast freewheeling diode, in order to return the negative current to the filter capacitor provided at the input of the converter.

The diagram of a three-phase two level voltage source inverter is shown in Figure 4.4

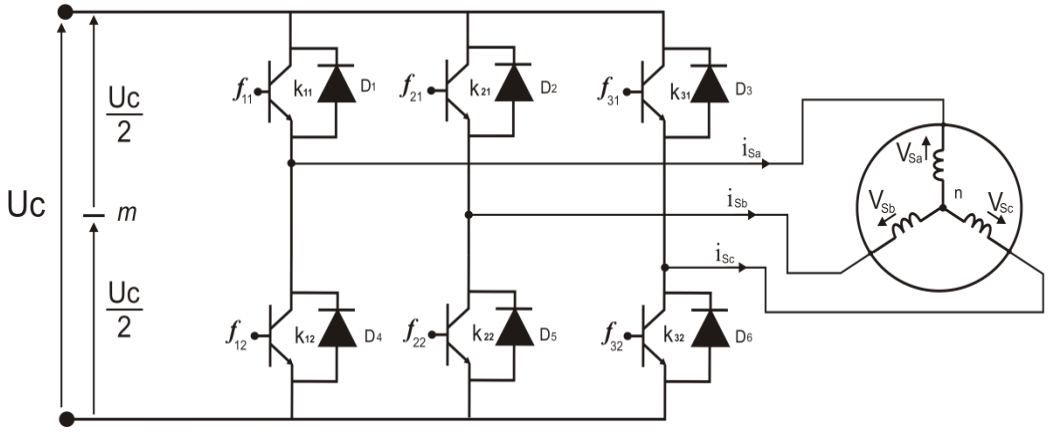

Figure 4.4 Schema of inverter

The inverter is controlled by analog values with f_{ci} ($c \in \{1, 2,3\}$, $i \in \{1, 2\}$) associated as the state of switches k_{ci} , we have:

$$\begin{cases} f_{11} = 1 - f_{10} \\ f_{21} = 1 - f_{20} \\ f_{31} = 1 - f_{30} \end{cases} \quad \text{(IV.18)}$$

With:

f_{ci}= 1 if the switch is ON

f_{ci}= 0 if the switch is OFF

Hence, the simple and composed voltages vectors which depends on the control signals and the input voltage:

$$\begin{cases} u_{sab} = U_c(f_{11} - f_{21}) \\ u_{sbc} = U_c(f_{21} - f_{31}) \\ u_{sca} = U_c(f_{31} - f_{11}) \end{cases} \quad \text{(IV.19)}$$

The stator voltage ensures the equation (III.20):

$$v_{sa} + v_{sb} + v_{sc} = 0 \quad \text{(IV.20)}$$

Hence:

$$\begin{bmatrix} v_{sa} \\ v_{sb} \\ v_{sc} \end{bmatrix} = \frac{U_c}{3} \begin{bmatrix} 2 & -1 & -1 \\ -1 & 2 & -1 \\ -1 & -1 & 2 \end{bmatrix} \begin{bmatrix} f_{11} \\ f_{21} \\ f_{31} \end{bmatrix} \quad \text{(IV.21)}$$

IV.3.3 Inverter control

In general, inverters are controlled by a Pulse Width modulation (PWM) technique which is characterized by the generation of constant amplitude V_r and the frequency f_r and comparing with a triangular signal (called carrier wave) characterized by a frequency significantly greater than of the reference $f_p >>> f_r$, and the amplitude V_p. When two signals take the same value and generated the duty cycle, the later involves turning the switches change the state.

The most used methods are:

-Voltage-controlled PWM techniques (SVM).

-Current - controlled PWM techniques (ex: hysteresis controllers).

The principle operation of later is illustrated in Figure 4.5. When the motor current in phase A, for example, becomes greater (or less) than the current reference value by the hysteresis $\pm$H in the comparator HCA, the inverter leg is switched to the negative (or positive) pole of the dc link supply.

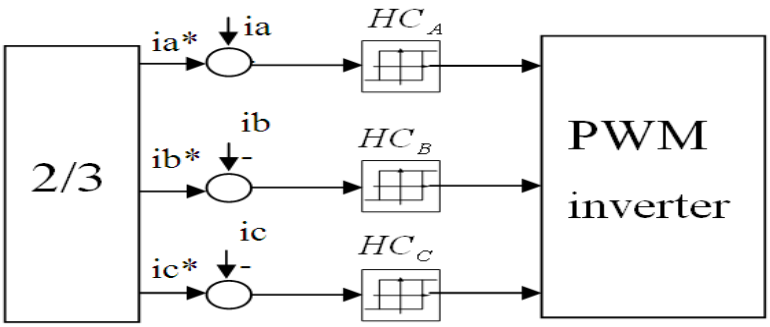

Figure 4.5 PWM inverter with hysteresis loop

IV.3.4 Pump

Different pumps are cited in the literature, it classified under two categories based on operating principal: dynamic pumps and positive displacement pumps, the latter pumps operate in applications characterized by a constant discharge speed, low flow rates or at high heads. These pumps generally tend to be larger than equal-capacity dynamic pumps.

Dynamic pumps operate by developing a high liquid velocity and pressure in diffusing flow passage. It has comparatively lower maintenance requirements [105]. Centrifugal pumps and axial flow pumps are dynamic pumps.

Centrifugal pumps are economical from shallow to medium lifts with large flow rates. Axial flow pumps are dynamic pumps that use the propeller to create a lift action of the fluid in the pipe. These pumps used in wet-pit drainage, storm water applications, and low pressure irrigation [105].

Each centrifugal pump applies a load torque proportional to the square of the rotor speed [106, 107].

$$T_L = K_p \Omega_r^2 \quad \text{(IV.22)}$$

Where K_p is the proportionality constant and it is given by

$$K_P = P_{np} / \Omega_{rn}^3 \quad \text{(IV.23)}$$

The water rate and pressure of the pump depend on the available mechanical power at the rotating impeller and the total head. The determination of the pump's output parameters can be simplified using affinity laws [109, 111] which require only pump ratings and actual input parameters; rotor speed and torque.

$$\begin{cases} H' = (\Omega_r / \Omega_{rn})^2 .H \\ Q' = (\Omega_r / \Omega_{rn}).Q \\ P' = (\Omega_r / \Omega_{rn})^3 .P \end{cases} \quad \text{(VI.24)}$$

Where H, Q and P are the rated parameters of the pump at speed Ω_{rn}, H', Q' and P' are the parameters of pump at speed Ω_r different than the rated speed.

IV.4 Indirect Rotor Field Oriented Controller-Induction motor

When the pump operating, the complexity of the induction machine control is due to non-linearity of the motor model and the effect of the inherent coupling between the direct axis (d) and the quadratic axis (q) , thanks to the vector control eliminates this problem by positioning in a privileged position ($\phi_{rd}=\phi_r$ and $\phi_{rq}=0$). This technique consists in controlling independently the flux and the current at a constant speed, by acting on the mechanic speed and the rotor flux ϕ_r, using the direct and the quadrature components of the stator current I_{sd} and I_{sq} respectively (Figure 4.6). Now the flux and the current are controlled independently. In this case, it imposes the electromagnetic torque T_{em}. Hence equation (VI.11) becomes [1].

$$T_{em} = \frac{pM}{L_r} \phi_{rd} i_{sq} \quad \text{(IV.25)}$$

When the rotor flux is not accessible, it is estimated using the direct current component I_{sd} as follows:

$$T_r \frac{d\phi_r}{dt} + \phi_r = M i_{sd} \quad \text{(IV.26)}$$

The angle θ_s can then be determined with the speed of the machine as follows:

$$\theta_s = \int \left(p\Omega + \frac{i_{sq}^*}{T_r i_{sd}^*} i_{sd} \right) dt \qquad when: i_{sd}^* = \frac{\phi_r^*}{M} \quad \text{(IV.27)}$$

Where: (*) is the index of reference value.

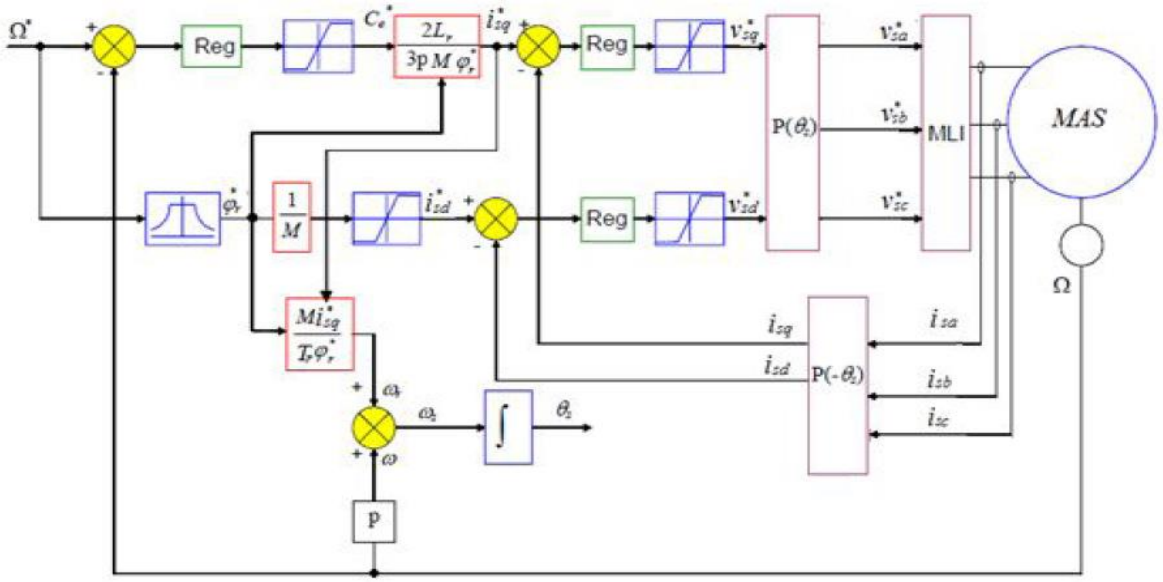

Figure 4.6 Block diagram of IFOC for an induction motor.

In the IRFOC, the regulation of the current and the speed is done via PI regulators.

IV.5 Steady state performance of solar water pumping system using MPPT

Figure 4.7 shows the bloc diagram of SWPs with induction motor, the whole system is composed of a PV generator, a Boost chopper, a PWM voltage source inverter and squirrel cage driving a centrifugal pump. We can be noticed that the water tank which replaces the battery is not shown in the diagram as long as the objective is to maximize the solar power harvesting. Yet, to completely utilize the solar power, the size of the tank should be compatible with the capacity of the PVG together with the maximum of insulation available at the location of usage.

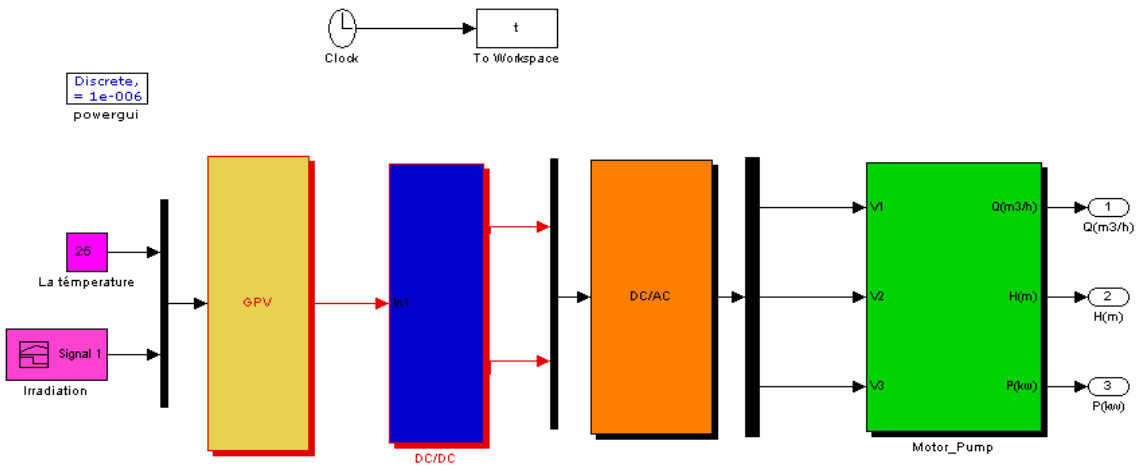

Figure 4.7 MATLAB/Simulink programs of the SWPS

IV.6 Control system

The extraction at each moment of the maximum power available at the terminals of the PV and transfer it to the motor is the objective of the control system. Figure 4.8 is illustrates the block diagram controlling by MPPT, optimal speed selection and IRFOC block. The duty cycle of the boost chopper is adjusted using an MPPT algorithm, which it is harvested that maximum power from the PVG. To ensure a maximum power transfer to the pump, an optimal selection of the rotor speed must be done. The speed allows obtaining maximum water rate for given sun's irradiance. To satisfy this condition, the induction motor must run at the operating point characterized by the above optimal rotor speed. To this, the inverter must be controlled by IRFOC such that appropriate stator voltages are generated across the induction motor. The main part of the control system is the MPPT algorithm. In the present work a GSS-based one will be applied and therefore to show its performances; the conventional P&O algorithm is introduced for comparison purposes.

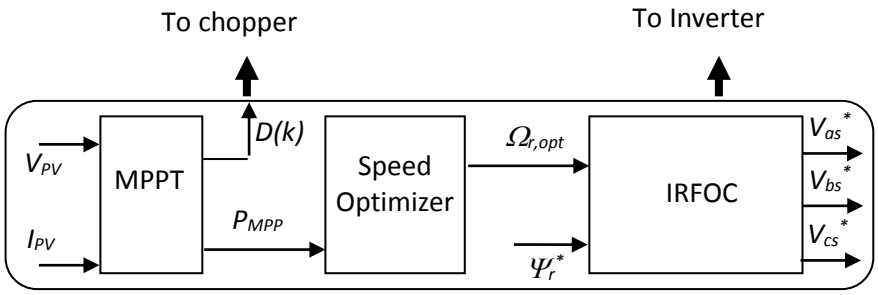

Figure 4.8 Control system components

IV.6.1 Rotor speed selection

When we are extracted the maximum power from the PVG, it is needs to be transferred to the motor-pump. The speed of the latter is controlled by IRFOC through PWM inverter. As long as the power is function of the speed and torque, a function relating the PVG power and the rotor speed can be derived if the motor losses are ignored. In steady state operation and upon neglecting friction losses, the motor torque will be the same as the pump torque which is given by [110]

$$T_{em} = T_L = K_p \Omega^2 \quad \text{(IV.28)}$$

If both sides of the above equation are multiplied by the rotor speed, the following equation of the power can be obtained:

$$P \approx T_L \Omega = K_p \Omega^3 \quad \text{(IV.29)}$$

PWM inverters are known by their very high efficiency and therefore the output power that is the induction motor's input is nothing but the PVG's output power, and the rotor speed which ensures maximum power transfer can be derived as follows:

$$\Omega_{opt} = \sqrt[3]{\left(\frac{P_{opt}}{K_p}\right)} \qquad \text{(IV.30)}$$

IV.7 Simulation Results and Discussion

Using the parameters of the Bp SX150S being derived from the datasheet at STC (TableII.1) and considering the size of the required PVG (N_{ser} x N_{par} =6x7) allow obtaining the P (V) and I (V) characteristics of the PV generator. At rated irradiance, E=1kW/m^2, the PVG delivers a maximum power of 6x7x150=6.3kW at voltage 6x34.5=207V if the load being connected to the PVG is able to absorb such amount of power, such as a resistance. By increasing the irradiance, the PVG's peak power output increases while operating voltage and current levels will be different as well. In solar water pumping system, the motor is connected to the PVG and the maximum power that can be extracted cannot exceed the rated power of the motor. To this the PVG is designed such that maximum power that can be obtained at STC (1kW/m^2) is greater than that of the motor demand. With Bp SX150S module being chosen and the motor-pump having the power of 5.5kW (Table IV.1), the optimal combination to satisfy the requirement in terms of power and voltage at the same time is an array of 6x7 modules. By using a boost chopper, the voltage is stepped up to much the requirement of the inverter fed-induction motor in terms of voltage.

Table IV.1 Pump-motor parameters

P=5.5kW	H=180(m)
Ω_m=2950(r/min)	Q=4.7(m^3/h)

The different components constituting the SWPS described in the previous section have been modeled using Malab/Simulink software. Sim Power System toolbox of Matlab has been used to model the power electronics part of the system; boost chopper and inverter. The values of capacitors and inductor used in the program are shown in Table IV.2.

Table IV.2 Boost chopper parameters

Element	Rating
Input capacitor, C1	225 µF
Inductor	0.481mH
Output capacitor, C2	5.8 µF

The curve of the PVG power can be carried by multiplying the PV current and PV voltage for three levels of insulation Figure 4.9 (E= [600, 800, 1000] w/m^2) with constant temperature (25^{0}C) Figure 4.10 (a-b).

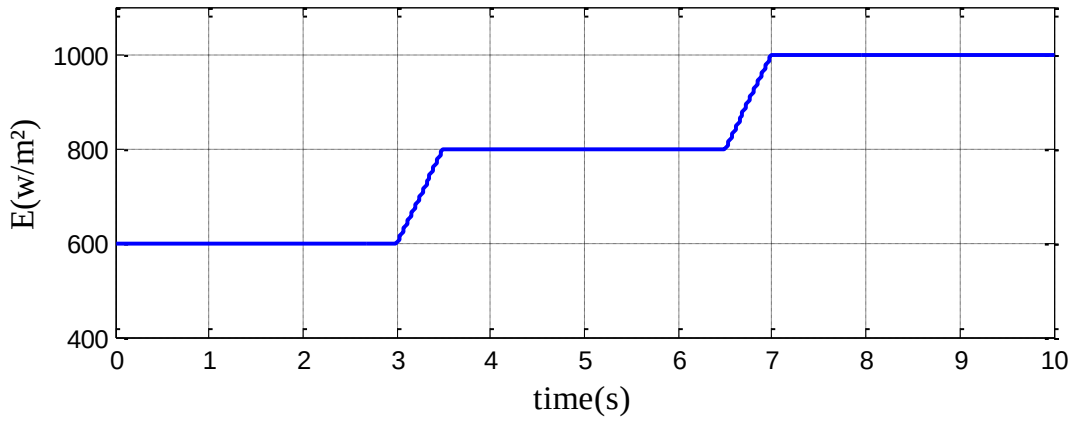

Figure 4.9 the irradiance level

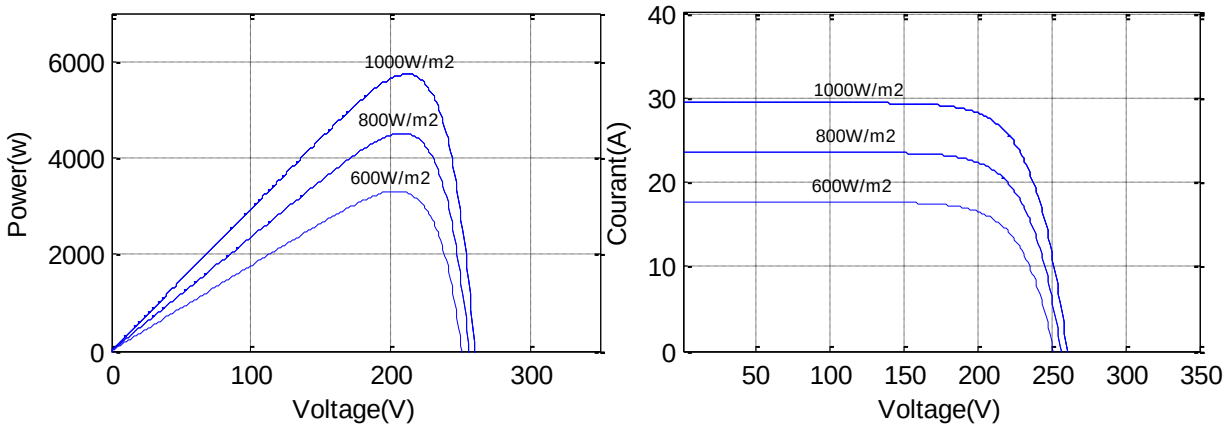

(a) (b)

Figure 4.10 P (V), I (V) characteristics at 25^{0}C

IV.7.1 SWPS using P&O algorithm

The transient characteristics of the MPP during a transient of solar irradiance it can be observed that the PV power, the PV output voltage and the PV output current, adjust to their optimal values during the solar irradiance variation, consequently the power of pump, the

rotation speed Ω converges to their reference values and flow rate as shown in Figure 4.11 (a, b, c, d and e).

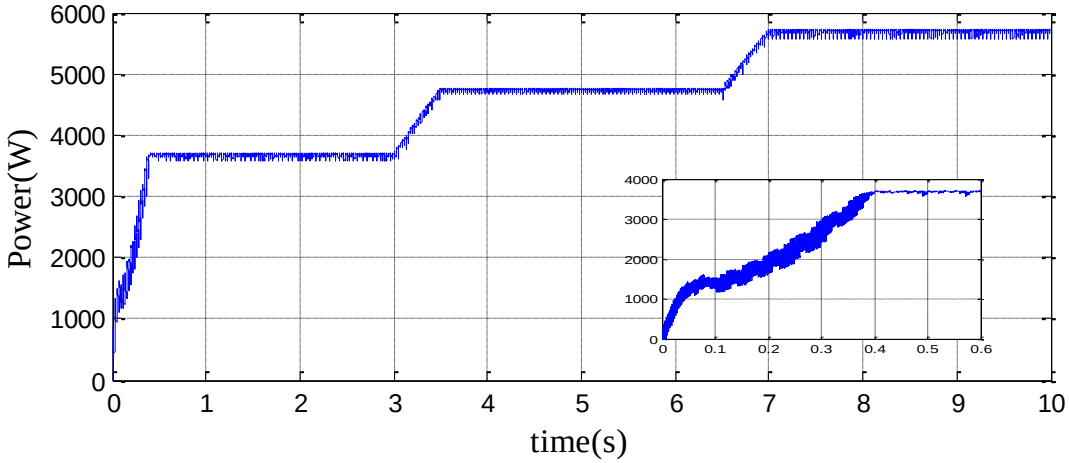

(a)

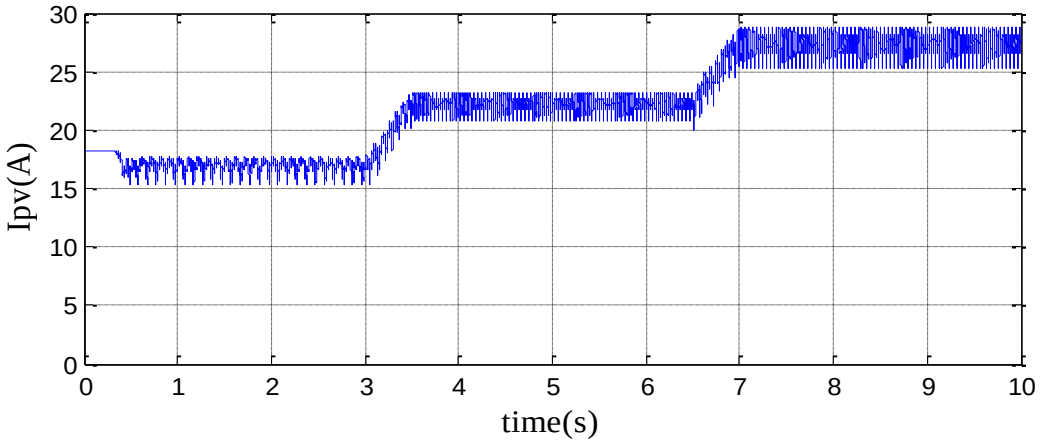

(b)

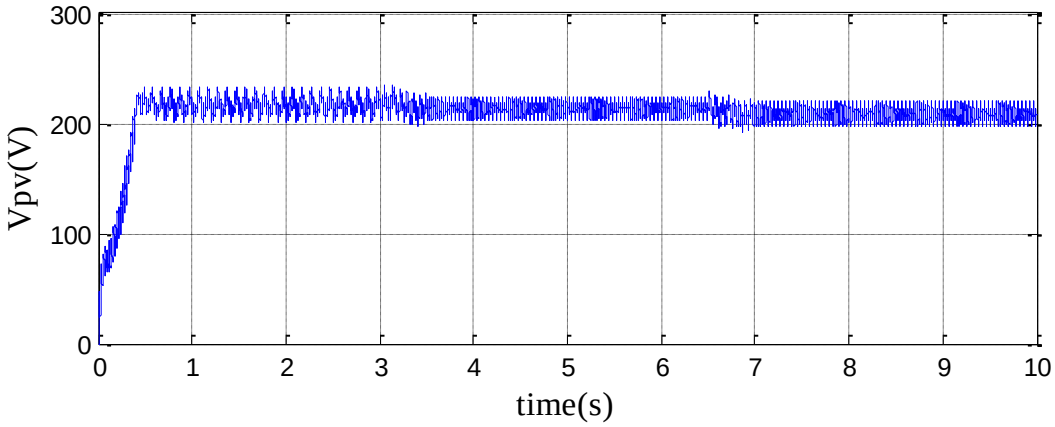

(c)

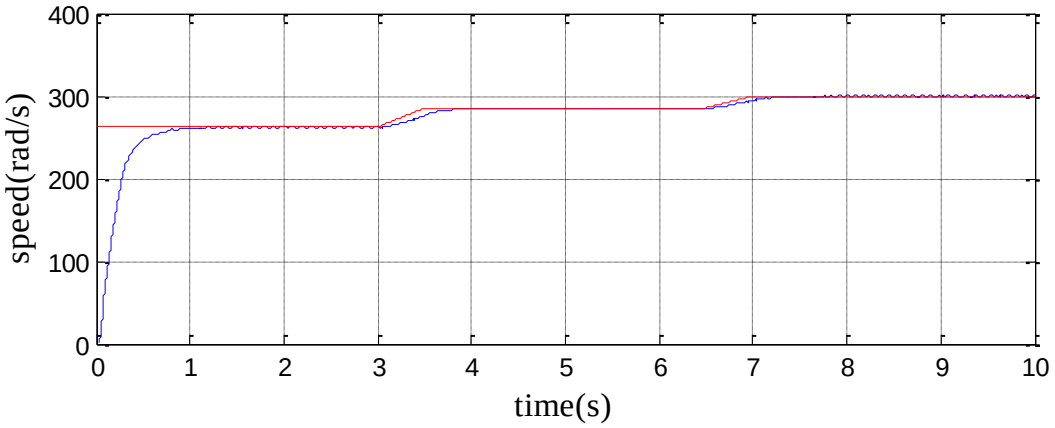

(d)

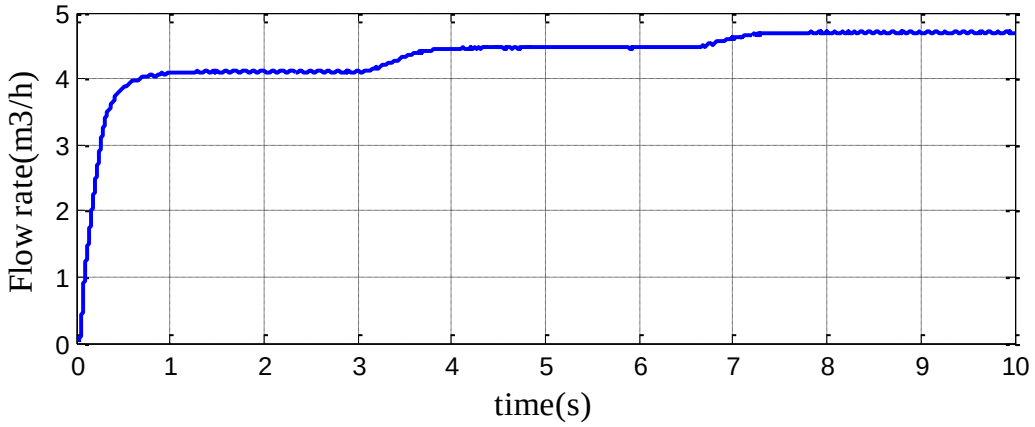

(e)

Figure 4.11 a) the photovoltaic power, (b) PV courant. (c) PV voltage of P&O. (d) Induction motor speed. (e) Water flow rate.

IV.7.2 SWPS using Golden section algorithm

In this section, the simulation is performed under different climatic conditions to verify the validity of the proposed search algorithm. Figure 4.12 shows the PV output power, current and voltage for the GSS control proposed in this research, the good speed and flow rate tracking has presented also in good tracking of the PVG power and hence maximum power transfer to the water pump.

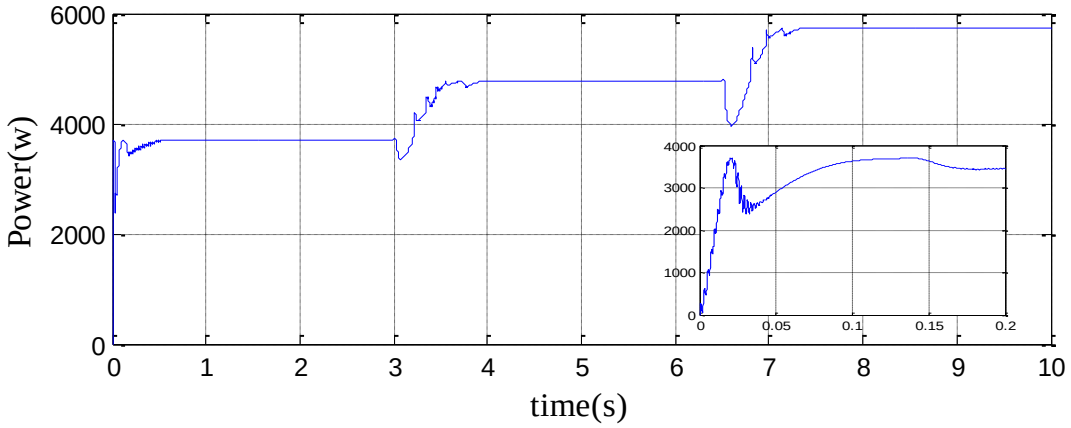

(a)

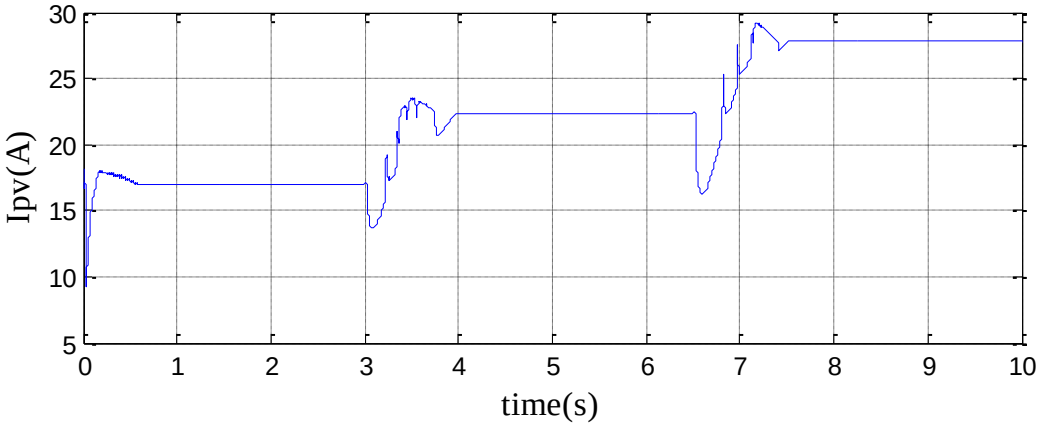

(b)

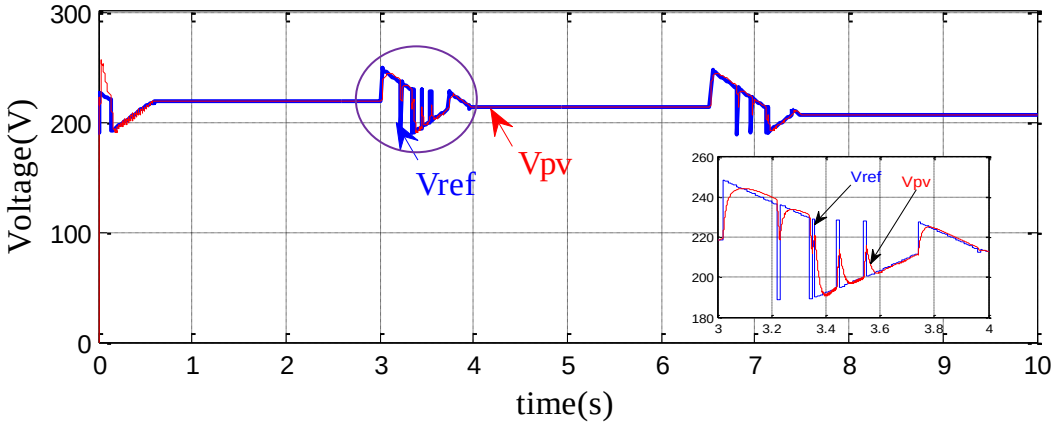

(c)

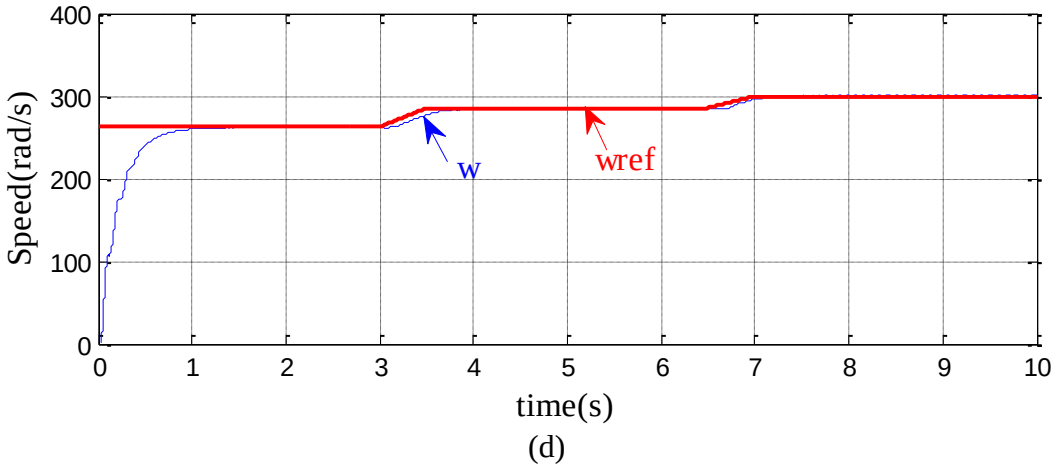

(d)

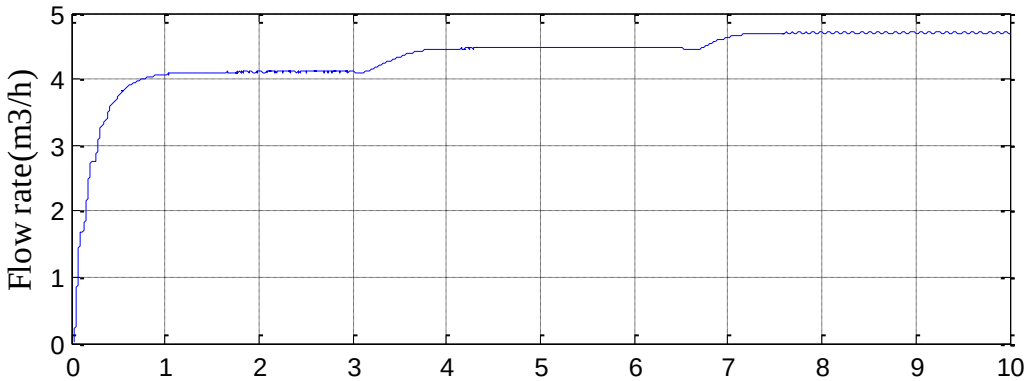

(e)

Figure 4.12(a) the photovoltaic power. (b) PV courant. (c) PV voltage and reference voltage using GSS. (d) Induction motor speed. (e) Water flow rate.

The variation of the reference voltage generated by the GSS based MPPT reaches the voltage at MPP. When the convergence is reached, and in order to ensure the transfer of this electric power to the motor, the speed of the motor is adjusted according to the irradiance. The motor speed is well controlled using the field oriented control, Figure 4.12(d). The increase in power will result in the increase of the water flow rate as depicted in Figure 4.12(e).

IV.7.2.1 Dynamic performance tracking of proposed technique

It is clear in previous section; the effectiveness of the proposed architecture in tracking the maximum power has been undertaken the irradiance changes from one level to another. However, the efficiency is affected also by the dynamic response and as well as the steady state error. To this, the concept of dynamic efficiency is introduced which represents the aptitude in tracking the MPP under variable climatic conditions. This efficiency is determined

by special variation of the irradiance according to the European Standard EN50530 [110]. In this case, the test sequence varies the irradiance from low level (30% of STC) to high level (100% of STC) with a step of 100 W/m^2. The pattern starts with an initial setup time and ends with the same period of time as shown in Figure 4.13. The values of the parameters used in Figure 4.13 are given in Table IV.3 where t1 represents the rise time, t2 is the dwell time on high irradiation level, t3 is the fall time, and t4 is the dwell time on low irradiation level, n is the repetition number [111]. Finally, the dynamic efficiency is computed as:

$$\eta_{dynamic} = \frac{\int_0^T P_{pv} dt}{\int_0^T P_{\max} dt}.100 \qquad \text{(IV.31)}$$

Where: P_{pv} represents the measured instantaneous power at the output of the PV generator; P_{max} illustrates the available maximum power at the PV generator.

Table IV.3 the test pattern applied in our study

Test no.	N	Step (W/m^2)	Initial setting time(s)	t1(s)	t2(s)	t3(s)	t4(s)	T(s)
1	1	100	10	7	10	7	10	44

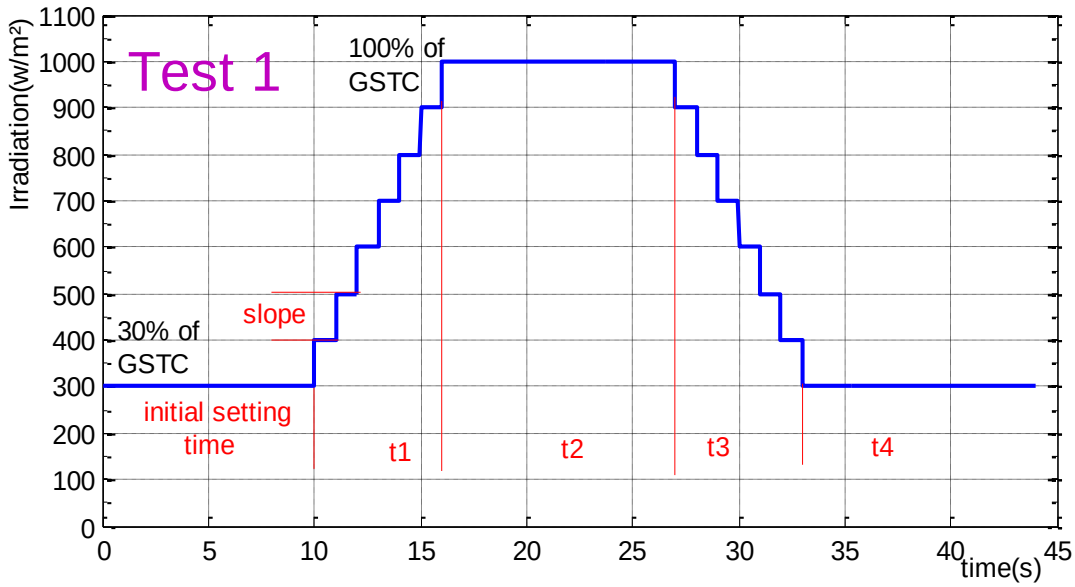

Figure 4.13 the test pattern for the dynamic efficiency of MPPT

The dynamic power tracking behavior and tracking error are depicted respectively in Figure 4.14(a) and Figure 4.14(b). The latter is the difference between the theoretical power corresponding to the irradiance shown in Figure 4.14 and the extracted one. One can notice from Figure 4.14(b) the occurrence of oscillations around the MPP just after each variation of the irradiance. These are the result of varying the voltage across the array before convergence. It can be noticed that theoretical maximum power that can be extracted at $1kW/m^2$ is approximately the sum of the motor's rated power and losses in it. Dynamic efficiency that is the ratio of maximum electric energy extracted over theoretical energy with Equation (IV.31). The dynamic efficiency has been found to be 99.15%.

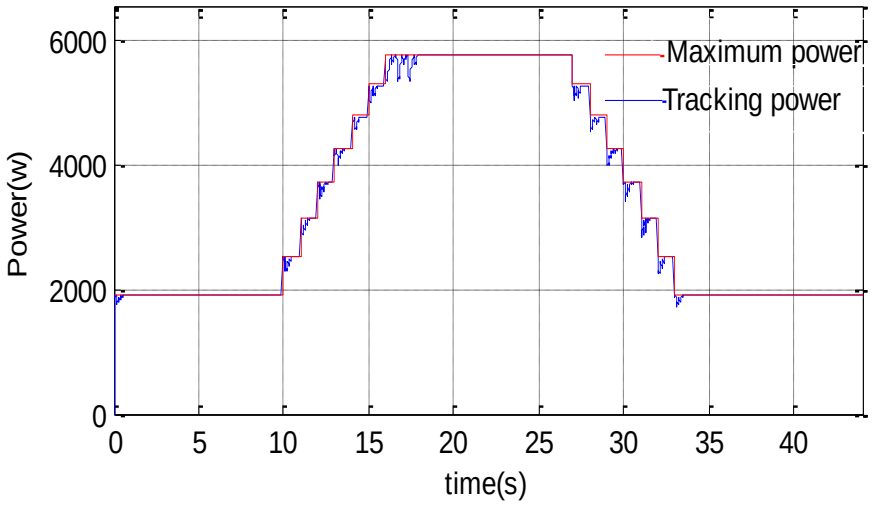

Figure 4.14.a Dynamic power tracking result

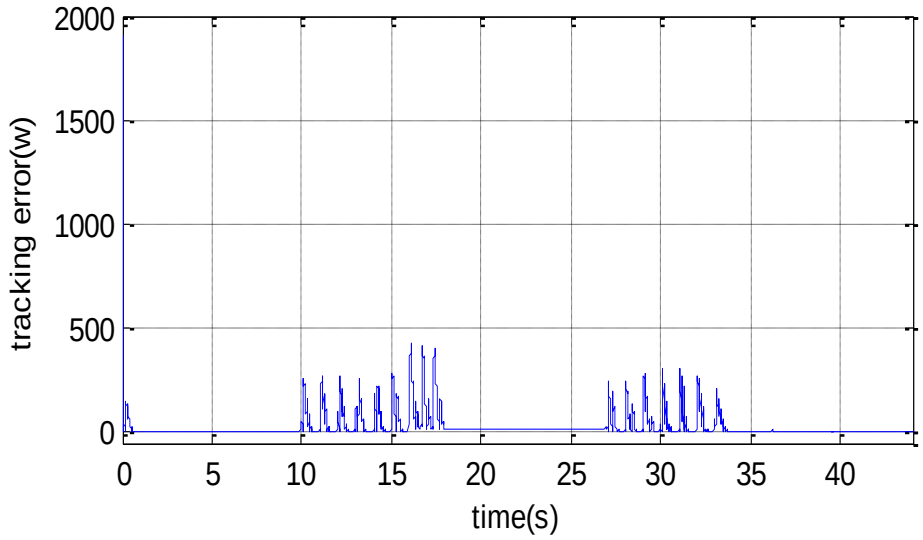

Figure 4.14.b Dynamic tracking error

IV.7.3 Comparison with P&O algorithm

The irradiance has been changed according to the profile shown in Figure 4.9 and the MPP traces obtained have been recorded for both P&O and GSS-based MPPTs controlled. The comparison of the two traces shown in Figure 4.15(a) and Figure 4.15(b), it can be easily noticed that GSS-based MPPT converges to the MPP without oscillations. The latter increases the electric energy waste and will undoubtedly affect the dynamic efficiency. Furthermore, Figure 4.15(b) shows that oscillation amplitude (power versus voltage) is greater than that of the P&O. This is to the due to the principle of GSS-based MPPT.

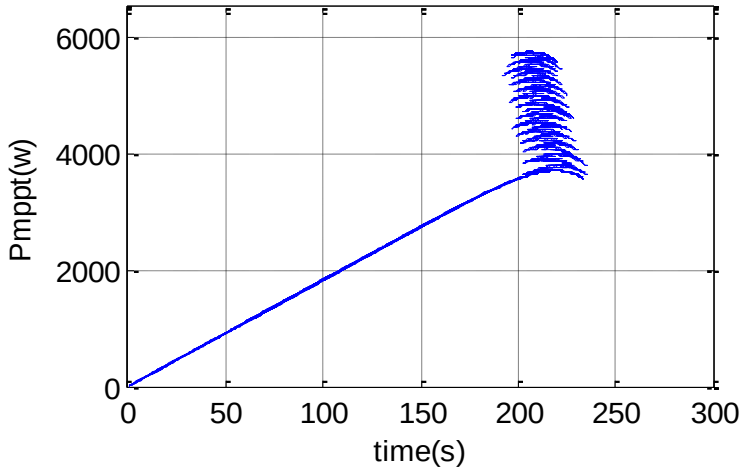

(a)

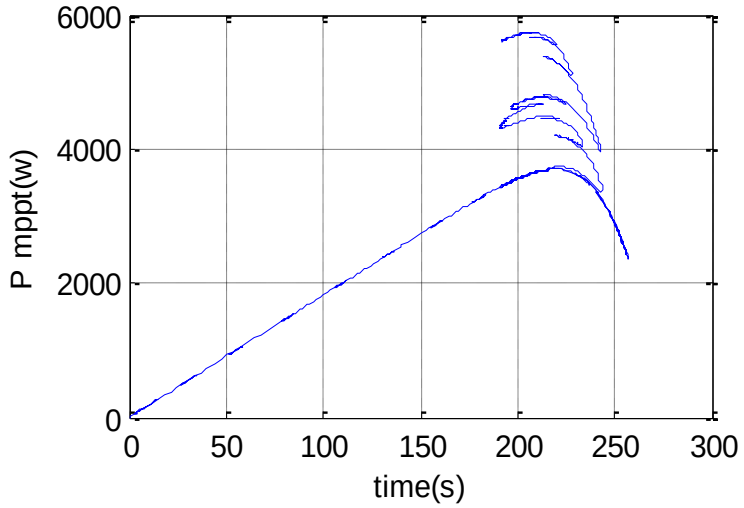

(b)

Figure 4.15 the PV power tracking; (a) P&O MPPT method. (b) GSS Proposed MPPT method

The simulation has been plotted in time domain as to show the time response of both maximum power extraction methods. The comparison of the power convergence to the right MPP illustrate in Figure 4.16 while the irradiance has undergone the variation profile given in Figure 4.9. It is clear that GSS-based MPPT is faster than the classical P&O MPPT technique. Other results of comparison are recorded in Table IV.4. Comparison is done in terms of dynamic efficiency, time response, perturbation and complexity level.

Table IV.4 Comparison the dynamic efficiency and complexity level

MPPT algorithm	$\eta_{dynamic\ \%}$	Response time	Complexity level
P&O	98.95	0.35	easy
Proposed algorithm(GSS)	99.15	0.25	easy

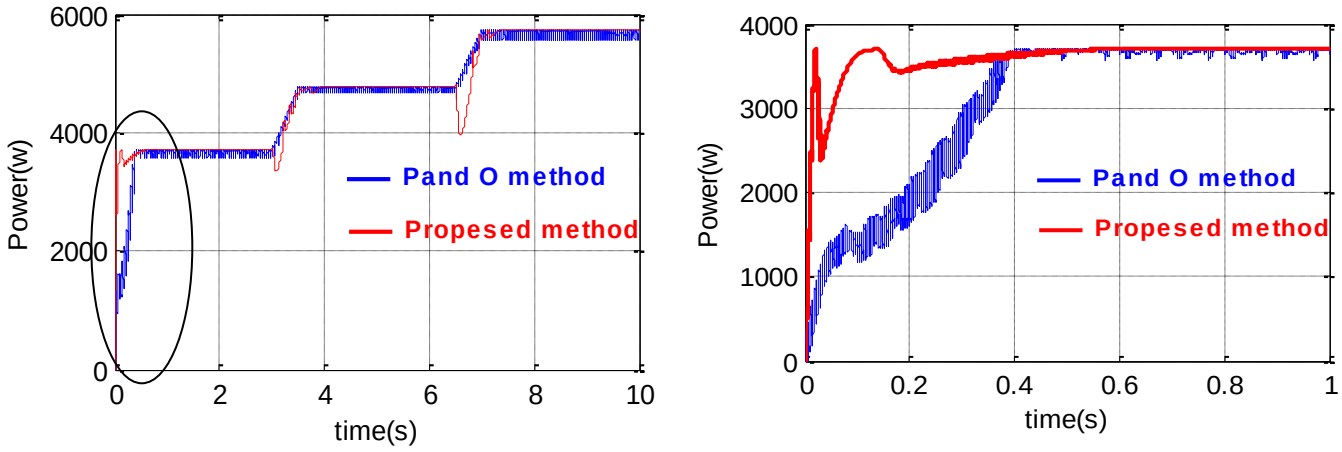

Figure 4.16 The PV powers of two MPPT methods under changing irradiance

IV.8 Conclusion

In this chapter, a comparison of SWPS performances using P&O and GSS-based MPPT is investigated. Selection of the induction motor to drive the centrifugal pump is justified by its robustness and low cost while the indirect field oriented controller is adopted to control the speed of the motor thanks to the availability of fast controllers with competitive prices. This thesis has presented the operation principle of the proposed GSS-based MPPT in order to

figure out its simplicity in comparison with P&O algorithm and its way of narrowing the search interval which results in fast convergence. Using the GSS-based MPPT in SWPS control systems is almost the same compared to that of the P&O method while the performances, following the obtained results, are much better in terms of time response, perturbation free and dynamic efficiency. This algorithm is intended to be applied for single-stage solar water pumping system. That is, the chopper component would be eliminated and the inverter will be controlled by a PWM algorithm. The latter, receives a reference value either voltage or current that is generated by the GSS –based MPPT algorithm.

As a general conclusion, we have shown that our proposed method is adequate for the searching of the MPP in the photovltaic pumping systems.

Chapter V

MPPT for Solar water pumping system using Dual Star Induction Motor

V.1 Introduction

The most popular application of the photovoltaic energy is stand-alone water pumping system driven by electrical motors. Indeed, it is the best adopted energy source to supply drinking and irrigating water in remote regions which economically cannot benefit from the national grid connection [112]. In such applications, high efficiency and reliability are required. Many types of motors are available for use in SWPS. For high power and/or when high reliability SWPS is required, AC induction motors seem to be the adequate alternative [113] compared to the aforementioned motors. The present chapter introduces the use of a multi-phase induction motor for SWPS.

For the development of power electronics and control technologies, the scope for AC machines continues to extend. The multiphase motor drive is a popular one and it has become attention due to developments in many popular applications, electric ship propulsion, traction (hybrid electric vehicles), the concept of aircraft, pumps, fans, compressors, rolling mills, cement mills, mine hoists…etc.) [114][115]. the advantages of multiphase machines over their compared to a three phases one or to a DC machines are: total rating of system is multiplied, the torque pulsations will be smoothed, the rotor harmonic losses as well as the harmonics content of the DC link current will be reduced, in *n*-phase machines it caused by 2n±1order harmonics, an increase for number of phases appear as the best solution of this problem and it have greater fault tolerance than the three phase which it's a total reliability with a much improved as the motor continues running with one of its many phases open- or short-circuited without much performance degradation [116]. A common type of multiphase machine is the dual star induction machine (DSIM). It is also known as the six-phase induction machine.

In this chapter, we focus on the study and analysis of performance (voltage, current, speed, torque, flow rate) of the DSIM through centrifugal pump fed by photovoltaic generator.

V.2 General description of the system

The DSIM being fed by solar panels by two PWM inverts drives the centrifugal pump. In order to improve the optimum operation of the system requires using of MPPT to investigate and exploit the maximum power delivered by solar panels with variation of irradiance and temperature [117]. However, the pump outputs which are water flow rate and head depends to variation of this power. Therefore, to optimize the SWPS, the speed of the

centrifugal pump must be set as to maximize the water flow rate. The proposed architecture is not able to guarantee the optimum speed operation. Optimized operation of SWPS has been achieved also however the derivation of the optimum speed leading to maximum efficiency is not discussed. Indirect rotor field oriented control scheme is selected to control the speed of the DSIM being coupled to the centrifugal pump [118]. In addition, it offers a fast torque and flux control response hence a fast speed control [119].

Speed control of DSIM is often undertaken using conventional PI controller. The design of the later requires the use of the motor model being linearized around the rated operating point. However, during the operation, the motor internal parameters and the operating point will be subject to variation and this alters the performance of the speed control [119,120]. Better global reliability as well as speed control would be obtained if less sensitive speed controller is used. In this work, it is suggested to use fuzzy sets-based PI controller instead of the conventional PI controller.

V.3 Modeling of SWPS

The system studied is a cascade constituting of photovoltaic generator (PVG), Boost converter controlled by the MPPT control, two PWM inverters, the DSIM and finally the centrifugal pump. The structure of this cascade is shown in Figure 5.1.

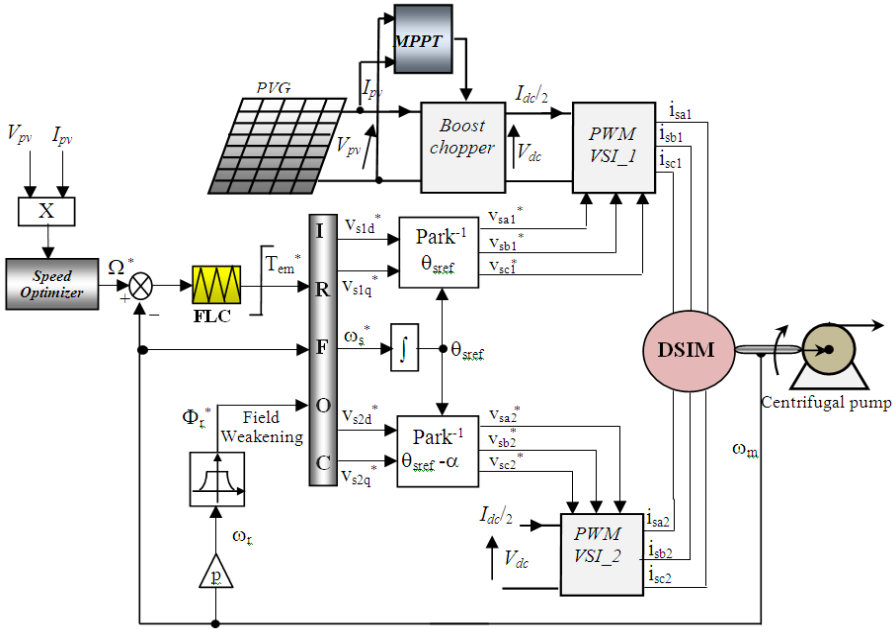

Figure 5.1 System simulation model of the proposed SWPS with DSIM

V.3.1 Photovoltaic generator and Boost converter

The solar panel has an optimal operating point which can supply the maximum power to the load, the power of the panel generator which study in Chapter I must be adjusted to the appropriate value by regulating the voltage of PV panel to the MPP operating voltage. The technique conventionally employed is to use an adaptation stage between the PVG and the load. In our study we use a boost converter, which is mostly used in photovoltaic applications, especially in photovoltaic pumping system.

This converter is important in PV system since it has the ability of regulating the output voltage [121]. The output voltage can be controlled to be greater than the input voltage by varying the duty cycle control. The control that makes the PVG's output power as close as possible to $P_{max}$is known as MPPT.

MPPT stands for maximum power point tracking which is essential for optimizing the PVG operation and the whole system performance. Improving the performances of PV-fed systems in general is very important issue for scientific community as well as for industrial investors as long as the central problem of the PVG is the low efficiency. There are several methods that have been widely used to track the MPP such as the P&O technique known for its speed, accuracy and quality of sizes obtained by the proper choice of the step increment [122], that it's used in this chapter.

V.3.2 PWM Voltage Source Inverter

The three-phase inverter is one of the structures used in energy conversion for powering AC loads; it consists of three independent legs. Each one includes two switches which are complementary and controlled by the Pulse Width Modulation (PWM) circuit [123].

The induction motor stator voltages (V_{sa}, V_{sb}, V_{sc}) are expressed in terms of states of the upper switches as below:

$$\begin{bmatrix} V_{sa} \\ V_{sb} \\ V_{sc} \end{bmatrix} = \frac{U_{pv}}{3} \begin{bmatrix} 2 & -1 & -1 \\ -1 & 2 & -1 \\ -1 & -1 & 2 \end{bmatrix} \begin{bmatrix} f_{11} \\ f_{12} \\ f_{13} \end{bmatrix} \quad \text{(V.1)}$$

U_{pv}: The photovoltaic voltage

f_{11}, f_{12} and f_{13} are the controller signals applied to the inverter's three upper switches. Figure 5.2 shows the control circuit which generates these signals using the classical sinusoidal pulse width modulation method (SPWM).

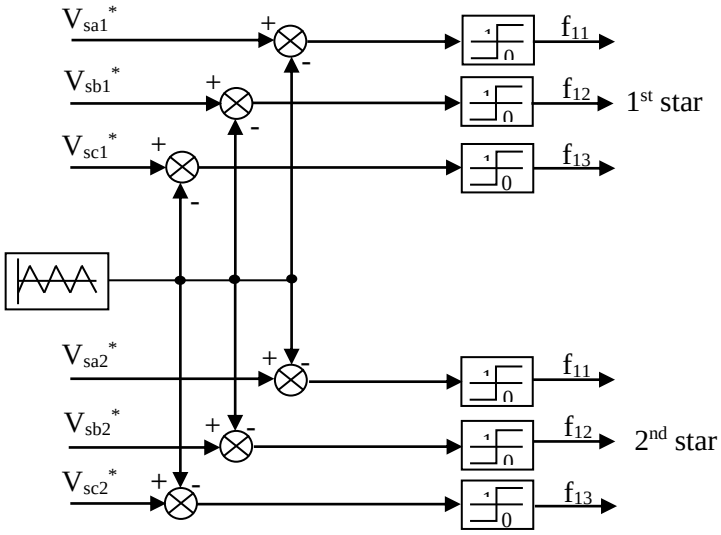

Figure 5.2 DSIM fed by SPWM controlled inverters

V.3.3 Dual Start Induction Motor

A schematic of the stator and rotor windings for a machine dual three phase is given in Figure 5.3 The six stator phases are divided into two wyes-connected three phase sets labeled As1, Bs1, Cs1 and As2, Bs2, Cs2 whose magnetic axes are displaced by an angle α=30°. The windings of each three phase set are uniformly distributed and have axes that are displaced 120° apart. The three phase rotor windings Ar, Br, Cr are also sinusoidal distributed and have axes that are displaced apart by 120° [124].

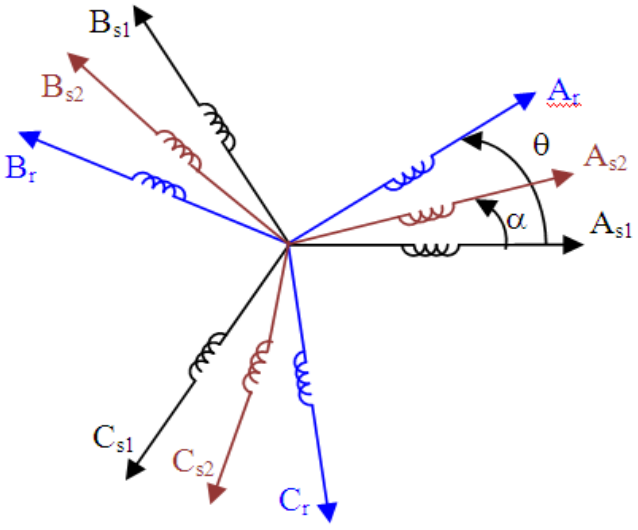

Figure 5.3 Windings of the dual star induction machine

V.3.3.1 Electrical equation

The voltage equations of the dual stator induction machine are as follow [119]:

$$[V_{s1}]=\begin{bmatrix}V_{sa1}\\V_{sb1}\\V_{sc1}\end{bmatrix}=[R_{s1}][I_{s1}]+\frac{d}{dt}[\Phi_{s1}] \quad (V.2)$$

$$[V_{s2}]=\begin{bmatrix}V_{sa2}\\V_{sb2}\\V_{sc2}\end{bmatrix}=[R_{s2}][I_{s2}]+\frac{d}{dt}\left[\Phi_{s2}\right] \quad (V.3)$$

$$[0]=\begin{bmatrix}V_{ra}\\V_{rb}\\V_{rc}\end{bmatrix}=[Rr][Ir]+\frac{d}{dt}[\Phi_{r}] \quad (V.4)$$

Where:

$R_{sa1} = R_{sb1} = R_{sc1} = R_{s1}$: Star resistance 1.

$R_{sa2} = R_{sb2} = R_{sc2} = R_{s2}$: Star resistance 2.

$R_{ra} = R_{rb} = R_{rc} = R_r$: Rotor resistance.

$$[R_{s1}]=\begin{bmatrix}R_{s1}&0&0\\0&R_{s1}&0\\0&0&R_{s1}\end{bmatrix};\ [R_{s2}]=\begin{bmatrix}R_{s2}&0&0\\0&R_{s2}&0\\0&0&R_{s2}\end{bmatrix};\ [R_{r}]=\begin{bmatrix}R_{r}&0&0\\0&R_{r}&0\\0&0&R_{r}\end{bmatrix} \quad (V.5)$$

$$[I_{s1}]=\begin{bmatrix}I_{sa1}\\I_{sb1}\\I_{sc1}\end{bmatrix};\ [I_{s2}]=\begin{bmatrix}I_{sa2}\\I_{sb2}\\I_{sc2}\end{bmatrix};[I_{r}]=\begin{bmatrix}I_{ra}\\I_{rb}\\I_{rc}\end{bmatrix} \quad (V.6)$$

V.3.3.2 Flux equation

$$[\Phi_{s1}]=\begin{bmatrix}\Phi_{sa1}\\\Phi_{sb1}\\\Phi_{sc1}\end{bmatrix};[\Phi_{s2}]=\begin{bmatrix}\Phi_{sa2}\\\Phi_{sb2}\\\Phi_{sc2}\end{bmatrix};[\Phi_{r}]=\begin{bmatrix}\Phi_{ra}\\\Phi_{rb}\\\Phi_{rc}\end{bmatrix} \quad (V.7)$$

The expressions for star and rotor flux are [119]:

$$\begin{bmatrix}[\Phi_{s1}]\\[\Phi_{s2}]\\[\Phi_{r}]\end{bmatrix}=\begin{bmatrix}[L_{s1s1}]&[L_{s1s2}]&[L_{s1r}]\\[L_{s2s1}]&[L_{s2s2}]&[L_{s2r}]\\[L_{rs1}]&[L_{rs2}]&[L_{rr}]\end{bmatrix}.\begin{bmatrix}[I_{s1}]\\[I_{s2}]\\[I_{r}]\end{bmatrix} \quad (V.8)$$

Where:

[Ls1s1]: Inductance matrix of the star 1.

[Ls2s2] : Inductance matrix of the star 2.

[Lrr] : Inductance matrix of the rotor.

[Ls1s2]: Mutual inductance matrix between star 1 and star 2.

[Ls2s1]: Mutual inductance matrix between star 2 and star 1.

[Ls1r] : Mutual inductance matrix between star 1 and rotor.

[Ls2r] : Mutual inductance matrix between star 2 and rotor.

[Lrs1] : Mutual inductance matrix between rotor and star 1.

[Lrs2]: Mutual inductance matrix between rotor and star 2.

V.3.3.3 Mechanical equation

The equation of the electromagnetic torque is then as follows [123] [124] [125]:

$$Tem = \left(\frac{p}{2}\right).\left([I_{s1}]\frac{d}{d\theta}[L_{s1r}][I_r] + [I_{s2}]\frac{d}{d\theta}[L_{s2r}][I_r]\right) \quad (V.9)$$

The above *ABC* model (V.2-V.9) of the DSIM is very complex for simulation as well as for control design. Apart of time-varying inductances elimination due to 90° between *d* and *q*-magnetic axes, (see Figure 5.4), Park transformation allows reducing the number of the differential equations and obtaining equivalent dc stator and rotor quantities to be used for vector control design. The obtained Park model of the dual star induction machine in the rotating reference frame described by subscript (*d*, *q*), is given below equations (V.10) [126].

V.3.4 The dynamic d-q model using PARK's transformation

The Park model of the dual star induction machine in the references frame at the rotating field (d, q), is defined by the following equations (V.10) [120].

The Figure 5.4 shows the DSIM windings (stator and rotor windings) in the rotating reference frame.

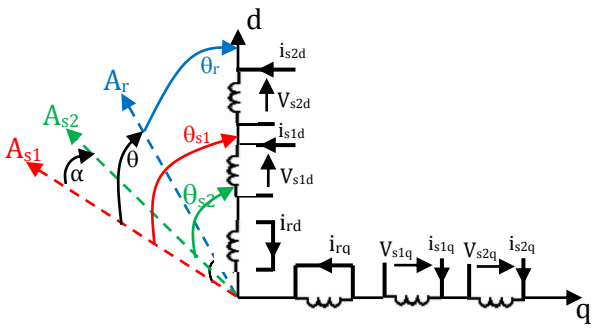

Figure 5.4 *d*-and *q*-windings of the DSIM in the rotating reference frame

$$
\begin{aligned}
V_{s1d} &= R_{s1}I_{s1d} + \frac{d}{dt}\Phi_{s1d} - \omega_s\Phi_{s1q} \\
V_{s1q} &= R_{s1}I_{s1q} + \frac{d}{dt}\Phi_{s1q} + \omega_s\Phi_{s1d} \\
V_{s2d} &= R_{s2}I_{s2d} + \frac{d}{dt}\Phi_{s2d} - \omega_s\Phi_{s2q} \\
V_{s2q} &= R_{s2}I_{s2q} + \frac{d}{dt}\Phi_{s2q} + \omega_s\Phi_{s2d} \\
0 &= R_rI_{rd} + \frac{d\Phi_{rd}}{dt} - \omega_{sr}\Phi_{rq} \\
0 &= R_rI_{rq} + \frac{d\Phi_{rq}}{dt} + \omega_{sr}\Phi_{rd}
\end{aligned}
\qquad (V.10)
$$

Where:

$$
\begin{aligned}
\Phi_{s1d} &= L_{s1}I_{s1d} + L_m(I_{s1d} + I_{s2d} + I_{rd}) \\
\Phi_{s1q} &= L_{s1}I_{s1q} + L_m(I_{s1q} + I_{s2q} + I_{rq}) \\
\Phi_{s2d} &= L_{s2}I_{s2d} + L_m(I_{s1d} + I_{s2d} + I_{rd}) \\
\Phi_{s2q} &= L_{s2}I_{s2q} + L_m(I_{s1q} + I_{s2q} + I_{rq}) \\
\Phi_{rd} &= L_rI_{rd} + L_m(I_{s1d} + I_{s2d} + I_{rd}) \\
\Phi_{rq} &= L_rI_{rq} + L_m(I_{s1q} + I_{s2q} + I_{rq})
\end{aligned}
\qquad (V.11)
$$

Where Lm is cyclic mutual inductance between star 1, star 2 and rotor

The mechanical equation is given by:

$$J\frac{d\Omega}{dt} = T_{em} - T_L - F_r\Omega \qquad (V.12)$$

With:

$$Tem = p\frac{L_m}{L_r + L_m}\left[\Phi_{rd}(I_{s1q} + I_{s2q}) - \Phi_{rq}(I_{s1d} + I_{s2d})\right] \qquad (V.13)$$

Where:

F_r is friction coefficient

T_{em} is electromagnetic torque

T_L is Load torque

p is number of pole pairs

V.3.5 Centrifugal Pump

Depending upon the intended application, the pump of the SWPS can be selected to be surface, submersible or floating pump described in section IV.3.4. In this chapter, we used the centrifugal pump.

V.3.6 IRFOC of DSIM

Field oriented control allows controlling the induction motor exactly as the separately excited DC motor. The stator current is optimally resolved to direct component which controls the flux level and to transverse component which controls the torque. In other words, in case or rotor flux orientation, if the *d*-axis of park frame is oriented towards the q-component of this flux will be null and its d-component will be the rotor flux. The IRFOC equations are obtained by making $\emptyset_{qr}=0$ while the direct component equals the reference rotor flux $\emptyset_r^*$ [127, 119].

By applying this principle ($\emptyset_{qr}=0$ and $\emptyset_{dr}=\emptyset_r^*$) to equations (V.5) (V.6) and (V.8), the electromagnetic torque and the slip frequency would be as follows [119]:

$$T_{em} = p\frac{L_m}{L_m + L_r}\Phi_r^* \left(I_{s1q}^* + I_{s2q}^*\right) \tag{V.14}$$

$$w_{sr}^* = \frac{R_r L_m}{\left(L_m + L_r\right)\Phi_r^*}\left(I_{s1q}^* + I_{s2q}^*\right) \tag{V.15}$$

The stator voltage equations are:

$$\begin{aligned}
V_{s1d}^* &= R_{s1}I_{s1d} + L_{s1}\frac{d}{dt}I_{s1d} - \omega_s^*\left(L_{s1}I_{s1q} + T_r\,\Phi_r^* w_{sr}^*\right)\\
V_{s1q}^* &= R_{s1}I_{s1q} + L_{s1}\frac{d}{dt}I_{s1q} + \omega_s^*\left(L_{s1}I_{s1d} + \Phi_r^*\right)\\
V_{s2d}^* &= R_{s2}I_{s2d} + L_{s2}\frac{d}{dt}I_{s2d} - \omega_s^*\left(L_{s2}I_{s2q} + T_r\,\Phi_r^* w_{sr}^*\right)\\
V_{s2q}^* &= R_{s2}I_{s2q} + L_{s2}\frac{d}{dt}I_{s2q} + \omega_s^*\left(L_{s2}I_{s2d} + \Phi_r^*\right)
\end{aligned} \tag{V.16}$$

Equations (V.14) and equation (V.16) show that there is still some coupling between d- and q-control voltages due to presence of ω_s^* in both equations. Thus, overcome this coupling between torque and rotor flux, we introduce new control variables:

$$
\begin{aligned}
V_{s1d} &= R_{s1} I_{s1d} + L_{s1} \frac{d}{dt} I_{s1d} \\
V_{s1q} &= R_{s1} I_{s1q} + L_{s1} \frac{d}{dt} I_{s1q} \\
V_{s2d} &= R_{s2} I_{s2d} + L_{s2} \frac{d}{dt} I_{s2d} \\
V_{s2q} &= R_{s2} I_{s2q} + L_{s2} \frac{d}{dt} I_{s2q}
\end{aligned}
\qquad (V.17)
$$

The system equations (V.17) show that the new stator voltages *(V_{s1d}, V_{s1q}, V_{s2d}, V_{s2q})* are now directly related to the stator currents (I_{s1d}, I_{s1q}, I_{s2d}, I_{s2q}). The torque and flux control voltages which will be applied to the PWM circuit are obtained after having compensating for the coupling by adding or subtracting the appropriate terms. The reference voltages (V_{s1d}^*, V_{s2d}^*, V_{s1q}^*, V_{s2q}^*) at constant flux are given by:

$$
\begin{aligned}
V_{s1d}^* &= V_{s1d} - V_{s1dc} \\
V_{s1q}^* &= V_{s1q} + V_{s1qc} \\
V_{s2d}^* &= V_{s2d} - V_{s2dc} \\
V_{s2q}^* &= V_{s2q} + V_{s2qc}
\end{aligned}
\qquad (V.18)
$$

Where

$$
\begin{aligned}
V_{s1dc} &= \omega_s^* (L_{s1} I_{s1q} + T_r \Phi_r^* w_{sr}^*) \\
V_{s1qc} &= \omega_s^* (L_{s1} I_{s1d} + \Phi_r^*) \\
V_{s2dc} &= \omega_s^* (L_{s2} I_{s2q} + T_r \Phi_r^* w_{sr}^*) \\
V_{s2qc} &= \omega_s^* (L_{s2} I_{s2d} + \Phi r^*)
\end{aligned}
\qquad (V.19)
$$

To realize the decoupling between torque and flux current components in terms of steady state error and time response, stator current PI controllers (I_{s1d}, I_{s1q}, I_{s2d}, I_{s2q}) can be inserted and the control stator voltages will be obtained at the output of these controllers. The block diagram of the structure and the system of voltage fed and rotor field Oriented controlled-DSIM is summarized in Figure 5.5.

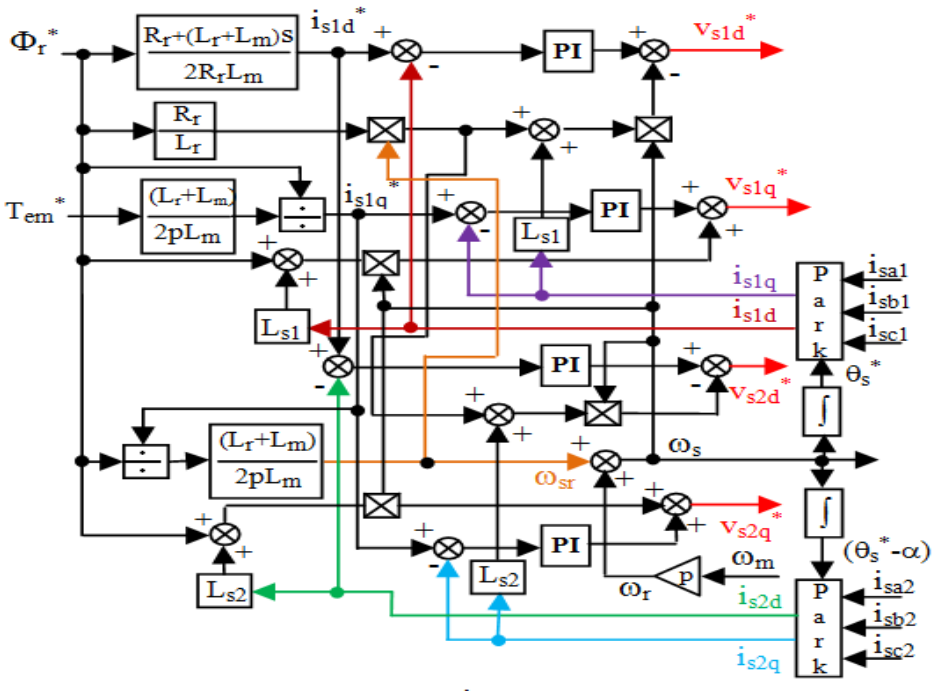

Figure 5.5 Voltage fed- DSIM with Rotor Field Orientation Control scheme

V.3.6.1 Speed optimizer

Global optimization technique of the SWPS requires that MPP of the PVG is transferred to the water pump. In [128, 129] it is proposed to determine a relationship between the irradiance and the rotor speed using curve fitting, however this approximation results in speed error and consequently near optimal speed operation [119]. Need the section IV.6.1, Table V.1 shows an example of computation of optimal rotor speed and represents the reference speed. For three different solar irradiations, the rotor speed is varied accordingly to guarantee this maximum power transfer.

Table V.1 variation of reference speed with respect to P_{max} and irradiance level

G(W/m2)	P_{mpp}(W)	Ω_{opt}(rad/s)
600	3050	263.52
800	3895	285.90
1000	4630	302.86

V.3.6.2 Speed Fuzzy logic control

Fuzzy logic control uses Fuzzy sets and Fuzzy inference to derive control laws in which no precise model of the plants is available, and most of the expertise is available only in qualitative form. The basic idea of Fuzzy Logic control is to make use of expert knowledge to

build a rule based controllers [130]. The Fuzzy control processing, in general, is typically divided into the following three stages: fuzzification, inference engine plus rules base and defuzzification, as shown in Figure 5.6. The Fuzzification process means that real world variables are translated into Fuzzy values using fuzzy sets (fuzzy set membership). The control algorithm is coded using Fuzzy statements in the block containing the knowledge base by taking into account the control objectives and the system behavior. The second stage includes the rules base and the Fuzzy inference engine. The control objectives taking into account the system behavior are coded under the form of rules "IF THEN". The way it is processed the fuzzy rule is decided by the inference engine. The results of the Fuzzy computations are translated in terms of real values for the Fuzzy control action by the Defuzzification block [130] [132].

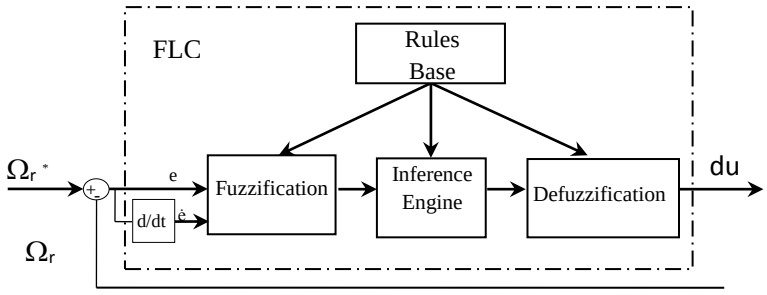

Figure 5.6 Fuzzy Logic Controller structure

There is no systematic methodology to select the FLC system parameters, such as the number fuzzy sets, the shape of membership functions, and the universe of discourse of input and output variables, etc. The greater is the number of linguistic values the more processing time it requires and better accuracy is obtained. In this chapter, following our experience in using fuzzy logic, we have chosen a Fuzzy logic controller with five fuzzy values (Negative Large, Negative, Zero, Positive, Positive Large) for each variable of the controller. The middle fuzzy values have triangle membership functions whereas the extreme values have rectangular shape [119]. Figure 5.7 shows the parameters of each variable used in the FL Controller.

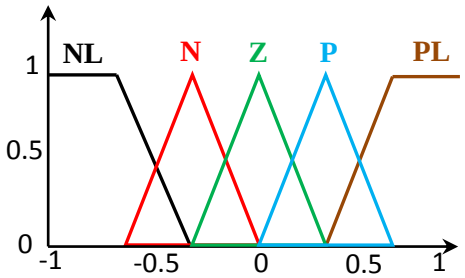

Figure 5.7Universe of discourse, fuzzy values and their membership functions

The inputs to the fuzzification process are the speed error and its derivative after being normalized according to the following expressions:

$$e(k) = \alpha_1.\left(\Omega_r^*(k) - \Omega_r(k)\right)$$
$$\dot{e}(k) = \alpha_2.\frac{\left(\Omega_r(k-1) - \Omega_r(k)\right)}{T_s} \quad \text{(V.20)}$$

Where

α_1, α_2 are the input normalization gains and T_s is the sampling time.

The rules base is essentially to establish the control strategy of the system. It is usually obtained from expert knowledge. It contains a collection of Fuzzy conditional statements expressed as a set of *If-Then* rules [131]. An example of rule type: if ***e*** is negative large, ***ė*** is positive large, then ***u*** is zero, where: ***e*** (speed error: is calculated with comparison between reference speed and speed signal feedback) and ***ė*** (The derivative of the error) represent two input variables of the Fuzzy controller and ***du*** represents the output variable (reference torque's variation) [119]. Table V.2 contains all the rules for all the fuzzy values of both input variables; the speed error «*e*» and its variation « ***ė*** » and the output variable «*du*».

Table V.2 Fuzzy rules base for speed control

du		***e***				
		NL	N	Z	P	PL
de	NL	NL	NL	NL	N	Z
	N	NL	N	N	Z	P
	Z	NL	N	Z	P	PL
	P	N	Z	P	P	PL
	PL	Z	P	PL	PL	PL

The used fuzzy controller has the same behavior as that of a conventional PI controller; therefore the output of the fuzzy controller will be torque variation and therefore the torque reference is given by

$$T_{em}^*(k+1) = T_{em}^*(k) + \alpha_3 du \quad \text{(V.21)}$$

Where

α_3 is the output normalization gains and du is the torque variation.

V.4 Simulation results and discussion

In this section, several simulations were performed under different operating conditions to verify the effectiveness and validity of the proposed search controllers applied to the photovoltaic water-pumping system using fuzzy indirect field oriented control, a simulation framework has been carried out. The proposed design scheme shown in Figure 5.1 is implemented using Matlab/Simulink software where the parameters of DSIM and centrifugal pump are given below.

Table V.3 Dual Stator Induction Machine parameters

P_n [kw]	4.5	R_r [Ω]	2 .12	J [kg.m²]	0.062
V_n [V]	220	L_{s1} [H]	0.022	F_r [Nms/r]	0.001
I_n [A]	6.5	L_{s2} [H]	0.022	f [Hz]	50
R_{s1} [Ω]	3.72	L_r [H]	0.006	p	1
R_{s2} [Ω]	3.72	L_m [H]	0.367	Cos φ	0.8

Table V.4 Pump model parameters

Q=4.7(m^3/h)	H=180(m)
N=2950(r/min)	

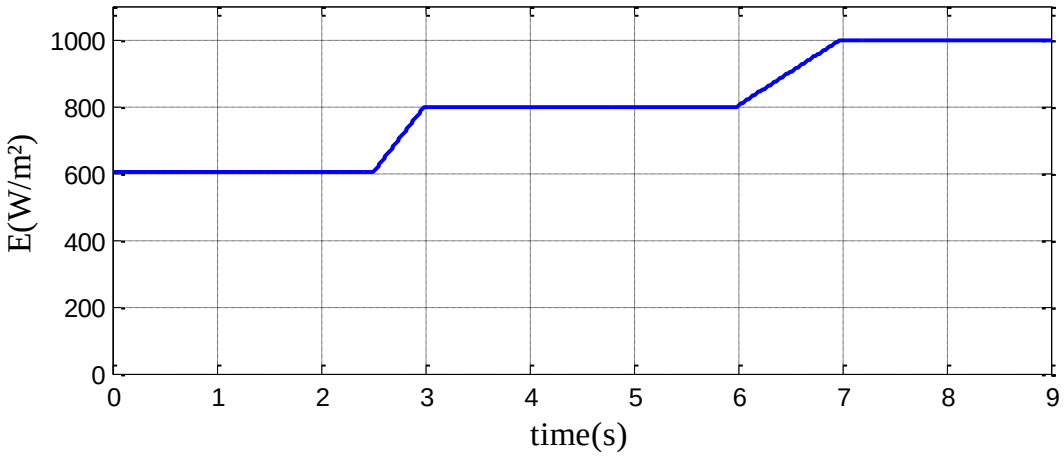

Figure 5.8 Irradiance level variations

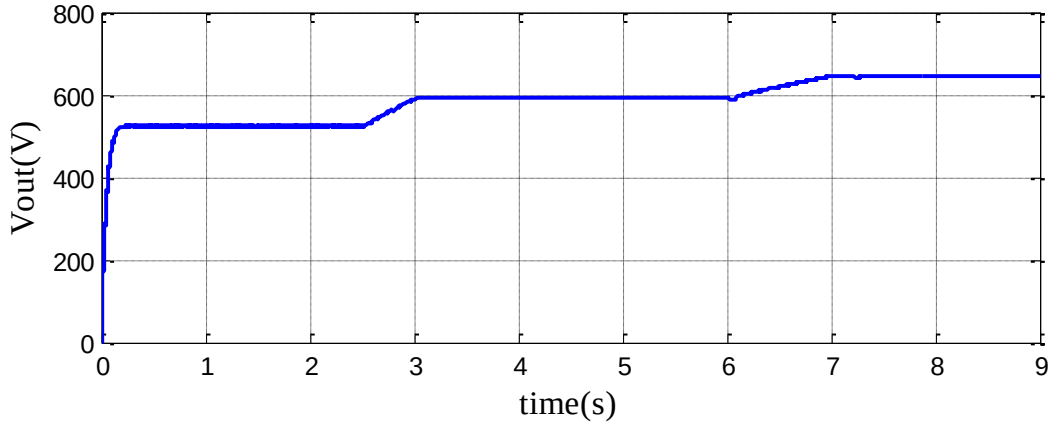

Figure 5.9 the output voltage

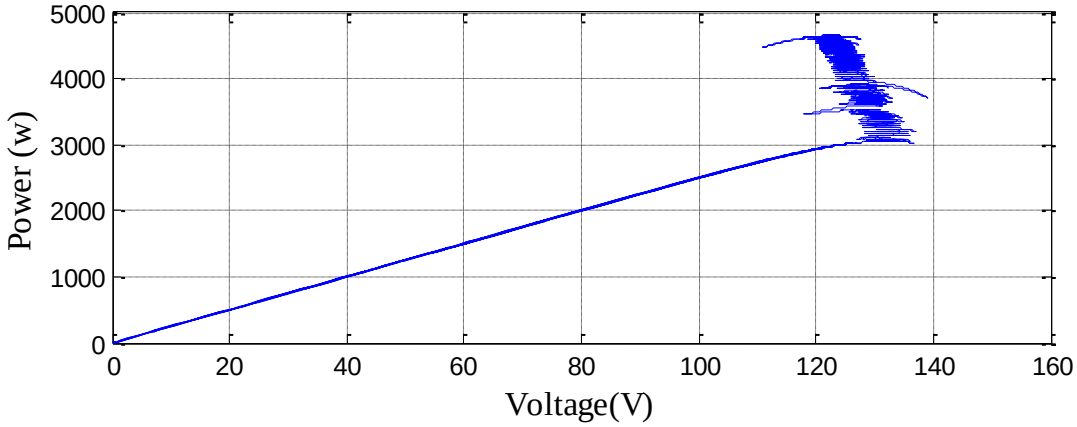

Figure 5.10 the MPPT trajectory

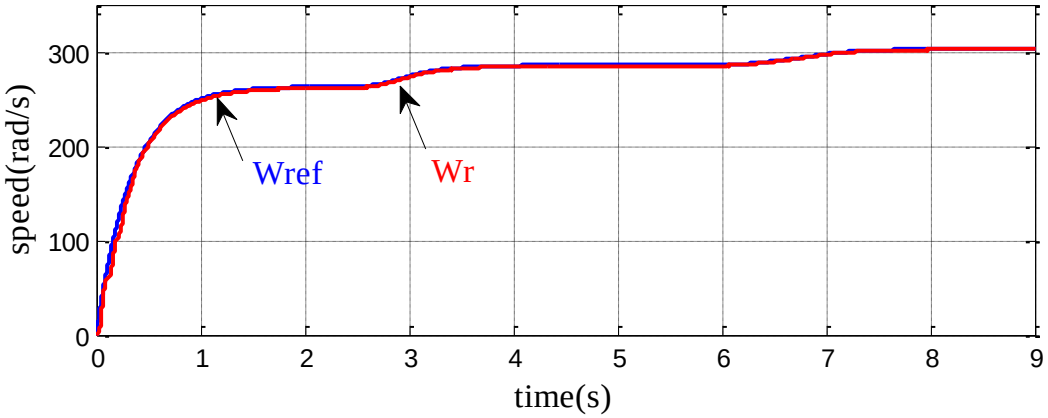

Figure 5.11 rotational speed and its reference

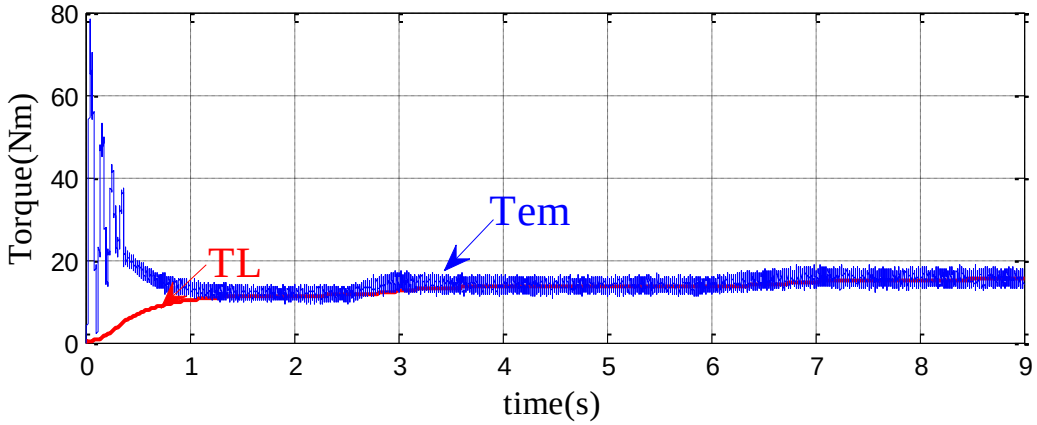

Figure 5.12 electromagnetic and load torque

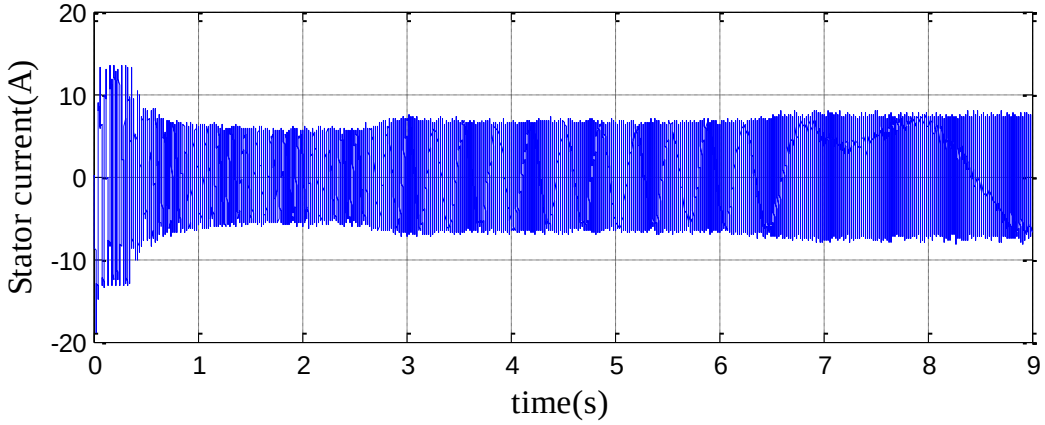

Figure 5.13 the stator current i_{sa1}

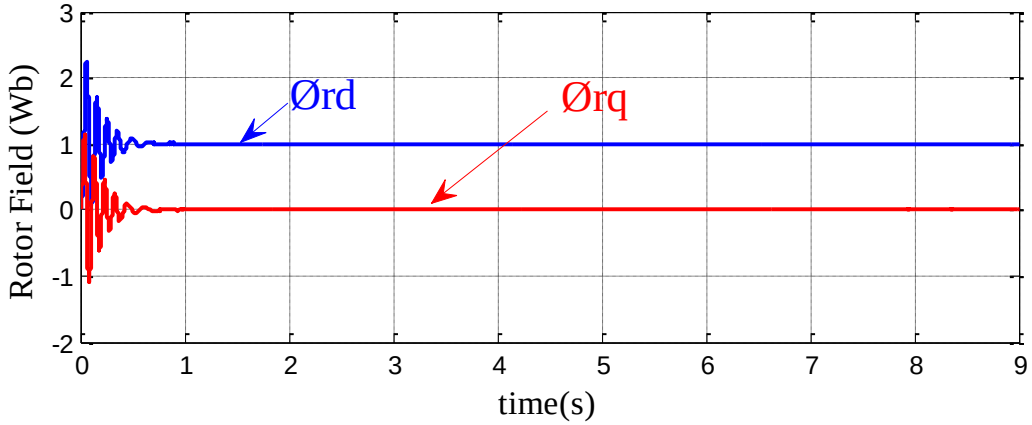

Figure 5.14 Rotor field orientation

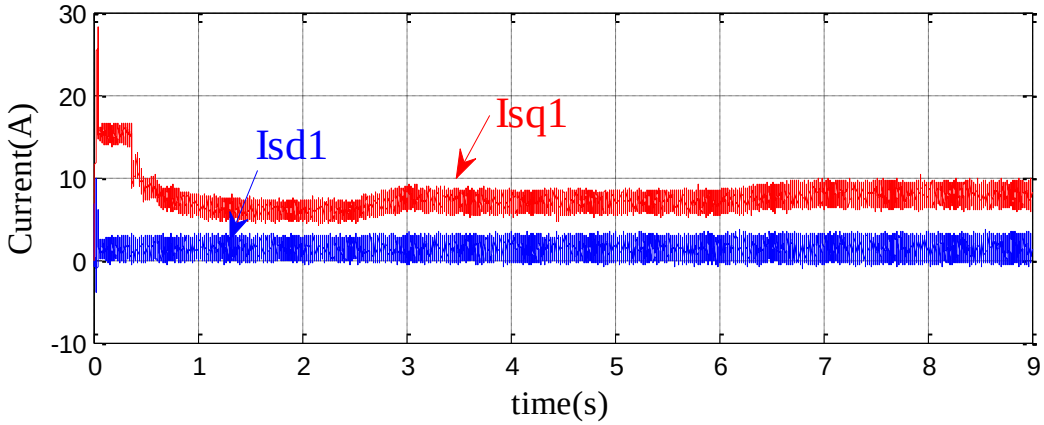

Figure 5.15 Decoupling between rotor flux and motor torque producing components

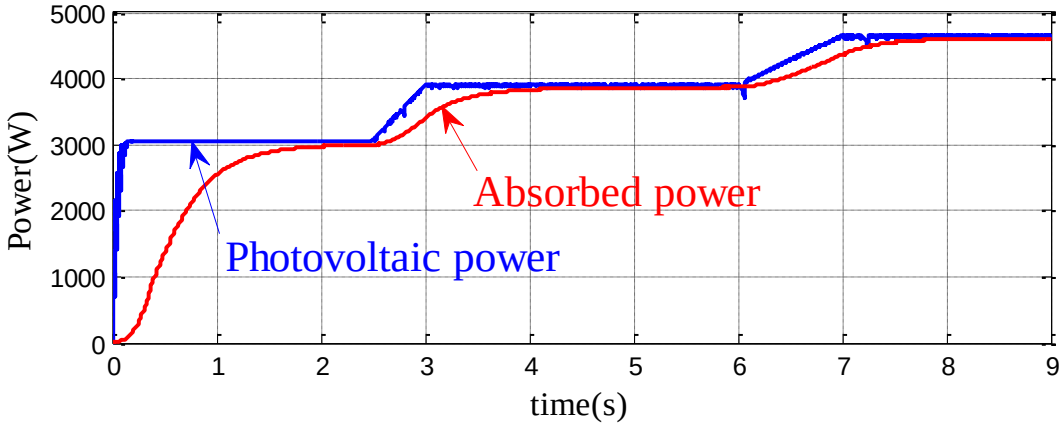

Figure 5.16 PV power and absorbed power

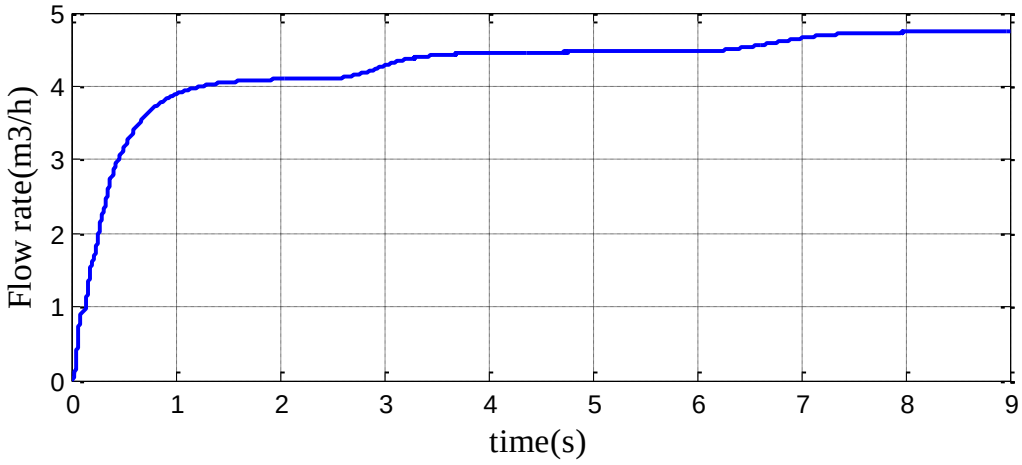

Figure 5.17 Evolution of flow rate

In order to have a clear view of the proposed system, The MPP algorithm tracks correctly to extract maximum power from the PVG. Figure 5.10 show the PV power trajectory of MPPT the PVG with the variation of solar irradiation which is varied from 600W/m^2 to 1000W/m^2 (Figure 5.8).

The PVG output voltage (Figure 5.9) is the input of the inverters that generates two three-phase voltages to feed the DSIM. The latter speed is varied accordingly by the fuzzy controller such that maximum power will be then applied to the water pump. Figure 5.11 shows the good tracking of the reference speed and the smooth control due to the use of fuzzy rules based control.

Regarding the motor –pump association, the IFOC has ensured that for variable irradiance, the torque of the motor is equal to that of the pump's need (Figure 5.12). Decoupling has made the torque control easier without affecting other parameters, Figure 5.13, for instance, shows that starting current is kept within safe limit ($I_{s1,\ start} \approx 20A$). The DSIM decoupling quality is shown by the dynamic variation of the flux as well as the variation of direct and transverse components of stator current.

- The direct rotor field *($\emptyset_{dr}$)* follows the reference value *(1Wb)* and the transverse component *($\emptyset_{qr}$)* is null (Figure 5.14). Thus, the flux orientation is satisfied.
- The direct component of stator current (i_{sd1}) is insensitive to the load torque variation (Figure 5.15) and depends only on the rotor flux level. The other component of the current (i_{sq1}) is the torque control component and therefore has the same shape as the output electromagnetic torque (Figure 5.15). This also can testify the good decoupling between the torque and rotor flux.
- The good speed tracking has resulted also in good tracking of the PVG power therefore maximum power transfer to the water pump (Figure 5.16).

Figure 5.17 illustrate the evolution of water flow rate. It shows that the water pump is operating at its optimum point where maximum water flow rate is at its maximum value.
The obtained maximum from the PVG (without an extra sensor of power, the power is computed using I_{pv} and V_{pv} which are the same inputs to the P&O MPPT algorithm) is used to compute the optimum rotor speed to be used by the Fuzzy controller.

V.5 Conclusion

A new architecture of SWPS is presented. We proposed in this architecture the use of DSIM with global optimization using Perturb and Observe MPPT algorithm and speed optimizer. Indirect field oriented control scheme is used to decouple the nonlinear structure of the DSIM and fuzzy sets based controller to handle the uncertainties related to the modeling of AC ploy-phase motors in general.

Fuzzy logic control has shown the ability to ensure fast speed response with minimum steady state error. Field oriented control of the DSIM allows the control of speed easier and consequently optimum operation of the pump is ensured.

The simulation results show the effectiveness and the good dynamic performances (speed response without overshoot, zero state error,…etc) of fuzzy speed control. Furthermore, the fuzzy controller design is performed without using the machine's mathematical model.

General Conclusion

General conclusion

In this thesis, a new GSS-based MPPT method is proposed and tested using MATLAB/Simulink Software. Accurate models of a PVG, as well as, a Boost converter were selected for implementation. The proposed technique requires only the initial interval to find the MPP for sure. This MPPT was tested under STC, rapidly changing conditions with different step variations on irradiance and temperature. This technique shows the Fast tracking, with no oscillations around the MPP, and it can provide an accurate and reliable tracking performance of the MPP when on irradiance or temperature changes.

GSS technique designed present important enhancements to the power extraction skills of the P&O for MPP, it is fast convergence speed and there is no requirement of derivatives of voltage and power measured from solar array.

A comparison of SWPS performances using P&O and GSS-based MPPT is presented. The induction motor is selected for driving centrifugal pump and the indirect field oriented controller is adopted to control the speed of the motor using the GSS-based MPPT in SWPS control systems, and it is almost the same compared to that of the P&O method while the performances, following the obtained results, are much better in terms of time response, perturbation free and dynamic efficiency. This technique is applied for single-stage solar water pumping system. That is, the Boost component would be eliminated and the inverter will be controlled by a PWM algorithm. The latter, receives a reference value either voltage or current that is generated by the GSS –based MPPT algorithm. The results validate that MPPT and can used for the searching of the MPP in the photovltaic pumping systems.

A new scheme of SWPS is presented, the DSIM is used for a global optimization using Perturb and Observe MPPT algorithm and speed optimizer. Indirect field oriented control scheme is implemented to decouple the nonlinear structure of the DSIM. Fuzzy logic control has shown the ability to ensure fast speed response with minimum steady state error. Field oriented control of the DSIM allows the control of speed easier and consequently optimum operation of the pump is ensured. The simulation results show the robustness, the effectiveness and the good dynamic performances (speed response without overshoot, zero state error,…etc) of fuzzy speed control. Furthermore, the fuzzy controller design is performed without using the machine's mathematical model.

References

[1] Imene Yahyaoui. Sizing and energy management for photovoltaic pumping, Thesis doctoral, university of Valladolid, April 2015

[2] Kala Meah, Steven Fletcher. Sadrul Ula, Solar photovoltaic water pumping for remote locations, Renewable and Sustainable Energy Reviews 12 (2008) 472–487

[3] Akbaba, M., Qamber, I., Kamal, A. Matching of separately excited dc motors to photovoltaic generators for maximum power output. Solar Energy 63 (1989) 375‑385.

[4] Appelbum, J. Starting and steady state characteristic of DC motor powered by solar cell generator, IEEE Trans. on EC 1 (1986) 17‑27.

[5] Z. Abidin Firatoglu, Bulent Yesilata. New approches on the optimization of directly coupled photovoltaic Water-Pumping System, Solar Energy77 (2004) 81–93.

[6] A. Terki, A. Moussi, A. Betka. N. Terki, An improved efficiency of fuzzy logic control of PMBLDC for PV pumping system, Applied Mathematical Modeling 36 (2012) 934–944.

[7] M. Nabil, S.M. Allam, E.M. Rashed. Performance improvement of a photovoltaic pumping system using synchronous reluctance motor, ElectPow Comp and Systems, 41 (2013) 447-464

[8] C. Gopal, M. Mohanraj, P. Chandramohan, P. Chandrasekar. Renewable energy source water pumping systems - A literature review, Renewable and Sustainable Energy Reviews 25 (2013) 351–370

[9] J. V. M. Caracas, G. C. Farias, L.F.M. Teixeira, L.A.S. Ribeiro. Implementation of a High-efficiency, High-lifetime, and low-cost Converter for an Autonomous Photovoltaic Water Pumping system, IEEE, Trans on Industry Applications, Vol. 50, No. 1, Jun/Feb. 2014

[10] Vitorine MA, Correa MBR, Jacobina CB, Lima AMN. An effective induction motor control for photovoltaic pumping, IEEE Trans Ind Electron 2011; 58 (4): 1162 - 70. doi: 10.1109/TIE.2010.2054053

[11] Biji G. Modeling and simulation of PV based pumping system for maximum efficiency. In: 2012 IEEE International Conference on Power, signals, Controls and Computation, EPSCICON, p.1-6, DOI: 10.1109/ EPSCICON.2012.6175266

[12] A. GEBREEL. Simulation and implementation of two level and three-level inverters by Matlab and rt-lab, The Ohio State University, 2011

[13] Akihiro Oi. design and simulation of photovoltaic water pumping system, Thesis for the Degree of Master, Faculty of California Polytechnic State University, September 2005

[14] UNEP, Water Policy and Strategy, (viewed on www.unep.org/dpdl/water/ , August2005)

[15] Fathi A O Aashoor. Maximum power point tracking techniques for photovoltaic water pumping system, thesis submitted for the degree of Doctor of Philosophy , University of Bath, May 2015.

[16] Foster R, Majid G, CotaA. A test book of solar energy Renew Energy Environ 2014 [accessed 07.06.1] Solar-Energy-Renewable-Environment

[17] S.S. Chandel et al. Review of solar photovoltaic water pumping system technology for irrigation and community drinking water supplies, Renewable and Sustainable Energy Reviews 49(2015)1084-1099

[18] Dhiaa Halboot Muhsen et.al. A review of photovoltaic water pumping system designing methods, control strategies and field performance, Renewable and Sustainable Energy Reviews 68 (2017) 70-86

[19] J. Appelbaum. Starting and steady-state characteristics of DC motors powered by solar cell generators, Energy Conversion, IEEE Transactions on, pp. 17-25, 1986.

[20] J. S. Ramos and H. M. Ramos, Solar powered pumps to supply water for rural or isolated zones: A case study, Energy for Sustainable Development, vol. 13, pp. 151-158, 2009.

[21] Vimal Chand Sontake et al. Solar photovoltaic water pumping system - a comprehensive review, Renewable and Sustainable Energy Reviews 59(2016)1038-1067

[22] Eker B. Solar powered water pumping systems. Trakia JSci2005; 3(7):7-11

[23] G. M. Masters, Renewable and efficient electric power systems: Wiley Inter science, 2005

[24] Abouda S, Nollet F, Chaari A, Essounbouli N, Koubaa Y. Direct torque control DTC of induction motor used for piloting a centrifugal pump supplied by a photovoltaic generator, Int J Electr Robot Electron Commun Eng2013; 7 (8):619-24

[25] Bhatnagar P, Nema RK. Maximum power point tracking control techniques: state of the art in photovoltaic applications, Renew Sust Energy Rev 2013; 23: 224-41. doi:10.1016/j.rser.2013.02.011

[26] Ishaque K, Salem Z. A review of maximum power point tracking control techniques of PV systems for uniform insolation and partial shading condition, Renew Sust Energy Rev 2013; 19: 475-88. doi: 10.1016/j.rser.2012.11.032

[27] Sontake VC, Kalamkar VR. Solar photovoltaic water pumping system a comprehensive review, Renew Sust Energy Rev 2016; 59:1038-67 doi: 10.1016/jrser. 2016.01.021

[28] Akihiro Oi Taufik, Anwari Makbul, Taufik Mohammad. Modeling and simulation of photovoltaic water pumping system, In: Proceedings of third Asia international conference on modeling simulation; 2009.p.497-02

[29] Elgendy MA, Zahawi B, Atkinson DJ. Assessment of perturb and observe MPPT algorithm implementation techniques for PV pumping applications, IEEE Trans Sustain Energy 2012; 3:21-33.

[30]Katan RE, Agelidis VG, Nayar CV. Performance analysis of a solar water pumping system, In: Proceedings of power electronics, drives and energy systems for industrial growth; 1996:18-11.p.81-87

[31]Mahmoud Marwan M, Kukhun Walied R, Daud Abdel-Karim. Efficiency improvement of a dual PV water pumping system on a desert well by solar matched load control, Int J Energy Eng 2013; 3(5):151-7

[32]Andoulssi R, Draou A, Jerbi H, Alghonamy A, Khiari B. Nonlinear control of a photovoltaic water pumping system.EnergyProcedia2013;42:328-36

[33]Lalouni Sofia, Rekioua Djamila. Comparison between MPPT controllers for optimal operating of photovoltaic pumping system, In: Proceedings of international conference on control, engineering information technology; 2013:2.p.62-67.

[34] Veerachary M, Yadaiah N. ANN based peak power tracking for PV supplied DC motors, Sol Energy 2000; 69:343-50

[35] Mazouz N, Midoun A. Control of a DC/DC converter by fuzzy controller for a solar pumping system, Int J Electr Power Energy Syst 2011; 33:1623-30

[36] Caton P, Design of rural photovoltaic water pumping systems and the potential of manual array tracking for a West-African village, Sol Energy 2014; 103:288-302

[37] Mozaffari Niapour SAK, Danyali S, Sharifian MBB, Feyzi MR. Brushless DC motor drives supplied by PV power system based on Z source inverter and FL-IC MPPT controller, Energy Convers Manag 2011; 52:3043-59

[38] Hamrouni N, Jraidi M, Chérif A. Theoretical and experimental analysis of the behavior of a photovoltaic pumping system, Sol Energy 2009; 83:1335-44

[39] Eskander MN, Zaki AM. A maximum efficiency-photovoltaic-induction motor pump system, Renew Energy 1997; 10:53-60

[40] Kumar B, Chauhan TK, Shrivastava V. A comparative study of maximum power point tracking methods for a photovoltaic-based water pumping system, Intern J Sust Energy 2014; 33 (4) 797-810. http://dx.doi.org/10.1080/14786451.2013.769990

[41] Mosaffari Niapour SAKH, Danyali S, Sharifian MBB, Feyzi MR. Brushless DC motor drives supplied by PV power system based on Z-source inverter and FL-IC MPPT controller, Energy Convers Manage2011; 52 (8-9): 3043-59. doi: 10.1016/ j.enconman. 2011.04.016

[42] Biji G. Modeling and simulation of PV based pumping system for maximum efficiency, In: 2012 IEEE International Conference on Power, signals, Controls and Computation, EPSCICON, p.1-6, DOI: 10.1109/ EPSCICON.2012.6175266.

[43]Lawrance W, Wichert B,Langridg D. Simulation and performance of a photovoltaic pumping system, In: Proceedings of 1995 international conference on power electronics and drive systems;1995:1.p.513-18

[44] Swamy CLP, Singh B, Singh BP, Murthy S. Experimental investigations on a permanent magnet brushless DC motor fed by PV array for water pumping system, In: Proceedings of the 31st inter society energy conversion engineering conference. IECEC 96; 11-16 August 1996: 3.p.1663-68

[45] Chandrasekaran N, Ganeshprabu B, Thyagarajah Dr.K. Comparative study of photovoltaic pumping system using a DC Motor and PMDC motor, In: Proceedings of IEEE international conference on advances in engineering, science and management. ICAESM-2012; March2012.p.129-32

[46] Singh Bhim, Swamy CL Putta, Singh BP, Analysis and development of a low cost permanent magnet brushless DC motor drive for PV array fed water pumping system, Sol Energy Mater Sol Cells1998;51(1):55-67

[47] Kolhe M, Joshi JC, Kothari DP. Performance analysis of a directly coupled photovoltaic water pumping system, IEEE Trans Energy Convers2004; 19 (3):613-8

[48] Daud AbdelKarim, Mahmoud Marwan M. Solar powered induction motor driven water pump operating on a desert well, simulation and field tests, Renew Energy 2005; 30:701-14.

[49]Zaki Aziza M, Eskander Mona N. Matching of photovoltaic motor pump systems for maximum efficiency operation, RenewEnergy1996; 7(3):279-88

[50] Bloos Hans, Genthner Markus, Heinemann Detlev, Janssen Andreas, Moraes Rejane.In: Proceedings of photovoltaic pumping systems a comparison of two concepts. EuroSun'96; 1996:p.583-87

[51] Chenni R, Zarour L, Bouzid A, Kerbache T. Comparative study of photovoltaic pumping systems using a permanent magnet synchronous motor (PMSM) and an asynchronous motor (ASM), Rev Energy Ren 2006;9:17-28

[52] Hamidat A. Simulation of the performance and cost calculations of the surface pump.RenewEnergy1999; 18:272-81

[53] Moulay Idriss C, Mohamed B. Application of the DTC control in the photovoltaic pumping system, Energy Convers Manag 2013; 65:655-62

[54] Odeh I, Yohanis YG, Norton B. Influence of pumping head, insulation and PV array size on PV water pumping system performance, Sol Energy 2006; 80:51-64

[55] Benlarbi K, Mokrani L, Nait Said MS. A fuzzy global efficiency optimization of a photovoltaic water pumping system. SolEnergy2004; 77:203-16

[56] Betka A, MoussiA . Performance optimization of a photovoltaic induction motor pumping system, RenewEnergy2004;29:2167-81

[57]Abdullah M. Noman and al. A Fuzzy Logic Control Method for MPPT of PV Systems, IEEE conference 2012,n0 978-1-4673-2421-2/12.

[58] Achour Betka. Perspectives for the Sake of Photovoltaic Pumping Development in the South, thesis submitted for the award of the degree of PHD University of Batna.

[59] C. Gopal, M. Mohanraj, P. Chandramohan, P. Chandrasekar. Renewable energy source water pumping systems - A literature review, Renewable and Sustainable Energy Reviews 25 (2013) 351–370

[60] J. V. M. Caracas, G. C. Farias, L.F.M. Teixeira, L.A.S. Ribeiro. Implementation of a High-efficiency, High-lifetime, and low-cost Converter for an Autonomous Photovoltaic Water Pumping system, IEEE, Trans on Industry Applications, Vol. 50, No. 1, Jun/Feb. 2014.

[61] Malki sihem. Maximum Power Point Tracking (MPPT) for Photovoltaic System, thesis submitted for the degree of Magister University of Boumerdes, 2011.

[62] Djamila rekioua and Ernest Matagne. Optimization of photovoltaic Power systems, Book of Green Energy and Technology, Springer-Verlag London Limited 2012

[63] Lewis Fraas, Chapter 1: history of Solar Cell Development, Low cost Solar Electric Power, Doi: 10.1007/978-3-319-07530-3_1, Springer, June 2014.

[64] A.M. Shraf and M. Reaz UI Haque. A stand alone photovoltaic (Ac) scheme for village electricity, 31st Photovoltaic Specialists Conference and Exhibition, January 3-7, 2005, Florida

[65] http://www.rfwireless-world.com/Articles/Solar-Cell-as-Renewable-Energy-Source.html

[66] A. Ghoneim. Design optimization of photovoltaic powered water pumping systems, Energy Conversion and Management 47 (2006) 1449–1463

[67] Ramesh K GOVINDARAJAN and al. A control scheme with performance prediction for a PV fed water pumping system, front. Energy 2014, 8(4): 480–489.

[68] C. S. Chin and al. Fuzzy Logic Based MPPT for Photovoltaic Modules Influenced by Solar Irradiation and Cell Temperature, UKSim 13th International Conference on Modelling and Simulation 2011.

[69] Jianbo Bai and al. Development of a new compound method to extract the five parameters of PV modules, Energy Conversion and Management 79 (2014) 294‑303

[70] F. Slama. Simulation of Photovoltaic generator Connected to a Grid, MJMS 01 (2014) 025–033.

[71] Belkacem Bouzidi. New sizing method of PV water pumping systems, Sustainable Energy Technologies and Assessments 4 (2013) 1‑10.

[72] bradley p. davenport. advanced thermo photovoltaic cells modeling, optimized for use in radioisotope thermoelectric generators (rtgs) for mars and deep space missions, thesis master of science in electrical engineering, naval postgraduate school, California, June 2004.

[73] Aissa Kheldoun, Salim Djeriou, Abdelmalek Kouadri, Larbi Refoufi. Using Golden Section Search Technique for Maximum Power Point Tracking in Photovoltaic Systems" 13th International Conferance o Clean Energy, June 2014 Istanbul

[74] Fathi A O Aashoor. Maximum power point tracking techniques for photovoltaic water pumping system, thesis submitted for the degree of Doctor of Philosophy , University of Bath, May 2015

[75] Shridhar Sholapur and al. Boost Converter Topology for PV System with Perturb And Observe MPPT Algorithm, IOSR Journal of Electrical and Electronics Engineering (IOSR-JEEE), Volume 9, Issue 4 Ver. II (Jul – Aug. 2014), PP 50-56.

[76] S. Kolsi and al. Design Analysis of DC-DC Converters Connected to a Photovoltaic Generator and Controlled by MPPT for Optimal Energy Transfer throughout a Clear Day, Journal of Power and Energy Engineering, 2014, 2, 27-34.

[77] Pratapsinh G. and al. A Review on DC-DC converters for Photovoltaic system, International journal of innovative research in electrical, electronics, instrumentation and control engineering (IJIREEICE), Vol. 3, Issue 12, December 2015

[78] Rashid, Muhammad H. Power Electronics - Circuits, Devices, and Applications 3rd Edition Pearson Education, 2004.

[79] Taufik EE527 Switching Power Supply Design - Lecture Note Cal Poly State University, San Luis Obispo, 2004

[80] M.tech scholars and al. Grid Connected Photovoltaic Power Plant with DC Boost converter Using MPPT Technique, International Research Journal of Engineering and Technology (IRJET), Volume: 04 Issue: 02 | Feb -2017.

[81] M.S.Sivagamasundari and al. Maximum Power Point Tracking For Photovoltaic System by Perturb and Observe Method Using Buck Boost Converter, International Journal of Advanced Research in Electrical, Electronics and Instrumentation Engineering, Vol. 2, Issue 6, June 2013.

[82] Adam TOMASZUK, Adam KRUPA. Step-up DC/DC converters for photovoltaic applications - theory and performance, PRZEGLĄD ELEKTROTECHNICZNY, R. 89 NR 9/2013

[83] ELIANA ISABEL ARANGO ZULUAGA. design of asymmetrical boost converters based on photovoltaic systems requirements, Dyna, year 79, Nro. 171, pp. 31-40. Medellin, february, 2012.

[84] Elgendy MA, Zahawi B, Atkinson DJ. Comparison of directly connected and constant voltage controlled photovoltaic pumping system. IEEE Trans Sust Energy2010; 1(3): 184 - 92. doi: 10.1109/TSTE.2010.2052936

[85] Nur Atharah Kamarzaman and al. A comprehensive review of maximum power point tracking algorithms for photovoltaic systems, Renewable and Sustainable Energy Reviews 37(2014)585–598

[86] Badescu, V.: Time dependent model of a complex PV water pumping system. Renew Energy 28(4), 543–60 (2003)

[87] Vitorine MA, Correa MBR, Jacobina CB, Lima AMN. An effective induction motor control for photovoltaic pumping, IEEE Trans Ind Electron2011, 58 (4): 1162 - 70. doi: 10.1109/TIE.2010.2054053.

[88] Elgendy MA, Zahawi B, Atkinson DJ. Assessment of incremental conductance maximum power point tracking algorithm, IEEE Trans Sust Energy2013, 4 (1): 108 - 17. doi: 10.1109/TSTE.2012.2202698

[89] Alireza Kouchakiand al. A new maximum power point tracking strategy for PV arrays under uniform and non-uniform insolation conditions, Solar Energy 91 (2013) 221–232

[90] Mohamed M. Algazar and al. Maximum power point tracking using fuzzy logic control'', Electrical Power and Energy Systems 39 (2012) 21–28

[91] A.R.N.M Reaz ul haque. Novel maximum power tracking for photovoltaic energy utilization schemes, Thesis for the Degree of Master, New Brunswick University, Novembre 2004

[92] B.AFIF and al. Power flow Controller of PV System, International Research Journal of Engineering and Technology (IRJET), Volume: 02 Issue: 08, Nov-2015

[93] Gailan Abdul Qadir, Majid S. Naghmash. Design and Simulation of Programmable AC-DC Converter Using Pulse Width Modulation (PWM) Techniques in MATLAB, International Journal of Soft Computing and Engineering (IJSCE), Volume-3, Issue-6, January 2014

[94] C. Johnson, Physics for Scientists 8thEdition, Ohio State University - 2003

[95] Curtis F. Gerald and Patrick O. Wheatley, Applied Numerical Analysis. Seventh Edition, Addison-Wesley, 2004

[96] http://numericalmethods.eng.usf.edu (see Numerical Methods university of South Florida-2002)

[97] Gurley, Numerical Methods Lecture 6-Optimization, Numerical Methods Lecture 6-Optimization, CGN 3421 - Computer Methods

[98] C. Gopal and al. Renewable energy source water pumping systems-A literaturere view, Renewable and Sustainable Energy Reviews 25(2013)351–370

[99] J.K. Kaldellis and al, Experimental energy analysis of a stand-alone photovoltaic-based water pumping installation, Applied Energy 88 (2011) 4556–4562

[100] Belkacem Bouzidi, New sizing method of PV water pumping systems, Sustainable Energy Technologies and Assessments 4 (2013) 1-10

[101] S.G. Malla, C.N. Bhende and S. Mishra, Photovoltaic based Water Pumping System, Indian Institute of Technology Bhubaneswar, 978-1-4673-0136-7/11/$26.00 ©2011 IEEE

[102] Geetanjali Manekar and al. Modeling Methods of Three Phase Induction Motor, National Conference on Innovative Paradigms in Engineering & Technology (NCIPET-2013)

[103] Canudas de Wit. Modélisation, contrôle vectoriel et DTC-commande des moteurs asynchrones, Vol. 1. Hermes Sciences Publications, ISBN 2-7462-0111-9. C. (2000)

[104] W. Y. Z. L. Haibing Hu. Design and Implementation of Three-Level Space Vector PWM IP Core for FPGAs, VOL 22, NO 6, NOVEMBER 2007.

[105] Djeriou S, Kheldoun A, Sadouni R. Fuzzy indirect field oriented control of a dual star induction motor water pumping system fed by photovoltaic generator. Eng Int Syst 2015, 23 (2): 63-76.

[106] Kumar R, Singh B, Chandra A, Al-haddad K. Solar OV array water pumping using BLDC motor drive with boost-buck converter. In: Proceedings of the IEEE Energy Conversion Congress and Exposition ECCE; 2015. p. 5741-5748, DOI: 10.1109/ECCE.2015.7310466.

[107] Thierry M, Christian G, Charles J, Benoît R. A simplified but accurate prevision method for along the sun PV pumping systems, Sol Energy 2008; 82 (11): 1009–1020. doi:10.1016/j.solener.2008.05.005

[108] Rawat R, Kaushik SC, Lamba R. A review on modeling, design methodology and size optimization of photovoltaic based water pumping, standalone and grid connected system, Renew Sust Energy Rev 2016; 57

[109] Sallem, Souhir; Chaabene, Maher; & Kamoun, Mohammed. Ben. Ali. (2009). Energy management algorithm for an optimum control of a photovoltaic water pumping system, Applied Energy, 86(12), 2671-2680

[110] Salim Djeriou, Aissa Kheldoun, Adel Mellit. Efficiency Improvement in Induction Motor-Driven Solar Water Pumping System Using Golden Section Search Algorithm, Arab J Sci Eng https://doi.org/10.1007/s13369-017-2972-6

[111] EN50530, Overall efficiency of grid connected photovoltaic inverters. 2010.

[112] Kala Meah, Steven Fletcher, Sadrul Ula, Solar photovoltaic water pumping for remote locations, Renewable and Sustainable Energy Reviews 12 (2008) 472–487, DOI:10.1016/j.rser.2006.10.008

[113] C. Gopal, M. Mohanraj, P. Chandramohan, P. Chandrasekar, Renewable energy source water pumping systems – A literature review, Renewable and Sustainable Energy Reviews 25 (2013) 351–370

[114] Umesh Chandra Dikshit and R. K. Tripathi, Direct Torque Control for Dual Three-Phase Induction Motor Drives, 978-1-4673-0455-9/12/$31.00 ©2012 IEEE

[115] Y. Zhao, T. A. Lipo , Space vector PWM control of dual three phase induction machine using vector space decomposition, IEEE Trans. Ind. Appl., vol. 31, no. 5, pp. 1100–1109,

[116] G.K. Singh, Multi-phase induction machine drive research - a survey, Electric Power Systems Research 61 (2002) 139–147

[117] T. S. Franklin, J. J. F. Cerqueira and E. S. de Santana, Fuzzy and PI Controllers in Pumping Water System Using Photovoltaic Electric Generation, IEEE latin america transactions, vol. 12, no. 6, september 2014 1049

[118] D. Hadiouche, Contribution à l'étude de la machine asynchrone double étoile modélisation, alimentation et structure, Thesis doctoral, university of Henri Poincaré, Nancy-1, Décembre 2001.

[119] Salim Djeriou, Aissa Kheldoun, Fuzzy indirect field oriented control of a dual star induction motor water pumping system fed by photovoltaic generator, Eng Int Syst (2015) 0: 1–14© 2015 CRL Publishing Ltd

[120] Z.Chen, AC.Williamson , Simulation Study of a Double Three Phase Electric Machine, International conference on Electric Machine ICEM'98, 1998, pp215-220

[121] C. S. Chin P. Neelakantan H. P. Yoong K. T. K. Teo, Fuzzy Logic Based MPPT for Photovoltaic Modules Influenced by Solar Irradiation and Cell Temperature, 978-0-7695-4376-5/11 $26.00 © 2011 IEEE, DOI 10.1109/UKSIM.2011.78

[122] S.AREZKI, M. BOUDOUR, Simulation and Modeling of a Photovoltaic System Adapted by a MPPT control reaction, Application on a DSIM, 2010 IEEE International Energy Conference, 978-1-4244-9380-7/10/$26.00 ©2010 IEEE

[123] G. K. Singh, K. Nam and S. K. Lim , A simple indirect field-oriented control scheme for multiphase induction machine, IEEE Trans. Ind. Elect., vol. 52, no. 4, pp. 1177–1184, August 2005.

[124] E.M. Berkouk, S. Arezki , Modélisation et Commande d'une Machine Asynchrone Double Etoile (MASDE) Alimentée par Deux Onduleurs à Cinq Niveaux à Structure NPC, , CNGE, Tiaret, Algeria 2004

[125] A.Igoudjil ; Y.Boudjema , Etude du changeur de fréquence à cinq niveaux à cellules imbriquées. Application à la conduite de la machine Asynchrone à Double Etoile, Master Thesis, university of USTHB , Algeria, June 2006.

[126] A.Aissaoui, M.Abid, H.Abid, A.Tahour and A.Zeblah, A Fuzzy Logic Controller for Synchronous Machine, Journal of ELECTRICAL ENGINEERING, VOL. 58, NO. 5, 2007, 285–290.

[127] S. Lekhchine, T. Bahi, Y. Soufi, Indirect rotor field oriented control based on fuzzy logic controlled double star induction machine, Electrical Power and Energy Systems 57 (2014) 206-211

[128] Marouani R., Bacha F., A maximum power point tracking algorithm applied to photovoltaic water pumping system", Proceeding of the 7th International Symposium on advanced electromechanical motion system & electric drives, 1-3 July, 2009.

[129] Faouzi Bacha, Moncef Gasmi, Sliding Mode Control of Induction-Motor-Pump Supplied by Photovoltaic Generator, IEEE International Conference on Industrial Technology (ICIT), 2011, pp.182-187

[130] Eker I., Torun Y., Fuzzy logic control to be conventional method, Energy Conversion and Management 47 (2006) 377–394

[131] Li Zhen, Longya Xu, Fuzzy learning enhanced speed control of an indirect field-oriented induction machine drive, IEEE Trans. on Cont. Syst. Techno. 8 (2010) 270–278

[132] A.Sivert, F. Betin , M. Moghadasian, A Yazidi, G. A. Capolino '' Position Control of Six-Phase Induction Motor using Fuzzy Logic: Application to Electric Power Steering 978-1-4673-0142-8/12/$26.00 ©2012 IEEE